2018

Netrin Guides Spinal Commissural Axons to the Midline at Long Range Through the Receptors DCC and Neogenin

Sze Sing Shaun Teo

NETRIN GUIDES SPINAL COMMISSURAL AXONS TO THE MIDLINE AT LONG RANGE THROUGH THE RECEPTORS DCC AND NEOGENIN

A Thesis Presented to the Faculty of

The Rockefeller University

in Partial Fulfillment of the Requirements for

the degree of Doctor of Philosophy

by

Sze Sing Shaun Teo

June 2018

NETRIN GUIDES SPINAL COMMISSURAL AXONS TO THE MIDLINE AT LONG RANGE THROUGH THE RECEPTORS DCC AND NEOGENIN

Sze Sing Shaun Teo, Ph.D.

The Rockefeller University 2018

During neurodevelopment, commissural axons are guided to the ventral midline in a remarkably precise and stereotyped way. Netrin, a secreted laminin-related protein, provides the major attractive cue for midline guidance. It is thought to act at long-range, functioning either in solution (chemotaxis) or bound to surfaces (haptotaxis). A gradient of Netrin-1 along the dorsal-ventral axis of the spinal cord is thought to attract commissural axons to the midline, with the floor plate being a major source of diffusible Netrin. However, this view has recently been challenged. To address this controversy and determine what role, if any, floor plate-derived Netrin-1 plays in commissural axon guidance, we quantitatively examined the phenotypes of mice specifically lacking floor plate *Netrin-1* expression. We observed that the loss of floor plate-derived Netrin-1 cause commissural axons to improperly project through the ventral motor column and resulted in fewer commissural axons that cross the ventral midline. The precrossing guidance defects observed at-a-distance from the floor plate supports the operation of Netrin as a long-range chemotropic factor.

To complement these studies, we investigated the differential roles for Netrin-1 receptors, Dcc and Neo1. How these two Netrin receptors collaborate during midline crossing has yet to be fully examined. Using transgenic embryos

that express Cre-recombinase within discrete spinal interneuron populations in combination with fluorescent reporter lines, we show that midline guidance of all commissural interneuron populations wholly depends on Netrin-1 signaling through the Dcc and Neo1 receptors. However, the genetic deletion of Dcc more severely perturbed midline guidance of the dorsal commissural neuron population compared to ventral interneurons, which predominantly express Neo1. The two populations differ in Dcc and Neo1 expression, both in terms of abundance and splice isoforms, and one of these differences could account for their differential dependence on Dcc for midline attraction.

To gain better insight into other genes that regulate midline guidance of commissural neurons, I generated a novel *Robo3*$^{Cre/+}$ mouse line to use in combination with fluorescent reporter lines to purify commissural neurons from embryonic spinal cord. Transcriptome analysis of isolated commissural neurons identified *RGMb*, a Neo1-specific ligand that is highly expressed by dorsal commissural neurons that could modulate Netrin signaling. Additionally, I profiled the transciptome of embryonic floor plate and characterized several floor plate-specific secreted proteins that were homologous to known guidance cues. The commissural neuron and floor plate transcriptomes will provide an invaluable starting point for testing the role of candidate guidance factors. The body of work performed here has reaffirmed the long-range nature of Netrin's attractive effect, showed that distinct neuronal populations express unique levels and isoforms of Dcc and Neo1 to achieve a common guidance outcome, and identified candidate factors that may collaborate with Dcc/Neo1 and Netrin in midline guidance.

Dedicated to the memory of

My grandmothers,
Lim Ah Jue (– 21 May 2009)
Anna Goh Ah Huay (16 May 1929 – 2 May 2012)

and my best friend,
Jude Alphonsus Tan Wei Xiong (14 Jun 1986 – 26 May 2012)

ACKNOWLEDGEMENTS

I must thank Marc for having me in the lab, and for his continued guidance and support throughout my graduate training. I am forever grateful to him for taking me under his wing. I am enriched with the scientific rigor he has imparted to me. Inspired by his leadership and professionalism, I hope to emulate these qualities in my future endeavors.

The Tessier-Lavigne lab has been a wonderful working environment. I owe a great deal to Olav, who has created an excellent learning and working environment. He has made it my home away from home. Olav has guided me every step of the way, and all these projects, experiments and dissertation would not be possible without him. I would also like to thank Kim, whose unwavering scientific and emotional support has been a pillar of strength for me. Together with Olav, they have also helped me become a better writer.

I owe special thanks to Zhuhao. As my mentor and collaborator, his passion for science and admirable patience with me exemplify what makes doing and learning science so enjoyable. His scientific rigor has made me a critical and better scientist. Alex and Nico also played a major part in teaching me the skills and techniques that make this work possible. I would also like to thank all other lab members for their camaraderie: my fellow graduate students Jason, Deanna, Dylan, Andy and Eliza, postdocs Dave, Dominik, Jianjin, Nick and Yuya, and research assistants Ricardo, Jinjoo, Mike and Paul.

I would like to thank the Dean’s Office for making my experience with the David Rockefeller Graduate Program so enjoyable. My thanks also go to my

faculty committee members Shai Shaham and Cori Bargmann for their guidance and advice as I progressed through my project, and to the various Rockefeller Resource Centers for making this work possible: Chingwen and her team at Gene Targeting, Rada and her team at Transgenic Services, Svetlana and her team at the Flow Cytometry Facility, and Connie and her team at the Genomics Center.

I want to thank my family and friends for their support, Andy's dog Howie for his attention, and very importantly to Faz, for his companionship and support on this journey.

This work was supported by fellowship funds from the Agency for Science, Technology and Research, Singapore (A*STAR). The *Kif26b*$^{+/-}$ mouse strain used for this research project was created by the Mouse Biology Program (*www.mousebiology.org*) at the University of California Davis using vector PRPGS00105_E_E07, generated by the trans-NIH Knock-Out Mouse Project (KOMP) and obtained from the KOMP Repository (*www.komp.org*). NIH grants to Velocigene at Regeneron Inc (U01HG004085) and the CSD Consortium (U01HG004080) funded the generation of gene-targeted vectors and ES cells for over 8500 genes in the KOMP Program and archived and distributed by the KOMP Repository at UC Davis and CHORI (U42RR024244).

TABLE OF CONTENTS

List of Figures ..... **ix**

List of Tables ..... **x**

List of Abbreviations ..... **xi**

Chapter 1. Introduction to axon guidance at the ventral midline **1**

Rationale for the current study 1
Overview of mammalian commissures 2
The trajectory of spinal commissural axons 3
The midline is the first intermediate target for commissural neurons 5
Molecular mechanisms of midline attraction 5
Molecular mechanisms that mediate axon guidance during and after crossing the midline 6
Netrins and their molecular structures 9
Netrin's chemotactic and haptotactic potential 9
Two distinct segments of commissural axon projections and their dependence on floor plate-derived chemoattractant(s) 10
Floor plate and ventricular zone expression of Netrin 11
The Netrin receptors Dcc and Neo1 11
Robo3 is a multifunctional receptor in precrossing axon guidance 13
The relative contribution of each signaling pathway to axon guidance is incomplete 15
Discrete interneuron populations in the spinal cord 16
Culturing spinal cord explants *in vitro* 17
Thesis outline 19

Chapter 2. Floor plate-derived diffusible Netrin is essential for long-range attraction **20**

Rationale 20
Floor plate-specific *Netrin-1* deletion reduces the ventral commissure size 20
Loss of floor plate Netrin-1 disrupts commissural axon guidance near the motor column 24
Netrin-1 does not direct commissural axons around the ventricular zone 29
Netrin-1 can travel from its site of production in the developing spinal cord 32
Conclusions 35

Chapter 3. Spinal commissural populations differentially express the Netrin receptors Dcc and Neogenin **36**

Rationale 36
Dorsal and ventral populations require Netrin-1 for proper guidance 36

Dorsal, but not ventral commissural neurons, require Dcc for midline crossing *in vivo* 43
Differential expression of Neo1 and Dcc across neuron populations along the dorsoventral gradient 51
In vitro Netrin receptor dynamics are similar in both dorsal and ventral populations 55
Dcc and *Neo1* splice isoforms differ across both populations 59
RGMb, a ligand of Neo1, is enriched in commissural neurons 62
RGMb is localized to precrossing and crossing axonal segments 65
Conclusions 67

Chapter 4. Revealing potentially new modulators of midline guidance factors using RNA-Seq of commissural neurons and floor plate 68

Rationale 68
Generation of a Robo3^{Cre} line to label commissural neurons and their axons 68
Gene profiling of factors expressed in commissural neurons 72
Functional knockdown screen for commissural-specific factors in axon guidance 76
Shortlisting commissural-specific candidates for further characterization 79
The Thsd7a ectodomain binds to axons *in vitro* 80
Grossly normal axonal projections in *Dner* and *Kif26b* mutant spinal cords 80
Gene profiling factors expressed in the floor plate 81
Considerations for shortlisting floor plate-specific candidates for further characterization 85
Lgi3 as a candidate for mediating midline guidance 86
Adamts16 as a candidate for midline guidance 91
Eva1c as a candidate for midline guidance 94
Conclusions 98

Chapter 5. Discussion 99

Floor plate-derived Netrin-1 is essential for midline guidance 99
Evaluating the reduction in ventral commissure size as a measure for axon guidance defects 99
Netrin-1 maintains the integrity of the CNS 101
Relative tissue-specific contributions to the Netrin-1 gradient 101
Netrin-1 has haptotactic modes of action and travels from its site of production 104
The canonical model of Netrin-1 in midline guidance revisited 105
Dcc and Neo1 mediate Netrin-dependent midline attraction 105
Population-specific mechanisms for midline attraction 106
Molecular correlates of differential Netrin-1 sensitivity: Receptor isoforms and modulators of Neo1 signaling 107
RNA-Seq transcriptomes provide a useful starting tool for identifying and verifying candidate guidance factors 109
Concluding remarks 111

Chapter 6. Materials and Methods 112

Mice....112
Histology and immunohistochemistry....114
Image processing and quantification....115
2D explant cultures....116
3D explant cultures....117
RNA extraction for RT-PCR....117
Tissue dissociation and FACS sorting of *Robo3*$^{Cre/+}$;*Rosa26*$^{Ai14/+}$ cells....118
RNA extraction of floor plate and dorsal spinal cord for RNA-Seq....119
RNA library preparation....119
RNA-Seq alignment and analysis....119
In situ hybridization....120
siRNA knockdown using whole embryo culture....123
AP-protein binding assay....123
CRISPR/Cas9 knockout mice generation....124
Statistics....124

References....125

List of Figures

Figure 1.1 The trajectory of commissural axons in the developing mouse spinal cord....4
Figure 1.2 Receptor-ligand pairs in midline crossing....8
Figure 1.3 *In vitro* 2D cultures of spinal cord explants....18
Figure 2.1. Floor plate specific Netrin-1 is deleted in *Shh^{Cre};Netrin-1$^{fl/fl}$* embryos....22
Figure 2.2. Floor plate-derived Netrin-1 controls axon guidance....23
Figure 2.3. Axon guidance around the motor column is disrupted in *Shh^{Cre};Netrin-1$^{fl/fl}$* embryos....27
Figure 2.4. Misprojecting axons in the ventricular zone of *Netrin-1$^{-/-}$* mutants are not commissural....31
Figure 2.5. Netrin-1 immunoreactivity in the ventral commissure and precrossing axons....34
Figure 3.1. An allelic series of *Netrin-1* mutations....38
Figure 3.2. A genetic screen identified 2 suitable mouse lines for commissural neuron subtype specific analysis....40
Figure 3.3. Dorsal and ventral populations require Netrin-1 for proper guidance....41
Figure 3.4. Differential Dcc and Neo1 expression *in vivo*....45
Figure 3.5. The phenotypic severity of *Dcc$^{-/-}$* differs between dorsal and ventral populations....47
Figure 3.6 Midline guidance is grossly normal in *Neo1$^{-/-}$* mutants....49
Figure 3.7 Differential Dcc and Neo1 expression of different neuronal populations *in vitro*....53
Figure 3.8 *In vitro* Netrin-1 sensitivities of both dorsal and ventral populations are similar....57
Figure 3.9 Differential expression of long and short isoforms of *Dcc* and *Neo1* in dorsal and ventral spinal cord....60
Figure 3.10 Identification and characterization of Rgmb expression in commissural neurons....63
Figure 3.11 Model for Dcc and Neo1 population-specific functions in midline attraction....66
Figure 4.1 Generation of a *Robo3^{Cre}* gene-targeted line....70
Figure 4.2 Expression of commissural neuron-specific transcripts....73
Figure 4.3 Characterization and genetic screening of commissural neuron-specific factors in axon guidance....77
Figure 4.4 RNA-Seq identification of candidate genes enriched in floor plate cells....82
Figure 4.5 *In situ* validation of gene expression of floor plate candidates....83
Figure 4.6 *In vitro* and *in vivo* characterization of Lgi3 in midline guidance....88
Figure 4.7 *In vivo* characterization of Adamts16 in midline guidance....93
Figure 4.8 Characterization of Eva1c in midline guidance....95

List of Tables

Table 1 Candidate genes shortlisted from the RNA-Seq of commissural neurons and subsequent verification of gene expression by *in situ* hybridization.....75
Table 2 Candidate genes shortlisted from the RNA-Seq of floor plate tissue and subsequent verification of gene expression by *in situ* hybridization.....84
Table 3 Primers used to generate *in situ* probes 122

List of Abbreviations

CNS	central nervous system
CMM	Congenital Mirror Movement
CRISPR	Clustered Regularly Interspaced Short Palindromic Repeats
CST	Corticospinal tract
Dcc	*Unc40/Deleted in Colorectal Cancer* gene
DRG	dorsal root ganglion
FACS	Fluorescence-activated cell sorting
HGPPS	Horizontal gaze palsy with progressive scoliosis
L1	Neural cell adhesion molecule L1
Neo1	*Neogenin-1* gene
Netrin-1	*Unc6/Netrin-1* gene
Rgma/b/c/d	*Repulsive guidance molecule a/b/c/d gene*
Robo1/2/3/4	*Roundabout* gene, 1/2/3/4
Shh	*Sonic hedgehog* gene
TAG-1	Transient axonal glycoprotein-1/Contactin-2
TuJ1	Neuron-specific class III β-tubulin

Chapter 1. Introduction to axon guidance at the ventral midline

Rationale for the current study

The central nervous system is made up of diverse populations of neurons that vary in their cell body location and axonal trajectory. Despite the anatomical complexity of the nervous system, synaptic connections are established in a remarkably precise and stereotyped way through axon guidance programs. Commissural neurons represent one neuronal class that has been intensely studied as a model for understanding axon guidance (Colamarino and Tessier-Lavigne, 1995; Tessier-Lavigne and Goodman, 1996; Dickson, 2002). Precise guidance of commissural axons is required for the proper wiring of several circuits including those that control breathing, audition and locomotion (Bouvier et al., 2010; Renier et al., 2010; Michalski et al., 2013), underscoring their biological relevance. In humans, aberrant guidance of commissural axons leads to neurological disorders such as horizontal gaze palsy with progressive scoliosis (HGPPS), congenital mirror movements (CMM) and agenesis of the corpus callosum (ACC) (Engle, 2010; Nugent et al., 2012; Chilton and Guthrie, 2016; Marsh et al., 2017; Whitman and Engle, 2017).

Many of the major guidance cues and their receptors have been identified, but our understanding of how these factors interact with each other remains fragmentary. For example, a previously well-accepted model of midline attraction has been recently called into question (Dominici et al., 2017; Varadarajan et al.,

2017). The desire to clarify the ligand-receptor relationships of these guidance factors and to uncover potentially novel guidance mechanisms provides the motivation for this study. To gain insight into these issues, we leveraged Next-Generation sequencing, as well as newly available genetic tools and mouse models to revisit classical axon guidance models. It is hoped that these studies will yield key insights into the process of axon guidance and, ultimately, circuit formation.

Overview of mammalian commissures

In metazoans, bilateral symmetry endows animals with opposing left and right sides. Commissural neurons project their axons across the midline to the contralateral side, thereby connecting both sides of the nervous system to integrate sensory and motor information (Colamarino and Tessier-Lavigne, 1995; Kaprielian et al., 2000; Kiehn and Kullander, 2004; Kiehn, 2006). These commissural neurons are diverse in their identity and occur at all axial levels of the CNS (Colamarino and Tessier-Lavigne, 1995). Further, the axons of these neurons cross the midline at well-defined regions to form prominent commissures. In mammals, the corpus callosum, hippocampal commissure and anterior commissure are a few of the major telencephalic commissures. The corticospinal tract (CST) is another longitudinal tract that originates in the telencephalon, connecting the motor cortex to the contralateral spinal cord. In the eye, retinal ganglion cells project to the optic chiasm, where a subset of axons cross to the contralateral side. In the spinal cord, commissural axons cross at the ventral midline to form the ventral commissure (Chédotal and Richards, 2010).

Spinal commissural neurons have been an intensely studied model for understanding axon guidance (Colamarino and Tessier-Lavigne, 1995; Tessier-Lavigne and Goodman, 1996; Dickson, 2002). As such, they are the model system studied in this thesis, and the mechanisms governing their development will be further elaborated in this Chapter.

The trajectory of spinal commissural axons

In the mouse, commissural neurons differentiate from neural progenitors shortly after neural tube closure at E9.5 and continuing until E11.5 (Altman and Bayer, 1984). During this period, their cell bodies migrate out of the ventricular zone and the axons of these spinal commissural interneurons project ventrally and medially toward the midline (Sabatier et al., 2004). The first axons begin to cross the midline at E10.5, and continue to do so until E12.5. Upon reaching the midline they cross it and exit into the contralateral side, where the majority make a right-angle turn to project longitudinally (Fig1.1) (Cajal, 1899; Colamarino and Tessier-Lavigne, 1995; Dickson and Zou, 2010).

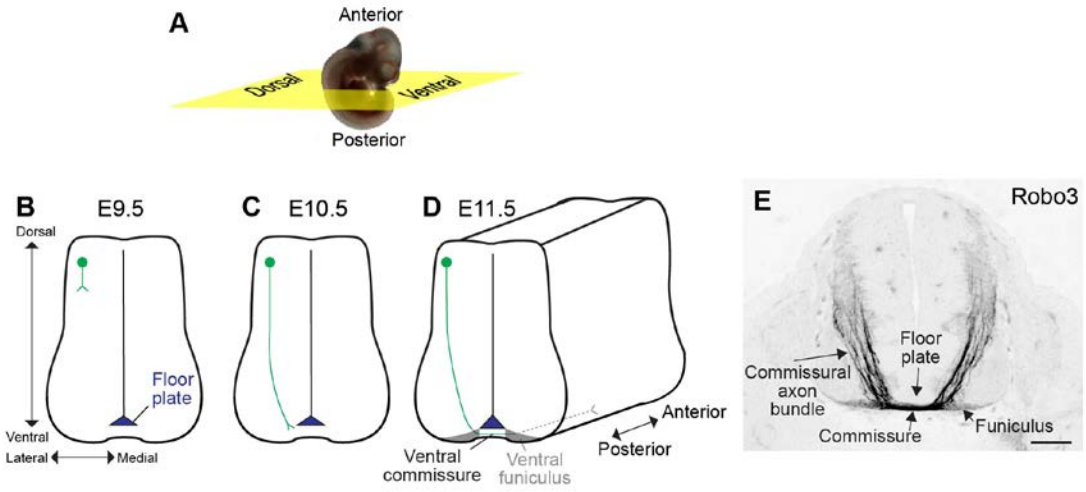

Figure 1.1 The trajectory of commissural axons in the developing mouse spinal cord

(A) Stereogram of an isolated mouse embryo at 11.5 days post-coitus (E11.5). Histological sections were prepared in the transverse plane (yellow), with the dorsal-ventral axis labeled. The orthogonal anterior-posterior axis is labeled as well. **(B-D)** The trajectory and development of commissural neurons (green). The floor plate is shown in blue. Commissural neurons are born at E9.5 (B), and their axons extend ventrally and medially towards the floor plate from E9.5-E10.5 (C). By E11.5 (D), these axons have crossed the midline and project into the contralateral ventral funiculus (grey). A majority of them turn into the transverse plane of the ventral funiculus and project anteriorly. **(E)** An E11.5 frozen section of the developing spinal cord stained for Robo3, a marker for commissural axons. The scale bar represents 100 μm.

The midline is the first intermediate target for commissural neurons

The final synaptic targets of neurons can be located several cell-body distances away, and in most instances, their axons can take one or more circuitous turns before reaching their eventual targets. These elaborate trajectories are precisely specified by a series of intermediate targets that are found along the trajectories of these axons during development. Intermediate targets are made up of morphogically distinct guidepost cells that express chemical cues to instruct axon guidance (Chao et al., 2009). For commissural neurons, the ventral midline is the first intermediate target their axons encounter. Columnar ependymal floor plate cells line the entire rostrocaudal axis of the midline (His, 1888; Placzek and Briscoe, 2005). When these cells fail to develop in *Drosophila melanogaster* and in *Mus musculus* mutants, commissural axons have aberrant trajectories (Bovolenta and Dodd, 1991; Klämbt et al., 1991; Matise et al., 1999), suggesting that the floor plate is critical for guiding commissural axons.

Molecular mechanisms of midline attraction

Floor plate cells secrete multiple diffusible factors that guide commissural axons toward and across the midline (Tessier-Lavigne et al., 1988). The first guidance cue that was biochemically isolated and identified was Netrin-1 (Kennedy et al., 1994; Serafini et al., 1994). Initially identified as *Unc-6* in *C. elegans* (Ishii et al., 1992), the Unc-6/Netrin proteins are evolutionarily conserved long-range chemoattractants that attract axons ventrally toward the midline in both vertebrates and invertebrates (Hedgecock et al., 1990; Colamarino and

Tessier-Lavigne, 1995; Wadsworth et al., 1996). This chemoattractive effect is mediated by the binding of Netrin to the Unc-40/DCC receptor and/or its close homolog Neogenin (Neo1), both of which are expressed on axons (Keino-Masu et al., 1996; Fazeli et al., 1997; Xu et al., 2014) (Fig 1.2). Consistent with a conserved role for Dcc in midline guidance, human mutations in Dcc that prematurely truncate the protein result in abnormal uncrossed CST projections and cause CMM (Srour et al., 2010; Jamuar et al., 2017).

Molecular mechanisms that mediate axon guidance during and after crossing the midline

In addition to mediating chemoattraction of commissural axons, the ventral midline in the spinal cord is also a rich source of chemorepellents. Semaphorin and Slit proteins are two examples of chemorepellents that are expressed by floor plate. Together, Slits and Semaphorins drive axons out of the midline after crossing, but also prevent them from re-crossing after they reach the contralateral side (Zou et al., 2000). Slits also coordinate the sorting of post-crossing commissural axons into distinct longitudinal tracts (Long et al., 2004). The actions of Semaphorins and Slits are mediated by the Class 3 Semaphorin receptor Neuropilin-2 (Npn2) and Roundabout receptors (with the exception of mammalian Robo3, see section on Robo3), respectively (Zou et al., 2000; Long et al., 2004) (Fig 1.2). As is the case with Netrins and their receptors, the midline repulsive role of Slits and their Robo receptors has been evolutionarily conserved (Dickson and Zou, 2010).

Other chemotropic functions of the midline have also been described in the mouse spinal cord. Within the floor plate, commissural axons are sensitive to midline-derived Stem Cell Factor (SCF), which through its receptor Kit promotes outgrowth and prevents axons from stalling within the floor plate (Gore et al., 2008) (Fig 1.2). There are also anterior-posterior gradients of Wnts and Shh that ensure a majority of axons turn anteriorly after midline exit (Lyuksyutova et al., 2003; Yam et al., 2012).

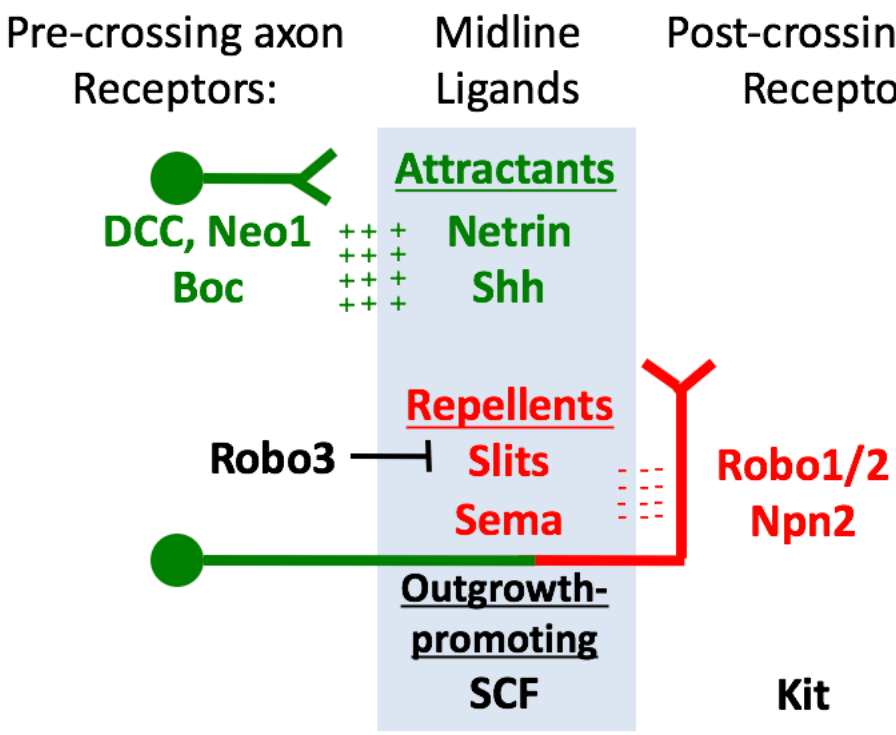

Figure 1.2 Receptor-ligand pairs in midline crossing

Precrossing axons are attracted towards the floor plate by chemoattractants (green). Attraction is mediated by the axonal receptors listed on the left. Note that Sonic hedgehog (Shh) is another chemoattractant for commissural neurons (Charron et al., 2003), and its action is mediated by the Boc receptor (Okada et al., 2006). Robo3 is a negative regulator that suppresses premature Slit signaling. After reaching the midline, axons are repelled from the floor plate by chemorepellents (red). Repulsion is mediated by the axonal receptors listed on the right (red). Kit promotes axon exit from the midline when it is bound by Stem Cell Factor (SCF).

Netrins and their molecular structures

Unc-6 was identified as a gene encoding a secreted protein that shares strong homology to laminins (Ishii et al., 1992). In parallel, two related axon outgrowth-promoting protein were purified from embryonic chick brain and found to be Unc-6 homologs. They were named Netrin-1 and Netrin-2 based on the Sanskrit word “netr” or “one who guides” (Serafini et al., 1994; Moore et al., 2007). All Netrins belong to the superfamily of laminin-related proteins (Yurchenco and Wadsworth, 2004), owing to the homology that their N-termini share with domains VI and V of laminins (Serafini et al., 1994). The N-terminus of secreted Netrins begins with a laminin domain VI followed by domain V. Domain V is made up of three cysteine-rich LN-type Epidermal growth factor (EGF)-like modules (LE1-3) (Xu et al., 2014). The protein ends with a ‘domain C’/Netrin-like domain (NTR) that is homologous to tissue inhibitor of metalloproteases and can bind to heparin (Kappler et al., 2000; Lai Wing Sun et al., 2011).

Netrin’s chemotactic and haptotactic potential

Since their purification, Netrins have been characterized as soluble outgrowth-promoting factors that are membrane-associated (Serafini et al., 1994). They were proposed to diffuse but become bound to surfaces, leaving open the question whether they mediate their effect in solution (chemotaxis) or bound to surfaces (haptotaxis) (Kennedy et al., 1994). Later, immunochemical data showed that Netrin protein is enriched in particular regions of the spinal cord, including in the vicinity of pial surfaces. These data supported the idea that Netrin-binding sites help accumulate and present Netrin to axons for haptotaxis

(Kennedy et al., 2006). A Netrin protein gradient that increases along the dorsal-to-ventral axis was identified by quantitative immunofluorescence (Kennedy et al., 2006).

Two distinct segments of commissural axon projections and their dependence on floor plate-derived chemoattractant(s)

There are two distinct segments in the trajectory that commissural axons make before reaching the midline: (1) a parallel and ventral path along the pial edge, termed “circumferential”, and subsequently, (2) a ventromedial path in which axons break away from the pial edge and begin to migrate toward the floor plate. In chick and mice, this second path lies within the environment of the motor column (Colamarino and Tessier-Lavigne, 1995). Previously, *in vivo* studies using dorsalized mutants in mouse and chick lacking floor plate revealed that axons successfully project to the midline, indicating that circumferential axon growth does not depend on long-range floor plate-derived cue(s) (Colamarino page 507). This appears to contradict the essential role for the chemotropic Netrin gradient established by the floor plate in midline attraction (Serafini et al., 1996). Bear in mind, however, that the mutants used in these early studies were dorsalized and, thus, also lacked a motor column. This apparent contradiction could be resolved by the hypothesis proposed in 1995: “Circumferential” growth along the edge of the spinal cord is not dependent on floor plate-derived chemoattractant(s) but possibly dependent on a ventricular zone-derived local cue; on the other hand, ventromedial guidance around the environment of the

motor column is dependent on floor plate-derived chemoattractant(s) (Colamarino and Tessier-Lavigne, 1995).

Floor plate and ventricular zone expression of Netrin

The floor plate and ventricular zone provide two discrete sources of Netrin in the developing embryo. In chick, *Netrin-1* is expressed in the floor plate, whereas *Netrin-2* is expressed in the ventricular zone (Kennedy et al., 1994). In mouse and rat, only *Netrin-1* is expressed and its expression pattern reflects the combined expression pattern of *Netrin-1* and *-2* in the chick. In both cases, Netrin expression is higher in the floor plate than the ventricular zone. Interestingly, Netrin-2 specific antibodies reveal that it does not diffuse far from its source and accumulates on the pial edge. Netrin-1 specific antibodies showed that Netrin-1 is found at a distance from the floor plate source. These data raised the possibility that the measured Netrin gradient may be established primarily from floor plate-derived Netrin (Kennedy et al., 2006).

However, two recent studies that used conditional mutants to investigate the roles of ventricular zone and floor plate Netrin sought to argue against a long-range action of Netrin in guidance to the midline (Dominici et al., 2017; Varadarajan et al., 2017). Their arguments against the established model are investigated in Chapter 2.

The Netrin receptors Dcc and Neo1

Three families of Netrin receptors have been described: (1) the Dcc family, (2) the Unc-5 family and (3) Down syndrome cell adhesion molecule (DSCAM).

All are single-pass type I transmembrane proteins and belong to the immunoglobulin (Ig) superfamily (Lai Wing Sun et al., 2011).

The prominent family members of the Dcc receptor family are Dcc and Neo1 in mouse (Cho et al., 1994; Vielmetter et al., 1994), Unc-40 in *C. elegans* (Chan et al., 1996) and Frazzled (Fra) (Kolodziej et al., 1996) in *D. melanogaster* (Lai Wing Sun et al., 2011). Their extracellular domain comprises four Ig domains and six fibronectin III domains (FNIII I-6). Crystal structures demonstrate that the N-terminal Laminin VI domain of Netrin binds to FNIII 4 and 5 of Dcc and Neo1 (Geisbrecht et al., 2003; Kruger et al., 2004; Xu et al., 2014).

The crystal structures of Dcc and Neo1 are interesting because when bound to Netrin, the receptors can form very different complexes: a continuous Netrin-receptor assembly or a 2:2 heterotetramer. Which complex is energetically favored depends on the length of the FNIII 4-5 linker region (Xu et al., 2014). Dcc and Neo1 both undergo alternative splicing at this region, resulting in either long or short isoforms (Shen et al., 2002). Formation of the 2:2 heterotetramer is favored and possible only with longer linkers that are present in Dcc_{long} and $Neo1_{short/long}$ but not Dcc_{short} (Xu et al., 2014).

Although Dcc and Neo1 both contribute to midline attraction (Xu et al., 2014), the relative abundance and function of the different Dcc and Neo1 isoforms remains undefined. Furthermore, it is unclear if there are additional Netrin receptors that mediate midline attraction within the spinal cord. To fully account for Netrin-dependent midline attraction, it is imperative to compare the phenotypic severity of Netrin mutants with those lacking both Dcc and Neo1.

Previous studies have relied on a *Netrin-1* hypomorph, and residual Netrin-1 activity in these hypomorphs makes it difficult to compare phenotypic severity with mutants of the cognate receptors. A comparison using a *Netrin-1* null mutant is reported in Chapter 2. Further, it is important to determine the relative expression of the different splice variants within commissural neuron populations to fully understand how these receptors function. These issues are addressed in Chapter 3.

Robo3 is a multifunctional receptor in precrossing axon guidance

The balance of chemoattraction and chemorepulsion is an important and intriguing aspect of mammalian commissural axon guidance. As discussed above, the floor plate is a source of both attractants and repellents. Therefore, precrossing axons must preferentially respond to Netrin-mediated attraction over Slit-mediated repulsion. In flies, this is mediated by *comm*, an intracellular trafficking receptor that is expressed by precrossing axons. Comm prevents Robo receptors from being trafficked to the surface of the growth cone and targets it for lysosomal degradation, thereby preventing premature Slit repulsion (Dickson, 2002; Dickson and Gilestro, 2006). However, a mammalian Comm homolog has not been reported. In mice, precrossing commissural axons express Robo3, a receptor that silences Slit/Robo signaling, thereby preventing premature Slit repulsion and allowing for axons to be attracted to the midline on their initial trajectory (Fig 1.2). Only when axons have reached the contralateral side do Robo3 levels decline and commissural axons gain Slit responsiveness. Genetic deletion of *Robo3* in mice confers premature Slit sensitivity to

precrossing commissural axons and results in the complete loss of the ventral commissure (Sabatier et al., 2004). Similarly, loss-of-function *Robo3* mutations in Horizontal Gaze Palsy with Progressive Scoliosis (HGPPS) patients result in uncrossed descending fibers (Jen et al., 2004), underscoring the evolutionarily conserved function of Robo3.

Unlike other Robo family members, the divergent mammalian Robo3 has lost its ability to bind to Slits (Zelina et al., 2014). Interestingly, Nell2 (neural epidermal growth factor-like 2) is a ligand for Robo3 that is expressed by motor neurons. The Nell2-Robo3 interaction signals repulsion and steers axons away from the motor column to the ventral midline (Jaworski et al., 2015). Robo3 also has gained the ability to potentiate Netrin-1 attraction. This potentiation is not mediated by a direct binding of Netrin-1 to Robo3. Instead, Netrin-1 phosphorylates Robo3 via Src kinases, and forms a complex with Dcc (Zelina et al., 2014).

In summary, Robo3 supports the migration of precrossing axons to the midline through several mechanisms: Robo3 silences Slit repulsion, potentiates Netrin-1 attraction and signals Nell2 repulsion. These simultaneous actions of Robo3 help to precisely guide commissural axons to the midline, and explains why *Robo3* mutants have a severe complete-failure-to-cross phenotype in mouse.

Given the central role of Robo3 in regulating midline attraction and repulsion, a Cre-driver was made to specifically label all commissural neurons. We then crossed this mouse line to a TdTomato-Cre reporter, effectively

fluorescently labeling all commissural neurons for fluorescence-activated cell sorting (FACS) and purifying this population for RNA-Seq analysis to uncover additional commissural neuron-specific factors that involved in midline guidance. This will be described in Chapter 4.

The relative contribution of each signaling pathway to axon guidance is incomplete

Despite having identified several guidance receptors and cues, it is unclear whether all commissural axons rely on all these mechanisms or if some mechanisms are redundant. For example, genetic mutants of either *Dcc* or gene-trapped *Netrin-1* do not completely block guidance to the midline (Serafini et al., 1996; Fazeli et al., 1997), suggesting that a subset of commissural axons might reach the midline through Dcc- or Netrin-independent mechanisms. Further, in *Npn2* mutant embryos (see Fig 1.2), many normal post-crossing trajectories are observed as well (Zou et al., 2000; Tran et al., 2013).

One possibility is that there are redundant mechanisms operating in all axons. Multiple attraction and repulsive cues exist, and it is possible that other receptors/ signaling pathways might compensate for the loss of one guidance receptor or cue. A complementary possibility is that discrete populations of commissural neurons utilize different guidance programs. Several observations support this idea: (1) Only a subset of spinal commissural neurons express Npn2 (Tran et al., 2013), (2) The Kit transcript is expressed in most but not all of commissural axons (Gore et al., 2008), (3) After crossing the floor plate, commissural axons sort into distinct mediolateral funiculi based on the different

Robo receptor(s) that they express (Kadison and Kaprielian, 2004; Long et al., 2004).

In the case of Netrin, two mammalian receptors Dcc and Neo1 contribute to axon guidance. However, these two Netrin receptors have spatially and temporally distinct expression patterns during development (Gad et al., 1997). How these expression profiles influence axon guidance and how these receptors collaborate during midline crossing have yet to be fully examined. The protein and transcript levels across the spinal cord will be described in Chapter 3.

Discrete interneuron populations in the spinal cord

In the embryonic mouse spinal cord, discrete neuronal populations with genetically distinct programs are defined by chemical gradients of several morphogens that are differentially expressed along the anterior-posterior and dorsoventral axes (Tanabe and Jessell, 1996; Alaynick et al., 2011). Indeed, the heterogeneity of spinal commissural neurons has been well documented across several vertebrates (Colamarino and Tessier-Lavigne, 1995). Several examples support the hypothesis that distinct spinal cord interneuron populations utilize distinct guidance mechanisms to signal Netrin-1 dependent midline attraction. In *Drosophila*, differential expression of Netrin-1 receptors within discrete motor neurons underlies their distinct axon trajectories (Labrador et al., 2005). Further, analysis of mouse cortical neurons reveals that distinct neuron populations possess unique Netrin-1 sensitivities in terms of elongation rates and receptor trafficking dynamics (Blasiak et al., 2015). In the context of mouse spinal commissural neurons, the ventral-most excitatory V3 commissural subtype is

uniquely unaffected in *Netrin-1* hypomorphs (Rabe et al., 2009). However, the possible population-specific differences in Netrin-1 dependent mechanisms mediating midline attraction remain largely unexplored. Useful genetic Cre-driver mouse lines that label distinct populations will be identified and used for population subtype analysis in Chapter 3.

Culturing spinal cord explants *in vitro*

Little is known about subpopulation specific guidance mechanisms because axons are highly fasciculated *in vivo*. Therefore, it has not been possible to discern differences in receptor expression between various neuron populations. *In vitro* systems where spinal cord explants are cultured in a collagen matrix are also not insightful, because axons remain highly fasciculated. This thesis capitalizes on a novel 2D culture system developed in our laboratory (together with Drs. Olav Olsen and Zhuhao Wu) in which axons defasciculate to achieve single growth cone resolution on an N-Cadherin coated glass surface (Fig 1.3). This 2D system allows identification of guidance receptor expression in defined subpopulations of axons immunohistochemically, and characterization of their chemoresponsiveness. This could yield new insights as to how multiple guidance receptors might rely on the same chemoattractant, Netrin-1, to achieve the identical outcomes, that is, accurate midline attraction.

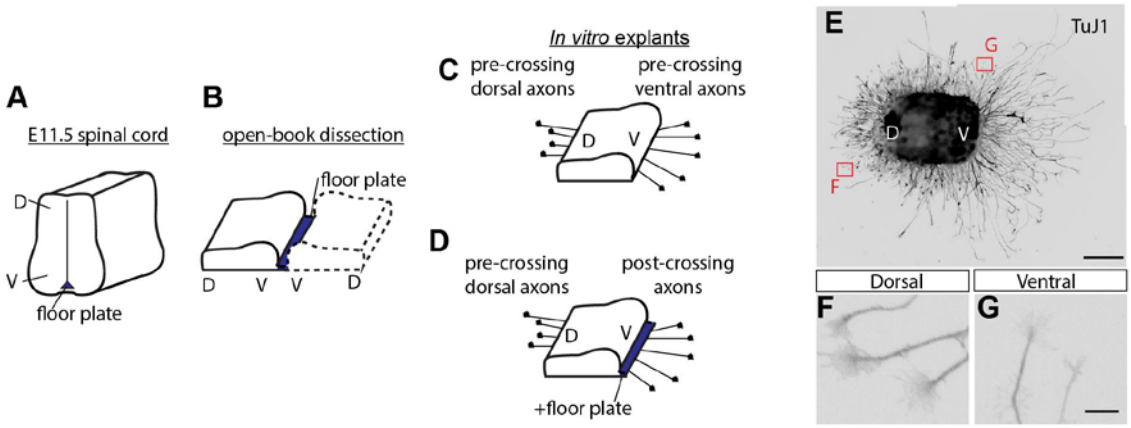

Figure 1.3 *In vitro* 2D cultures of spinal cord explants

(A) Diagram of an isolated E11.5 spinal cord, with the dorsal (D) and ventral (V) regions of the spinal cord marked. **(B)** Diagram of a spinal cord in the 'open-book' configuration, which is obtained when the meninges are removed from the spinal cord. In this configuration, the roof plate (not shown here) falls apart, leaving the spinal cord to open, and the halves of the spinal cord is held together by the floor plate. A further cut can be made at one edge of the floor plate to isolate half a spinal cord (dotted lines) (C), or half a spinal cord with the floor plate still attached (solid lines) (D). **(C-D)** When both halves are cultured on glass slides coated with N-Cadherin, different populations can be studied. In preparations without a floor plate (C), precrossing dorsal and ventral axons are observed. In preparations with a floor plate (D), post-crossing axons are observed coming out from the ventral edge. **(E-G)** An example of an E11.5 spinal cord explant without a floor plate cultured for 16 hr *in vitro* that was fixed and stained for the axonal marker TuJ1. Details of dorsal-population axons and ventral-population axons are shown in (F) and (G). Note that the axons defasciculate and individual growth cones can be observed. The scale bar in E represents 200 μm and the scale bar in G represents 15 μm.

Thesis outline

This thesis aims to define the guidance mechanisms that are common and unique to various classes of commissural neurons. We begin in Chapter 2 by addressing two papers that challenge the canonical model by clarifying the modes of Netrin-1 chemoattraction that govern midline attraction. In Chapter 3, we define the unique roles of multiple Netrin-1 receptors by considering their place and function in distinct commissural neuron subpopulations. We conclude in Chapter 4 by characterizing the transcriptome of commissural neurons and floor plate, which offers the promise of uncovering additional modulators or effectors of axon guidance.

Chapter 2. Floor plate-derived diffusible Netrin is essential for long-range attraction

Rationale

The prevailing view is that floor plate-derived diffusible Netrin-1 establishes a chemotropic gradient that contributes to attracting commissural axons to the midline (Colamarino and Tessier-Lavigne, 1995). This model is supported by the observation that ventricular zone and floor plate Netrin-1 establish gradients within the spinal cord, that are enriched in the vicinity of the pial surface (Kennedy et al., 2006). However, this model was questioned by two similar studies in mouse claiming that ventricular zone-specific, but not floor plate-specific, deletion of *Netrin-1* perturbs commissural axon extension toward and across the midline in spinal cord and hindbrain (Dominici et al., 2017; Varadarajan et al., 2017). We sought to determine whether floor plate-derived Netrin-1 plays an essential role in midline attraction, and, if so, to determine what aspects of midline attraction were perturbed. To reconcile the apparent contradictions between the new claims made by the two recent papers and the established model, we revisited these claims using quantitative methods.

Floor plate-specific *Netrin-1* deletion reduces the ventral commissure size

To explore the role of floor plate derived Netrin-1 in midline crossing, we crossed a *Netrin-1* conditional mouse line (Brunet et al., 2014; Varadarajan et al., 2017) to a mouse line in which Cre recombinase expression is driven by the endogenous *Sonic hedgehog* (*Shh*) promoter (Harfe et al., 2004). At E10.5 and

E11.5, we detected, in wild-type control embryos, *Netrin-1* transcripts in the various progenitors within the ventricular zone and floor plate of control embryos, an observation that is consistent with previous reports (Kennedy et al., 2006). Consistent with the restriction of *Shh* to the floor plate proper, in $Shh^{Cre};Netrin\text{-}1^{fl/fl}$ embryos, *Netrin-1* expression was lost specifically in the floor plate without affecting expression in the neighboring ventricular zone, and in particular, the ventral-most V3 progenitors (Fig 2.1A-B).

Next, we visualized the ventral commissure size in control and mutant embryos by staining with 2 markers: neuron-specific class III β-tubulin (TuJ1), which labels all axons, and Robo3, a commissural axon-specific marker that is highly expressed in precrossing and crossing axon segments. Strikingly, compared to controls, the ventral commissure size is consistently smaller in $Shh^{Cre};Netrin\text{-}1^{fl/fl}$ embryos at E10.5 and E11.5 (Fig 2.1C-D and 2.2A). Interestingly, similar reductions can be seen in representative images of floor plate-specific *Netrin-1* deleted embryos that are shown in both recent papers in question, but this phenotype went unreported in both manuscripts (see Extended Fig 3a and 3d in Dominici et al., 2017, and Fig 1P and 1X in Varadarajan et al., 2017).

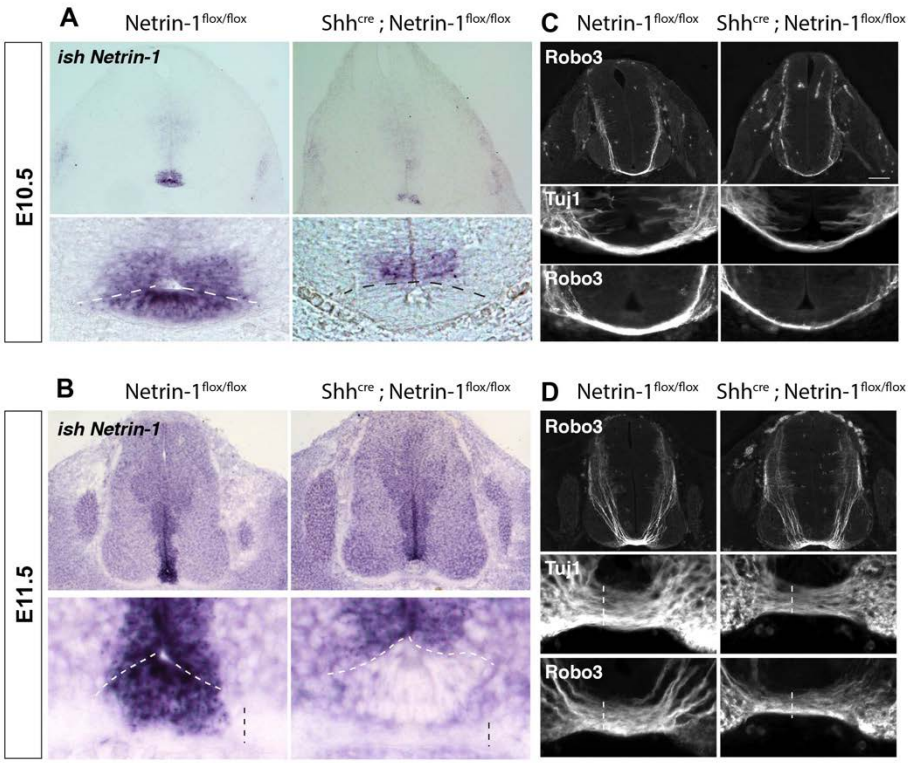

Figure 2.1. Floor plate specific Netrin-1 is deleted in *Shh^{Cre};Netrin-1$^{fl/fl}$* embryos

(A-B) *In situ* hybridization of E10.5 (A) and E11.5 (B) spinal cord sections for *Netrin-1* in *Netrin-1$^{fl/fl}$* controls (left) and *Shh^{Cre};Netrin-1$^{fl/fl}$* mutants (right). In controls, expression was detected within the various progenitors of the ventricular zone and the floor plate, whereas within the *Shh^{Cre};Netrin-1$^{fl/fl}$* embryos, no transcripts were detected.

(C-D) E10.5 (C) and E11.5 (D) spinal cord sections were stained for Robo3 and TuJ1 as labeled in *Netrin-1$^{fl/fl}$* controls (left) and *Shh^{Cre};Netrin-1$^{fl/fl}$* mutants (right). Compared to controls, the ventral commissure size is smaller in *Shh^{Cre};Netrin-1$^{fl/fl}$* embryos at both developmental stages. The dotted lines in (D) demarcate the width of the ventral commissure. The scale bar in (C) represents 100 μm and applies to the full-sized panels of the spinal cord in both (C) and (D).

(Figure prepared with Dr. Nicolas Renier)

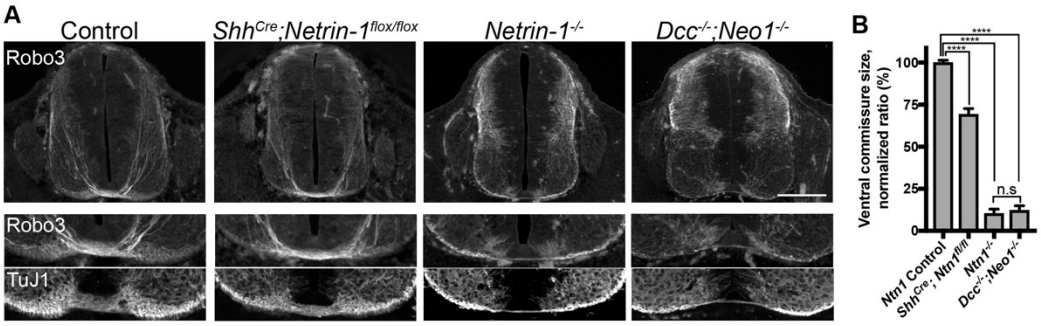

Figure 2.2. Floor plate-derived Netrin-1 controls axon guidance

(A) Cross sections of E11.5 *Netrin-1* controls, *Shh^{Cre}; Netrin-1$^{floxf/lox}$* (both from the same litter), *Netrin-1$^{-/-}$* and *Dcc$^{-/-}$; Neo1$^{-/-}$* mouse embryos at the brachial spinal level, stained for Robo3 (top). The details of the ventral commissure from the same embryo are shown in the next two rows, stained for Robo3 (middle) and neuron-specific class III β-tubulin (TuJ1) (bottom). Compared to controls, floor-plate specific Netrin-1 deletion mutants (*Shh^{Cre}; Netrin-1$^{flox/flox}$*) have a smaller ventral commissure, as is the case with *Netrin-1* knockouts (*Netrin-1$^{-/-}$*). Mutants in which two Netrin-1 receptors are deleted (*Dcc$^{-/-}$; Neo1$^{-/-}$*) have a similar ventral commissure size as *Netrin-1$^{-/-}$* mutants. Scale bar represents 200 μm (top) and 100 μm (bottom two rows).

(B) Ratio of the commissural axon bundle size to the dorsoventral spinal cord length of E11.5 embryos, normalized to controls. For each genotype, the mean ratio ± SEM of at least three embryos are plotted. For each embryo, the mean ratio from at least 5 sections were taken. Compared to *Netrin-1* controls (*n*=3), *Shh^{Cre}; Netrin-1$^{flox/flox}$* mutants (*n*=3) have a 30.8 ± 3.8 % significantly thinner ventral commissure (one-way ANOVA with Bonferroni post-test for all comparisons in this section, P<0.0001, ****), *Netrin-1$^{-/-}$* mutants (*n*=4) have a 89.8 ± 2.0 % significantly thinner ventral commissure (****) and *Dcc$^{-/-}$; Neo1$^{-/-}$* mutants (*n*=4) have a 87.9 ± 2.1 % significantly thinner ventral commissure (****). No significant difference in ventral commissure size was observed between *Netrin-1$^{-/-}$* mutants and *Dcc$^{-/-}$; Neo1$^{-/-}$* mutants (P>0.99).

By quantifying the thickness of the ventral commissure, we found that the total ventral commissure size was significantly reduced by 30.8 ± 3.8 % in *Shh^{Cre};Netrin-1$^{fl/fl}$* embryos compared to controls (Fig 2.2B, one-way ANOVA with Bonferroni post-test for this test and subsequent comparisons in this section, P<0.0001). We also confirmed a significant ventral commissure size reduction in *Netrin-1$^{-/-}$* embryos (Fig 2.2B, P<0.0001), as has been described (Bin et al., 2015; Yung et al., 2015). To test whether Dcc and Neo1 receptors accounted for all Netrin-1 mediated attraction, we examined the size of the ventral commissure in *Dcc$^{-/-}$;Neo1$^{-/-}$* embryos. Defects in commissure size matched those of *Netrin$^{-/-}$* embryos (Fig 2.2B, P>0.99), suggesting that Netrin-1 mediated guidance of commissural axons is fully attributable to signaling through Dcc and Neo1 receptors. The loss of thickness in the ventral commissure in floor plate-specific *Netrin-1* deletion mutants suggest that a significant number of axons fail to make it to the ventral midline. These data demonstrate an important role for floor plate-derived Netrin-1 in spinal commissural midline guidance and argue against the recent assertions (Dominici et al., 2017; Varadarajan et al., 2017) that floor plate-derived Netrin-1 is dispensable for guidance.

Loss of floor plate Netrin-1 disrupts commissural axon guidance near the motor column

A longstanding model in the field posits that a diffusible chemotropic factor attracts axons at a distance, and is essential for directing growth through the motor column (Colamarino and Tessier-Lavigne, 1995). We have already shown that Netrin expression by floor plate cells is necessary for the proper formation of

the ventral commissure in spinal cord (Fig 2.1-2.2). However, to provide further evidence that Netrin-1 can act at a distance, we also examined whether floor plate derived Netrin affects directional commissural axon growth as the axons navigate toward the midline. To this end, we used antibodies against the homeobox transcription factor HB9, which specifically labels motor neurons (Thaler et al., 1999), to define the ventral motor column, and we examined the trajectory of commissural axons in the E11.5 ventral spinal cord. In control embryos, the major commissural axon bundles pass adjacent to, and for the most part avoid entering the motor column, with the exception of a few commissural axon misprojections (Fig 2.3A, C, E). However, in *Shh^{Cre};Netrin-1$^{fl/fl}$* embryos the main commissural bundles were displaced laterally, where they project through the ventral motor column. Further, we observed an 89.1 $\pm$ 22.9% increase (Fig 2.3G, unpaired *t*-test, P=0.027) in the number of commissural axons misprojecting within the motor column, as assessed by quantification of Robo3 immunofluorescence in that region (Fig 2.3B, D, F). We also examined the organization of pre- and post-crossing axons near the ventral edge of the spinal cord. Precrossing and crossing axons express higher levels of Robo3.1 (collectively termed Robo3^{high}) than the L1-expressing postcrossing axons in the ventral funiculus (Chen et al., 2008). In control embryos, Robo3^{high} axons largely avoid L1-expressing postcrossing axons in the ventral funiculus, occupying only 165 $\pm$ 10.3 μm of the ventral edge of the spinal cord (Fig 2.3A, E and H). However, in *Shh^{Cre};Netrin-1$^{fl/fl}$* embryos, these Robo3^{high} axons occupy a greater length within the ventral edge (231 $\pm$ 4.7 μm, unpaired *t*-test, P=0.0041, Fig 2.3B,

F and H), indicating a loss of segregation of pre- and post-crossing axons. These data support the model that floor-plate derived Netrin-1 acts at a distance (~150-250 μm) to prevent precrossing commissural axons from entering both the motor column and the ventral funiculus (Fig 2.3I).

Figure 2.3. Axon guidance around the motor column is disrupted in *Shh^{Cre};Netrin-1$^{fl/fl}$* embryos

(A-F) Cross sections showing the ventral half of spinal cords of E11.5 *Netrin-1* controls (A, C and E) and *Shh^{Cre}; Netrin-1$^{floxf/lox}$* littermates (B, D and F), stained for Robo3 (green), Hb9 (red), and L1 (blue). Inverted grayscale images of Hb9 alone (C and D) or Robo3 alone (E and F). The motor column was traced manually using Hb9 immunostaining (C-F, red dashed outlines). The expected normal location of the main commissure bundle as axons project toward the midline was defined as the region between the Hb9^{+} region and the more medial neuroepithelial neurons that are Hb9^{+} (green arrows). The total length occupied by precrossing and crossing commissural axons (Robo3^{high}) in the ventral commissure and funiculus combined was measured by using Robo3 as a marker (blue arrows). (E), in *Netrin-1* controls, few axons are found in the motor column. (F), in *Shh^{Cre}; Netrin-1$^{floxf/lox}$* embryos, several commissural axons invade the motor column (red arrows), and the main commissural bundle is displaced laterally, with part of this bundle invading the motor column (red arrowhead). Robo3^{high} axons also occupy a greater length of the ventral funiculus (blue arrows). Scale bar in (B) represents 100 μm and applies to all panels. **(G)** Robo3 immunofluorescence intensity per unit area within the motor column, normalized to controls. The mean normalized intensity ± SEM of 3 embryos of each genotype are plotted. For each embryo, the mean Robo3 intensity from at least 7 sections were taken. Compared to *Netrin-1* controls (*n*=3), *Shh^{Cre}; Netrin-1$^{flox/flox}$* mutants (*n*=3) have 89.1 ± 22.9 % more commissural axons invading the motor column (Unpaired *t*-test, P=0.027). **(H)** Length of Robo3^{high} axons occupying the left and right ventral funiculi and ventral commissure in controls and mutants. The mean length ± SEM of 3 embryos of each genotype are plotted. For each embryo, the mean straight-line length of high Robo3 expression from at least 7 sections were measured. Compared to *Netrin-1* controls (*n*=3), *Shh^{Cre}; Netrin-1$^{flox/flox}$* mutants (*n*=3) have precrossing axons that occupy 67.0 ± 11.3 μm more of the left and right ventral funiculi (unpaired *t*-test, P=0.004). **(I)** Model of the role of floor-plate derived Netrin-1. Top left, in wild-type ventral spinal cord, floor-plate (blue) derived Netrin-1 acts at a distance, and attracts commissural axons medially towards the ventral midline, preventing them from projecting into the motor column (MC). The commissural axon trajectory is typically “V-shaped” (green). Top right and bottom, in *Shh^{Cre}; Netrin-1$^{flox/flox}$* mutants, the loss of floor-plate Netrin-1 attraction results in (1) a laterally displaced main commissural axon bundle, resulting in a characteristic “U-shape” (red), (2) increased aberrant misprojections into the MC, (3) more precrossing axons occupy the ventral funiculus, and (4) fewer commissural axons successfully reach the midline, resulting in a significantly smaller ventral commissure. An overlay of the wild-type trajectory (green) is shown for comparison.

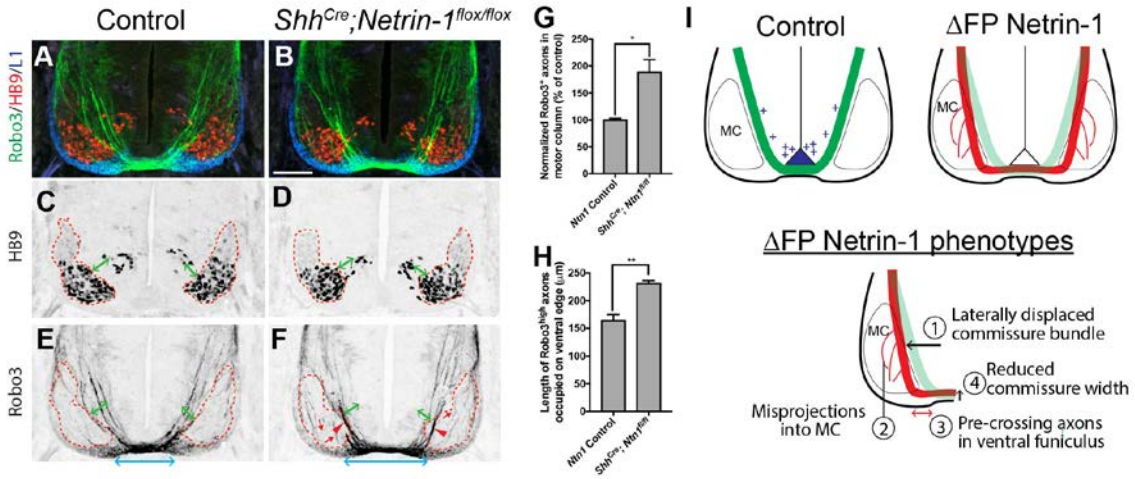
Control
Shh^Cre;Netrin-1^flox/flox
Robo3/HB9/L1
H B9
Robo3
A
B
C
D
E
F
G
Normalized Robo3+ axons in motor column (% of control)
Ntn1 Control
Shh^Cre; Ntn1^flox
H
Length of Robo3^high axons occupied on ventral edge (μm)
I
Control
ΔFP Netrin-1
MC
ΔFP Netrin-1 phenotypes
Laterally displaced commissure bundle
Reduced commissure width
Misprojections into MC
Pre-crossing axons in ventral funiculus

Netrin-1 does not direct commissural axons around the ventricular zone

Within the dorsal region of the spinal cord, Varadarajan et al., 2017 showed that neurofilament $(NF)^+$ spinal axons "robustly extend into the ventricular zone" in *Netrin-1* mutants (see Fig 1I and 1U). However, previous studies would suggest that these axons are likely to originate from sensory neurons rather than spinal neurons. Netrin-1 binds to Unc5c expressed on dorsal root ganglion (DRG) sensory axons to mediate repulsion, which is important for regulating the entry of primary afferents into the spinal cord (Watanabe et al., 2006). To better characterize the identity of the axons misprojecting toward the ventricular zone in *Netrin-1* mutants, we stained *Netrin-1*$^{-/-}$ embryos using an antibody for Transmembrane Axonal Glycoprotein-1 (TAG-1) (Xu et al., 2014) that is stronger than the one used by Varadarajan et al., 2017. TAG-1 stains axons less broadly than NF, thereby allowing us to trace them to their origin. Contrary to what was reported by Varadarajan et al., 2017, we found these dorsal projections in the ventricular zone of *Netrin-1*$^{-/-}$ spinal cords were in fact TAG-1^+ and that these axons originate from the dorsal root entry zone (Fig 2.4A-B). Our data are consistent with a previous report that also observed premature entry of sensory axons into spinal cord via the dorsal root entry zone, a site where Netrin-1 is normally enriched (Watanabe et al., 2006). Further, the projection of dorsal spinal axons appear normal in *Netrin-1* mutants, as was observed in *Atoh1/Math::taugfp* embryos (reported by Varadarajan et al., 2017 but as data not shown), and dorsal commissural axons neither express nor require any Unc5 receptor family member for proper guidance (see Varadarajan et al., 2017 Fig S2G-M).

Therefore, Netrin-1 is required to keep sensory, not spinal, axons from invading the ventricular zone.

The reduction of the ventral commissure size is a measure that faithfully reflects the loss of Netrin-1 attraction for commissural formation (Serafini et al., 1996), which we have shown previously in Fig 2.1 and 2.2. Consistent with Netrin-1 mediating midline attraction (Serafini et al., 1996), we observed commissural axons wandering randomly (both laterally and ventrally) in the ventral spinal cord of *Netrin-1*$^{-/-}$ mutants (Fig 2.4A-B). In *Netrin-1* mutants, Varadarajan et al., 2017 describe a previously unreported phenotype, observing an increase in the number of NF^{+} commissural axons invading the ventricular zone. However, NF staining is not specific to commissural axons and the axons being analyzed in their study would also include Unc5 expressing motor axons that are usually repelled by Netrin-1. Thus, this measurement is not specific to commissural axons, and it is therefore difficult to stand by their conclusion that there is an increase in the number of commissural axons invading the ventricular zone in *Netrin-1* mutants (see Varadarajan et al., 2017 Fig S2G-M). In our own studies, we do not observe a significant difference in the number of Tag1^{+} axons in ventral spinal cord between the *Netrin-1* mutants and control (Fig 2.4A-B). Taken together, there is no evidence to suggest that ventricular zone-derived Netrin-1 prevents commissural axons from growing into the ventricular zone.

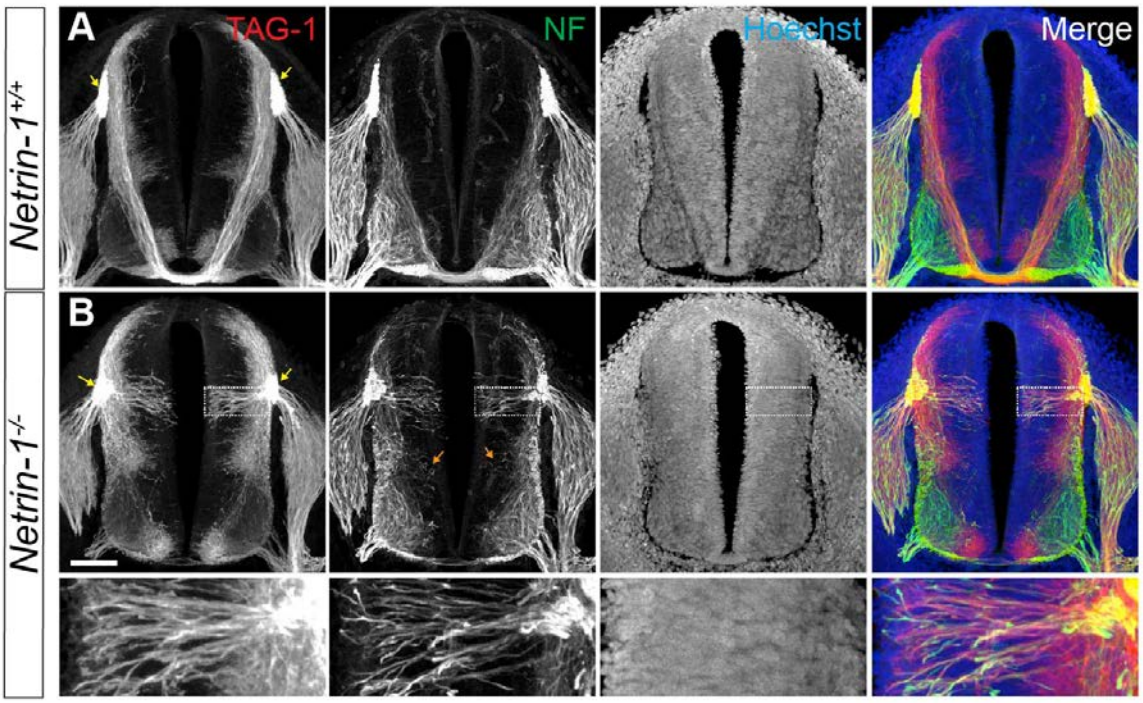

Figure 2.4. Misprojecting axons in the ventricular zone of *Netrin-1*$^{-/-}$ mutants are not commissural

E11.5 *Netrin-1*$^{+/+}$ (A) and *Netrin-1*$^{-/-}$ (B) spinal cord sections were stained for TAG-1 (red) and Neurofilament (NF, green). Sections were also stained for DNA (blue) to label cell bodies. In *Netrin-1*$^{+/+}$ wild-types, the dorsal root ganglion (DRG) axons project to the dorsal root entry zone (DREZ, yellow arrows), but in *Netrin-1*$^{-/-}$, the axons extended beyond the DREZ and invaded the dorsal spinal cord. NF^{+} axons were also seen invading the ventral region of the ventricular zone of *Netrin-1*$^{-/-}$ embryos (orange arrows) that were not observed in *Netrin-1*$^{+/+}$ embryos. In (A) and (B), this dorsal region of interest (dotted rectangle) is magnified and shown in the bottom row. The scale bar represents 100 μm for the top and middle row of panels, and 25 μm for the bottom panels.

Netrin-1 can travel from its site of production in the developing spinal cord

Varadarajan et al., 2017 and Dominici et al., 2017 also dispute that Netrin-1 diffuses, long-range, from its site of production in the floor plate. Our data shows that commissural axons improperly invade the motor column in mice lacking Netrin expression in the floor plate, already providing evidence to the contrary. However, to more directly address this point we also compared the distribution of Netrin-1 protein in the presence or absence of floor plate-derived Netrin-1 using floor plate-specific *Netrin-1* deleted embryos. We found that in *Shh^{Cre};Netrin-1$^{fl/fl}$* embryos, the ventral commissure retained Netrin-1 immunoreactivity (Fig 2.5D-D'). This result is consistent with the Netrin-1 immunoreactivity within the ventral commissure that is also seen in representative images of floor plate-specific *Netrin-1* deleted embryos in both publications (Fig 1L-M and 1L'-M' in Varadarajan et al., 2017, and Extended Data Fig 2g in Dominici et al., 2017). However, this phenotype went unreported in both papers. Because Netrin-1 is still detectable within the ventral commissure when Netrin-1 expression within the floor plate tissue is abrogated, Netrin-1 must be redistributed from the ventricular zone to the ventral commissure. This redistribution could be mediated by passive diffusion through the neuropil and/or active transport on the membranes of commissural axons. Further, we also found that the Netrin-1 immunoreactivity on precrossing axons was weaker in floor plate-specific *Netrin-1* mutants than in controls (Fig 2.5C-D). Thus, distribution of Netrin-1 within the ventral spinal cord is dependent on floor plate-derived Netrin-1, supporting the notion that floor plate-derived Netrin-1 is redistributed to other

regions of the spinal cord. Our data support the model that Netrin-1 is not spatially restricted to its site of production and can be redistributed.

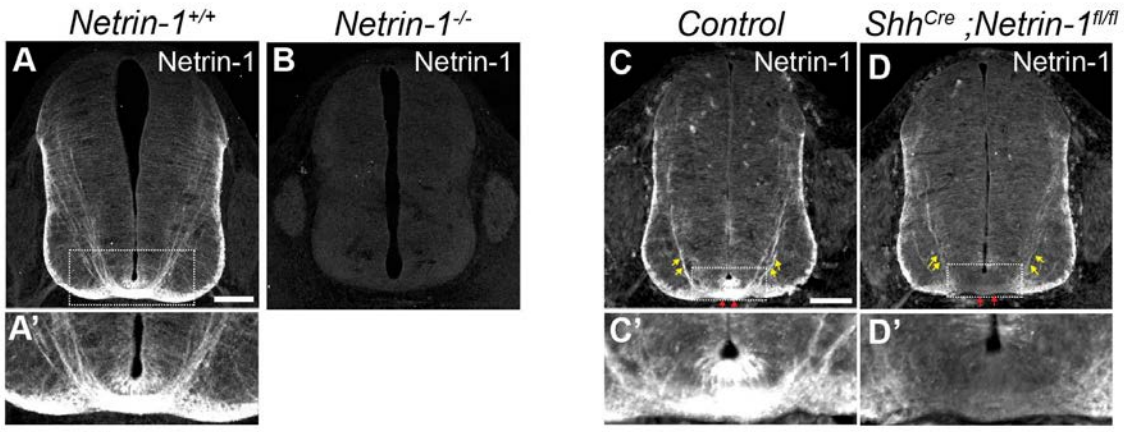

Figure 2.5. Netrin-1 immunoreactivity in the ventral commissure and precrossing axons

(A-B) E11.5 spinal cord sections of *Netrin-1*$^{+/+}$ (A) and *Netrin-1*$^{-/-}$ (B) embryos stained for Netrin-1. In *Netrin-1*$^{+/+}$, Netrin-1 immunoreactivity was detected on the pial surface, commissural axons, ventral commissures and floor plate (A). The ventral region of interest (white outline) in (A) is magnified and shown in panel A'. Labeling in all the above-mentioned structures were abolished in *Netrin-1*$^{-/-}$ (B), demonstrating Netrin-1 staining specificity. The scale bar in (A) represents 100 μm for panels (A) and (B), and 50 μm for panel (A'). **(C-D)** E11.5 spinal cord sections of control (C) and *Shh*^{Cre}*;Netrin-1*$^{-/-}$ mutant (D) embryos stained for Netrin-1. The ventral region of interest (white outline) in (C) and (D) is magnified and shown in panel (C') and (D') respectively. When compared to controls, residual Netrin-1 immunoreactivity was still detected in the ventral commissure (red arrows) of mutant embryos. Netrin-1 immunoreactivity of precrossing axons around the motor column (yellow arrows) was weaker in mutants (D) than controls (C). The scale bar in (C) represents 100 μm for panels (C) and (D), and 50 μm for panels (C') and (D').

Conclusions

Here we demonstrate that restricted elimination of Netrin-1 expression in floor plate cells causes significant guidance defects and reduces the number of commissural axons that successfully cross the floor plate. The reduced thickness in the ventral commissure in floor plate-specific *Netrin-1* deletion mutants suggests that a significant number of axons fail to make it to the ventral midline. This loss may, in part, be explained by defects in commissural axon guidance around the motor column and/or the ventral funiculus, whereby commissural axons inappropriately invade both structures. Given that axons near the motor column are still at a considerable distance away from the floor plate, floor plate-derived Netrin-1 must be acting as a long-range cue. In support of this idea, we detect Netrin-1 immunoreactivity within the ventral commissure even when Netrin-1 is no longer expressed in the floor plate cells that lie adjacent to it, and that floor plate-derived Netrin-1 contributes to precrossing axonal Netrin-1 immunoreactivity. Taken together, we show that the floor plate plays crucial guidance roles for commissural neurons as they navigate the ventral spinal cord, supporting the canonical model of Netrin-1 in midline guidance.

Chapter 3. Spinal commissural populations differentially express the Netrin receptors Dcc and Neogenin

Rationale

During development, commissural axons are guided to the midline by Netrin-1, a chemoattractant that is secreted by floor plate cells. Genetic deletion of the Netrin-1 receptor, Dcc, abrogates Netrin-1 mediated attraction of commissural axons and severely, but incompletely, disrupts formation of the ventral commissure. Neo1 also binds Netrin-1 and has recently been proposed to mediate the residual commissural axon crossing in Dcc knockouts (Xu et al., 2014). However, the relative contribution of Dcc and Neo1 to Netrin-1 signaling within distinct spinal cord interneuron populations remains unknown. Here, we compared two distinct commissural populations to determine whether they differentially rely on these Netrin receptors for midline guidance.

Dorsal and ventral populations require Netrin-1 for proper guidance

To determine Netrin-1 dependence of commissural neurons in midline crossing, we gathered an allelic series of mouse *Netrin-1* mutations: (1) *Netrin-1*$^{-}$, a *Netrin-1* null allele derived from a floxed *Netrin-1* exon 4 that has undergone Cre-loxP recombination (Brunet et al., 2014), (2) *Netrin-1*^{gt}, a gene-trapped hypomorph allele which expresses Netrin-1 at significantly lower levels than wild-types (Serafini et al., 1996), and (3), the *Netrin-1*$^{+}$ wild-type allele (Fig 3.1A). In *Netrin-1*$^{-/-}$ embryos, a ventral commissure was still detected, although it was only 10.9 $\pm$ 1.4 % of wild-types (Fig 3.1A), consistent with reports with other

homozygous *Netrin-1* null alleles (Bin et al., 2015; Yung et al., 2015) (Also see Fig 2.2). As expected, the phenotype was less severe in *Netrin-1*$^{gt/gt}$ hypomorph embryos (28.6 $\pm$ 4.8 % of wild-types, unpaired *t*-test, P=0.012, Fig 3.1A-B).

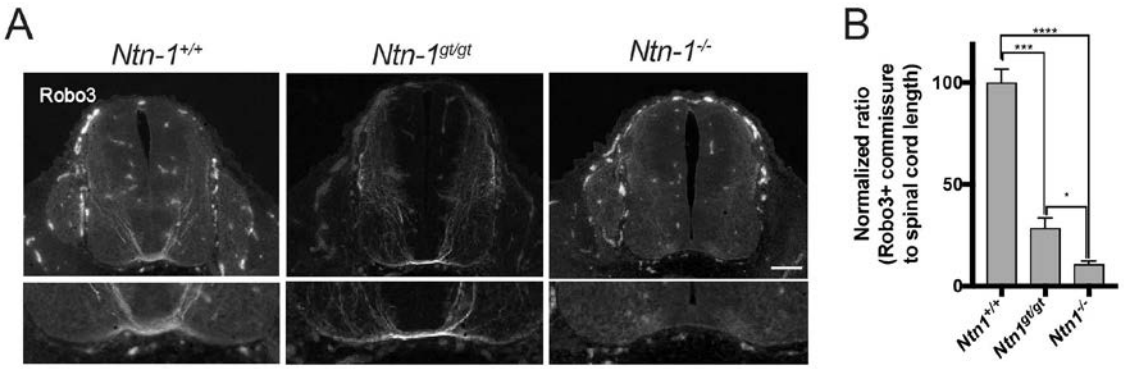

Figure 3.1. An allelic series of *Netrin-1* mutations

(A) Cross sections E11.5 of spinal cords from *Netrin-1* wild-type controls (left), genetrap hypomorphs (middle), and null mutants (right), stained for Robo3. Details of the ventral commissure of respective genotypes is shown in the bottom row. The scale bar represents 100 μm for top panels and 50 μm for bottom panels. **(B)** Ratio of the commissural axon bundle size to the dorsoventral spinal cord length of E11.5 embryos, normalized to wild-types. For each genotype, the mean ratio ± SEM of at least three embryos are plotted. For each embryo, the mean ratio from at least 5 sections were taken. Compared to *Netrin-1*$^{+/+}$ (*n*=4), *Netrin-1*$^{gt/gt}$ mutants (*n*=4) have a 71.4 ± 6.8 % significantly thinner ventral commissure (unpaired *t*-test, P=0.001, ***) and *Netrin-1*$^{-/-}$ mutants (*n*=4) have a 89.1 ± 6.8 % significantly thinner ventral commissure (unpaired *t*-test, P<.0001, ****). Compared to *Netrin-1*$^{gt/gt}$ mutants, *Netrin-1*$^{-/-}$ mutants (*n*=4) have a 17.8 ± 6.8 % thinner ventral commissure, (unpaired *t*-test, P=0.012, *).

After screening multiple transgenic Cre-driver mouse lines using a floxed-stop TdTomato-reporter allele (*Rosa26*^{Ai14}) (Madisen et al., 2010) (Fig 3.2), we identified *Math1:Cre* (Matei et al., 2005) and *Neurog3:Cre* (Schonhoff et al., 2004) as lines that were suitable for labeling distinct dorsal dI1 and ventral V0/V3 populations, respectively (Fig 3.3A). These populations are known to consist in part of commissural neurons (Sommer et al., 1996; Bermingham et al., 2001; Alaynick et al., 2011), and when each of these Cre-lines were crossed to the TdTomato-reporter line, the ventral commissure was fluorescently labeled (Fig 3.3B-C). We did not observe midline crossing of axons from either population in *Netrin-1*$^{-/-}$ Cre-expressing embryos that harbor the TdTomato Cre-reporter allele (Fig 3.3F'-G'). In the dorsal population, a significant number of axons stalled in the dorsal half of the spinal cord (Fig 3.3F, arrowhead). Axons also misprojected laterally into the ventral horn (Fig 3.3F, arrows). Our data show that the proper projection of axons from both the dorsal and ventral populations is wholly dependent on Netrin-1, as we predicted.

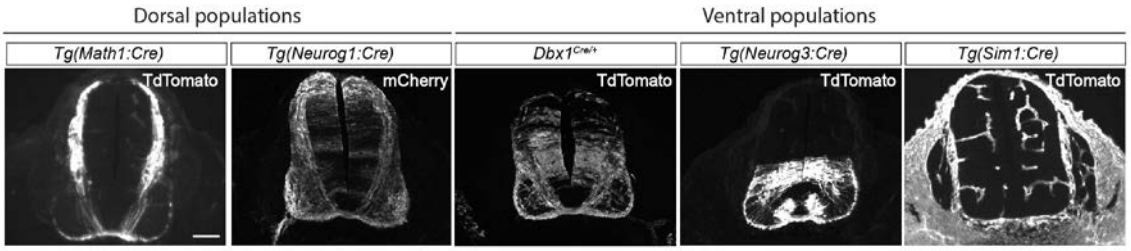

Figure 3.2. A genetic screen identified 2 suitable mouse lines for commissural neuron subtype specific analysis.

Transverse sections of E11.5 transgenic mouse embryos. *Tg(Math1:Cre), Tg(Neurog3:Cre), Dbx1*$^{Cre/+}$ and *Tg(Sim1:Cre)* mice were crossed to floxed-stop TdTomato mice (*Rosa26*$^{Ai14/Ai14}$), and stained for TdTomato. *Tg(Neurog1:mCherry)* mice were crossed to wild-types, and stained for mCherry. In *Tg(Math1:Cre)* embryos, the dorsal most progenitors are labeled, and the cell bodies are seen migrating ventrally. A significant number of these neurons send axons towards the midline. In the *Tg(Neurog1:mCherry)* and *Dbx1*$^{Cre/+}$ lines, a non-specific, broad domain of dorsal and ventral populations were labeled, showing that these alleles did not mirror expression of *Neurogenin1* and *Dbx1*, so these lines were not used. In *the Tg(Neurog3:Cre)* line, only the population from the ventral half of the spinal cord were labeled. An additional ventral-most population was labeled in *Tg(Neurog3:Cre)*. In *Tg(Sim1:Cre)*, within the spinal cord, only endothelial blood vessels were labeled instead of neurons, showing that this allele does not faithfully mirror the expression of *Sim1*, so it was not used. The scale bar represents 100 μm.

Figure 3.3. Dorsal and ventral populations require Netrin-1 for proper guidance

(A) Schematic summarizing the distinct dorsoventral populations. The populations labeled by the 2 transgenic Cre-driver lines used in this study are shown. **(B-C)** Spinal cord sections of E11.5 *Tg(Math1:Cre);Rosa26$^{Ai14/+}$;Netrin-1* wild-type (B) or *Tg(Neurog3:Cre);Rosa26$^{Ai14/+}$;Netrin-1* wild-type (C) embryos stained for TdTomato to reveal dorsal dI1 or ventral (V0 and V3) population-specific cell bodies and projections respectively. The detail of the ventral commissure is shown in B' and C'. **(D-E)** is the same as B and C, except that these are *Netrin-1$^{gt/gt}$* hypomorphs. The loss of population-specific projections was less severe than in null mutant embryos (F-G). **(F-G)** similar to (B-C), except that these are *Netrin-1$^{-/-}$* mutants. No axons from either population made it to the ventral commissure. The axons of the dorsal population remain more dorsal compared to wild-types (red arrowhead), and those axons that do project ventrally no longer avoid the ventral horn (red arrow). The scale bar is 100 μm for B-G and 50 μm for B'-G'. **(H-I)** Same embryos as in panels (B) and (D), except that a Robo3 stain is shown (green) as well. Detail of the motor column is shown in H' and I'. In wild-types, the main Robo3^{+} axon forms a well-defined bundle (arrows) (H'), and few axons were within the motor column, but in *Netrin-1$^{gt/gt}$* embryos, no clear bundle was observed, and several aberrant Robo3^{+} projections were observed in the motor column (I'). **(J)** Mean number of Robo3^{+} axons invading the motor column per 20 μm section. For each embryo, the number of axons were measured from at least 5 evenly-spaced sections, and the mean was calculated. Compared to wild-types (*n*=3), 6.8 ± 0.8 more Robo3^{+} axons were found invading the motor column in *Netrin-1$^{-/-}$* mutants (unpaired *t*-test, P=0.001, **). **(K)** Length of precrossing and crossing axons occupying the ventral funiculus and ventral commissure in controls and mutants. For each embryo, the straight-line length of high Robo3 expression were measured from at least 5 evenly-spaced sections, and the mean was calculated. Compared to *Netrin-1* controls (*n*=4), *Netrin-1$^{-/-}$* mutants (*n*=4) have precrossing axons that occupy 68.9 ± 16.5 μm more of the left and right ventral funiculi (unpaired t-test, P=0.006, **). For bar graphs (J and L), the mean ± SEM of at least three embryos of each genotype are plotted. The scale bar in (G) represents 100 μm for panels (B-G, H-I) and 50 μm for panels (B'-G', H'-I').

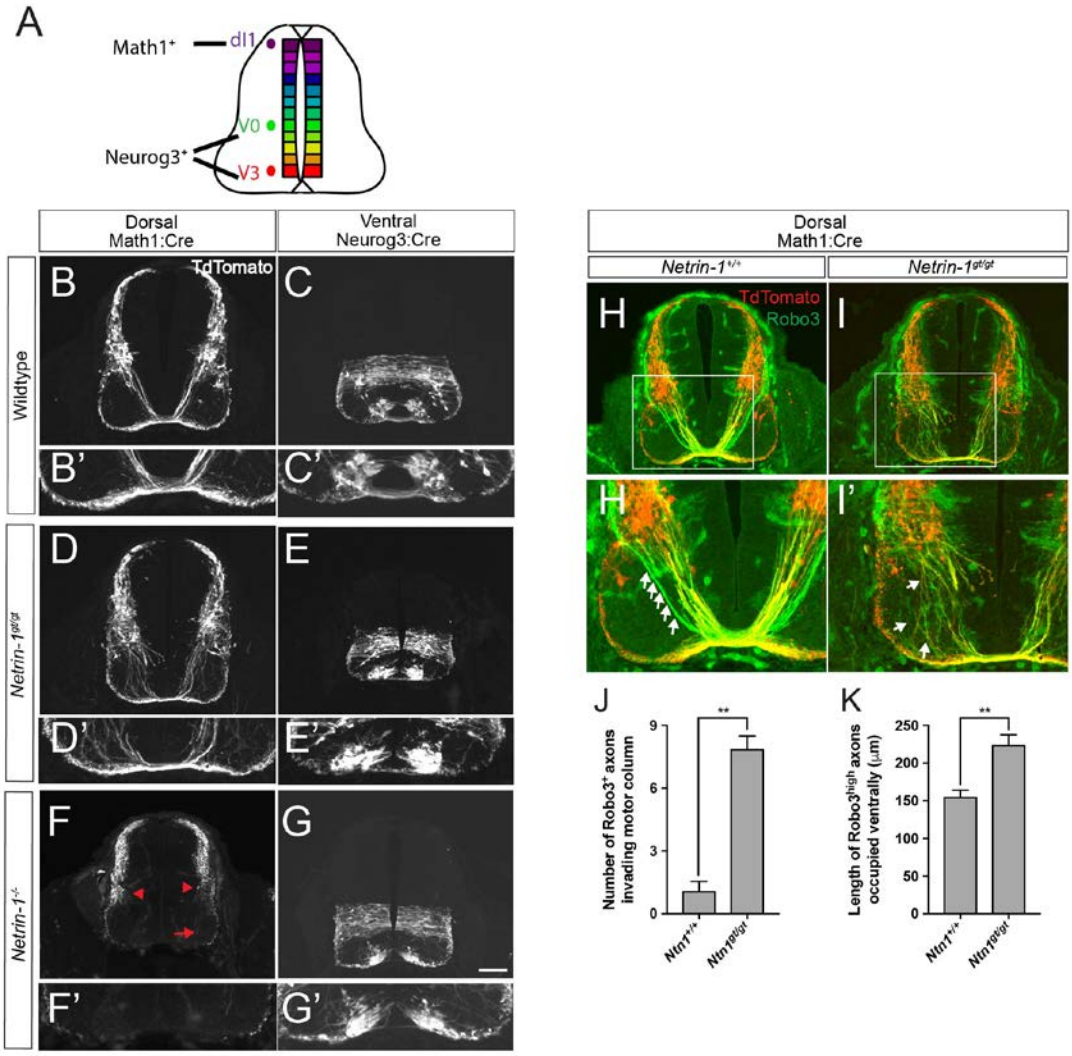
A
Math1+
dI1
V0
Neurog3+
V3
Dorsal
Math1:Cre
Ventral
Neurog3:Cre
Wildtype
TdTomato
B
C
B'
C'
Netrin-1gt/gt
D
E
D'
E'
Netrin-1-/-
F
G
F'
G'
Dorsal
Math1:Cre
Netrin-1+/+
Netrin-1gt/gt
TdTomato
Robo3
H
I
H'
I'
J
Number of Robo3+ axons invading motor column
9
6
3
0
**
Ntn1+/+
Ntn1gt/gt
K
Length of Robo3high axons occupied ventrally (μm)
250
200
150
100
50
0
**
Ntn1+/+
Ntn1gt/gt

To determine whether the dorsal and ventral commissural populations are sensitive to disruptions in the Netrin-1 gradient, we examined the trajectories of the dorsal and ventral axons in *Netrin-1*$^{gt/gt}$ hypomorphic Cre-expressing embryos that harbor the TdTomato Cre-reporter allele. The TdTomato^{+} axons from the dorsal population were disorganized as they failed to form a thick main commissural bundle, and several of these axons misprojected through the ventral motor column (Fig 3.3D and I). The overlapping cell bodies and axons of the ventral population precluded our ability to study the trajectories of commissural axons before they reached the midline. Using a Robo3 antibody to label all commissural neurons in the *Netrin-1* hypomorph, we observed a greater number of Robo3^{+} axons misprojecting in the motor column (unpaired *t*-test, P=0.001). We also observed that precrossing axons inappropriately occupied a greater length of the ventral funiculus (unpaired *t*-test, P=0.006) (Fig 3.3H-K). These results suggest that both the dorsal and ventral commissural populations are sensitive to disruptions in Netrin-1 expression, and the misguidance phenotypes in *Netrin-1*$^{gt/gt}$ mutants are similar to those in floor plate-specific *Netrin-1* mutants (Fig 2.3).

Dorsal, but not ventral commissural neurons, require Dcc for midline crossing *in vivo*

We considered whether expression of the different Netrin-1 receptors might differ in the dorsal and ventral populations. Only a small ventral commissure exists in *Netrin-1*$^{-/-}$ embryos (Figure 2.2). We found that the ventral commissure is similarly compromised in *Neo1*$^{-/-}$*;Dcc*$^{-/-}$ double knockout embryos

(Fig 2.2). Additionally, both the *Neo1*$^{-/-}$;*Dcc*$^{-/-}$ double knockout and *Netrin-1*$^{-/-}$ have fewer axons projecting into the ventral half of the spinal cord when compared to wild-type controls, and the few that are present misproject into the motor column (Fig 2.2). The fact that *Netrin-1*$^{-/-}$ embryos quantitatively phenocopy *Neo1*$^{-/-}$;*Dcc*$^{-/-}$ embryos indicate that Dcc and Neo1 account for the majority, if not all, of Netrin-1-dependent signaling in commissural neurons.

To examine Dcc and Neo1 expression, we performed immunohistochemistry on E11.5 spinal cords and found that Dcc is expressed along the entire trajectory of commissural axons, with the highest Dcc expression in the dorsal regions of the spinal cord (Fig 3.4A). However, no corresponding region of high expression is observed with Neo1 (Fig 3.4B). Instead, Neo1 protein expression is highest in the ventral population of *Neo1*$^{gt/gt}$ hypomorphs in which a significant amount of secretory gene-trapped protein is expected to accumulate in the endoplamic reticulum (Fig 3.4E), suggesting that Neo1 expression is enriched in ventral region of the spinal cord. This supports the hypothesis that Netrin-1 receptors may be differentially expressed across different commissural neuron populations.

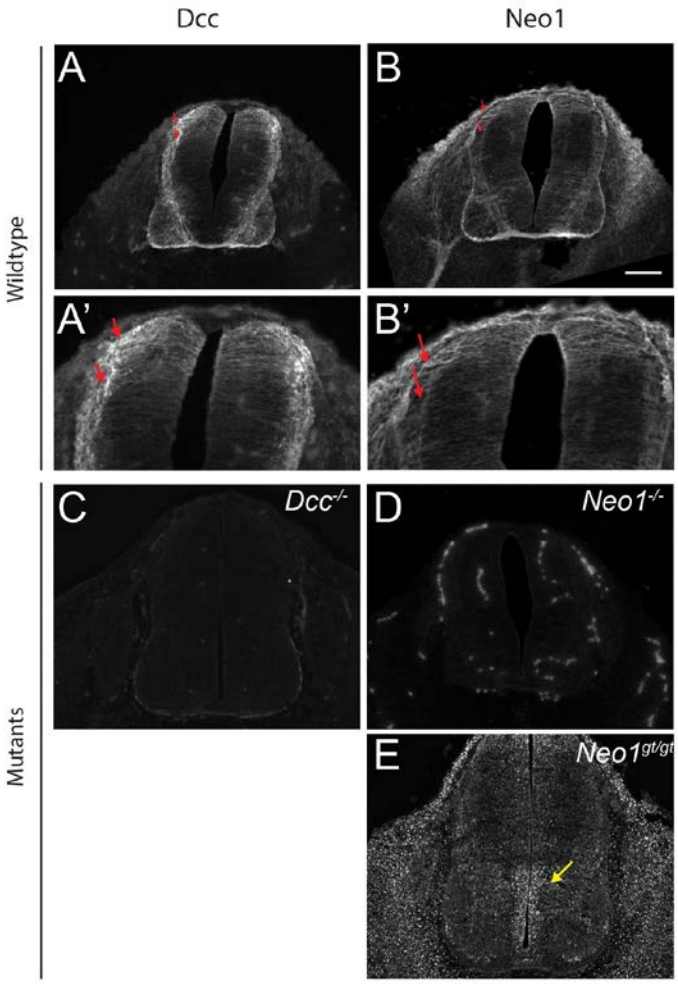

Figure 3.4. Differential Dcc and Neo1 expression *in vivo*

E11.5 spinal cord sections stained for Dcc (A, A' and C) or Neo1 (B, B', D and E), with A' and B' showing details of the dorsal spinal cord. The red arrows show regions that are enriched in Dcc. However, this region is not enriched for Neo1. The specificity of the antibody stain is shown in panels C and D. In (E), a *Neo1* gene-trap hypomorph is shown, and punctate Neo1 staining is observed because of the mutant protein is expected to be trapped in the endoplasmic reticulum. The yellow arrow shows the region of high Neo1 expression. The scale bar in (B) represents 100 μm.

Dcc mediates the midline attraction of commissural axons in response to Netrin-1 expression (Keino-Masu et al., 1996). Genetic deletion of *Dcc* results in fewer commissural axons reaching the midline and a thinner commissure (Fazeli et al., 1997) (Fig 3.5A-D). To determine if loss of Dcc more severely affects the guidance of dorsal or ventral commissural neurons, we examined the trajectory of axons from dorsal and ventral populations in *Dcc*$^{-/-}$ mutants using our genetically labeled mouse lines. Only a small number of axons from Math1 neurons were found in the ventral commissure in E12.5 *Dcc*$^{-/-}$ spinal cords (Fig 3.5F- H). In contrast, the number of axons from the ventral population that crossed the midline in the *Dcc*$^{-/-}$ were largely similar to the number of axons in the wild-type at E12.5 (Fig 3.5I- L). These results indicate that axons from the dorsal population, but not the ventral population, require Dcc for midline attraction. Further, the reduced commissure size in the *Dcc*$^{-/-}$ mutants largely reflects the loss of axons from the ventral neuron population.

Having characterized *Dcc* knockout mice, we next wanted to determine the phenotype of *Neo1*$^{-/-}$ embryos. Deletion of *Neo1* alone did not significantly affect the ventral commissure (Fig 3.6A-C, n=3, unpaired t-test, P=0.42). The finding that guidance of both dorsal and ventral populations was largely unaffected in *Neo1*$^{-/-}$ mutants (Fig 3.6D-G), suggests that Dcc can compensate for the loss of Neo1.

Figure 3.5. The phenotypic severity of *Dcc*$^{-/-}$ differs between dorsal and ventral populations

(A-D) Spinal cord sections of *Dcc*$^{+/+}$ (A and C) and *Dcc*$^{-/-}$ (B and D) at 2 developmental stages, E11.5 (A and B) and E12.5 (C and D), stained for Robo3. At each developmental stage, the ventral commissure in *Dcc*$^{-/-}$ was smaller than that of *Dcc*$^{+/+}$. However, in *Dcc*$^{-/-}$, there was a partial recovery of ventral commissure size from E11.5 to E12.5. The scale bar is 100 μm. **(E-L)** Spinal cord sections showing either the dorsal Math1:Cre population (E-H) or the ventral Neurog3:Cre population (I-L). Two developmental stages are shown here: E11.5 (E, F, I and J) and E12.5 (G, H, K and L). The detail of the ventral commissure is shown in E' - L'. At E12.5, unlike the dorsal population, in which only a few projections were found within the ventral commissure, several projections from the ventral population were observed. The scale bar in (L) represents 100 μm for full spinal cord sections (E-L), and 50 μm for panels showing only the ventral commissure (E'-L').

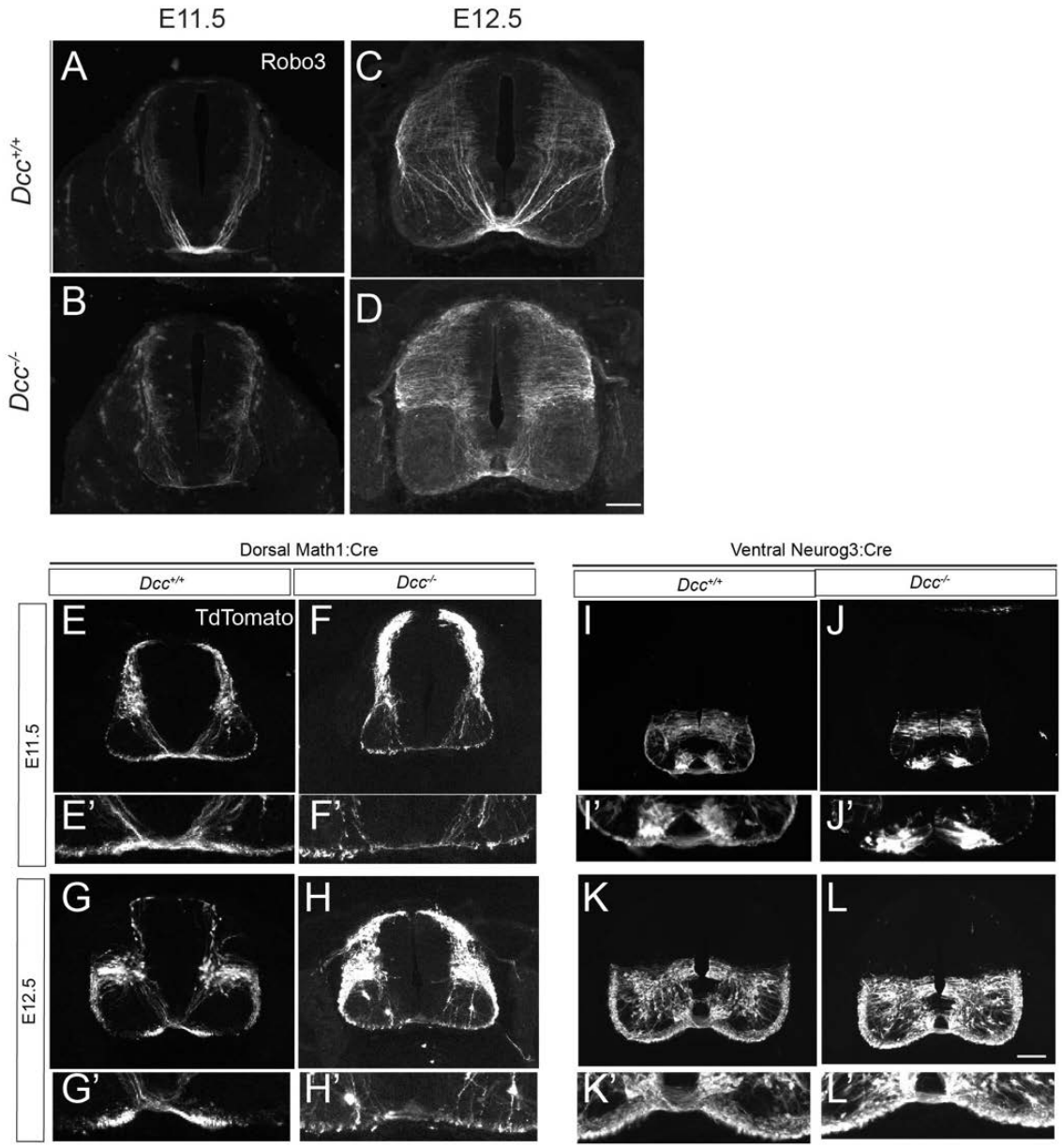
E11.5
E12.5
A
Robo3
C
Dcc+/+
B
D
Dcc-/-
Dorsal Math1:Cre
Ventral Neurog3:Cre
Dcc+/+
Dcc-/-
Dcc+/+
Dcc-/-
E
TdTomato
F
I
J
E11.5
E'
F'
I'
J'
G
H
K
L
E12.5
G'
H'
K'
L'

Figure 3.6 Midline guidance is grossly normal in *Neo1*$^{-/-}$ mutants

(A-B) Cross sections of E11.5 spinal cord sections of *Neo1*$^{+/+}$ (A) and *Neo1*$^{-/-}$ at the brachial spinal level, stained for TuJ1. The details of the ventral commissure from the same embryo are shown in the bottom row. Compared to *Neo1*$^{+/+}$, the size of the ventral commissure is similar in *Neo1*$^{-/-}$ mutants. Scale bar represents 100 μm (top) and 50 μm (bottom). **(C)** Ratio of the commissural axon bundle size to the dorsoventral spinal cord length of E11.5 embryos, normalized to controls. The mean ratio ± SEM of *n*=3 embryos are plotted. No significant difference in ventral commissure size was observed between *Neo1*$^{+/+}$ controls and *Neo1*$^{-/-}$ mutants (Unpaired *t*-test, P=0.42). **(D-G)** Similar to (A-B), except that sections were stained for TdTomato to label the dorsal population using *Tg(Math1:Cre);Rosa26*$^{Ai14;+}$ embryos (D-E), or the ventral population using *Tg(Neurog3:Cre);Rosa26*$^{Ai14;+}$ embryos (F-G). The trajectories of either population were similar in *Neo1*$^{+/+}$ and *Neo1*$^{-/-}$ embryos (E,G). The scale bar in (B) represents 100 μm, and applies to panels (D-G).

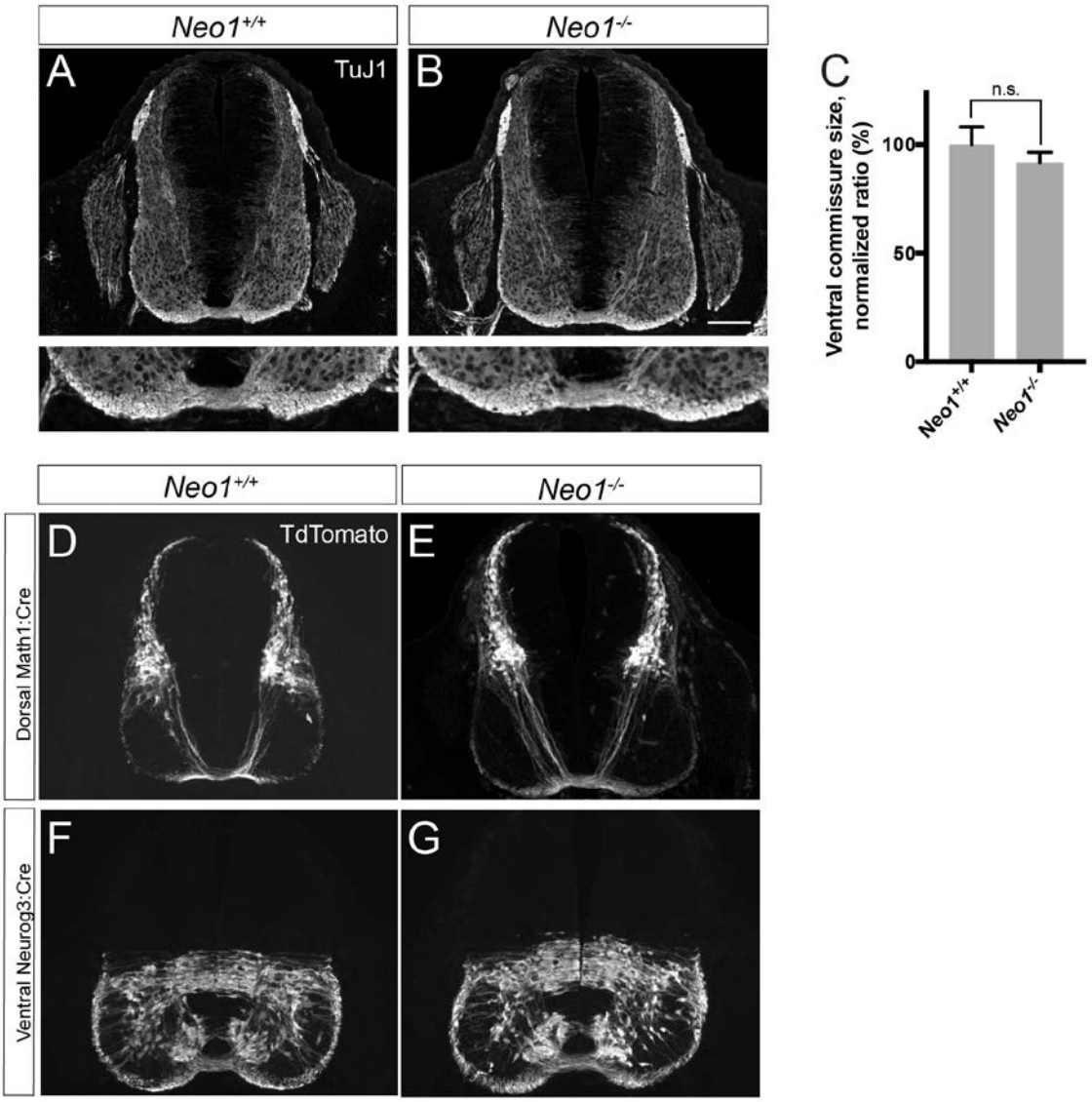
Neo1+/+
Neo1-/-
A
TuJ1
B
C
n.s.
Ventral commissure size, normalized ratio (%)
100
50
0
Neo1+/+
Neo1-/-
Neo1+/+
Neo1-/-
D
TdTomato
E
Dorsal Math1:Cre
F
G
Ventral Neurog3:Cre

Differential expression of Neo1 and Dcc across neuron populations along the dorsoventral gradient

To better characterize the molecular basis for differences in Netrin-1 receptor dependence between commissural neuron populations, we utilized a novel *in vitro* 2D culture system of spinal cord explants to examine Netrin-1 receptor expression and Netrin-1 sensitivity of discrete commissural neuron populations. In these cultures, E11.5 spinal explants are grown on glass slides coated with N-cadherin, which promotes axonal growth and defasciculation, ultimately achieving single growth cone resolution (Fig 3.7A). Consistent with our *in vivo* findings, Dcc receptor expression was higher in the growth cones of axons derived from the dorsal region (Fig 3.7B). In contrast, Neo1 expression was higher in the growth cones of axons derived from the ventral region (Fig 3.7C). Using spinal cord explants from the genetically labeled lines, we confirmed that both Dcc and Neo1 are expressed in both the dorsal *Math1* and the ventral *Neurog3* populations (Fig 3.7D-O). However, the relative expression of Dcc is greater in the dorsal *Math1* population (Fig 3.7 J-O), whereas Neo1 expression is higher in the ventral *Neurog3* population (Fig 3.7 D-I). These differences were significant: Dcc expression was 74.7 $\pm$ 12.6 % greater in dorsal growth cones compared to ventral growth cones (Fig 3.8A, B and G, dorsal n=4, ventral n=4, unpaired t-test, P=0.0011), and Neo1 expression was 59.1 $\pm$ 8.5 % greater in ventral growth cones compared to dorsal growth cones (Fig 3.8H, I and N, dorsal n=4, ventral n=4, unpaired t-test, P=0.0004). Taken together, the differential

expression patterns of Dcc and Neo observed *in vitro* are consistent with that observed *in vivo* along the dorsoventral axis (Fig 3.4A).

Figure 3.7 Differential Dcc and Neo1 expression of different neuronal populations *in vitro*

(A) Schematic of how E11.5 spinal cord explants were prepared. Left, an isolated spinal cord. Middle, a spinal cord dissected in an open-book configuration. One half of the spinal cord (dotted lines) is isolated from the floor plate tissue. Right, the isolated explant is cultured on glass slides *in vitro*. During this time, axons will be seen extending out of the explant on the slide, and each axon is led by a growth cone. D, dorsal; V, ventral. **(B)** E11.5 spinal cord explants were cultured for 16 hr, then fixed and stained for Dcc (green) and TuJ (red). Top row shows the entire explant, and the scale bar is 200 μm. Middle and bottom row shows a region of interest from the dorsal and ventral region respectively. The scale bar for these region of interests is 20 μm. Dorsal growth cones expressed higher levels of Dcc than ventral growth cones. **(C)** Same as (B), with the exception that explants were now stained for Neo1 instead of Dcc. Ventral growth cones expressed higher levels of Neo1 than dorsal growth cones. **(D-I)** Spinal cords from E11.5 *Tg(Math1:Cre);Rosa26*$^{Ai14/+}$ (D-F and J-L) or *Tg(Neurog3:Cre);Rosa26*$^{Ai14/+}$ (G-I and M-O) embryos were dissected, cultured, fixed and stained for TdTomato (red) and either Neo1 (D-I, green) or Dcc (J-O, green). TdTomato-labeled dorsal growth cones were found to express higher levels of Dcc (K) compared to the ventral population (L), and lower levels of Neo1 (E) compared to the ventral population (F). In contrast, TdTomato-labeled ventral growth cones were found to express higher levels of Neo1 (I) compared to the dorsal population (H), and lower levels of Dcc (O) compared to dorsal growth cones (N). Scale bar in M represents 200 μm for whole explants (D,G,J,M) and the scale bar in O represents 10 μm, and applies to all other panels.

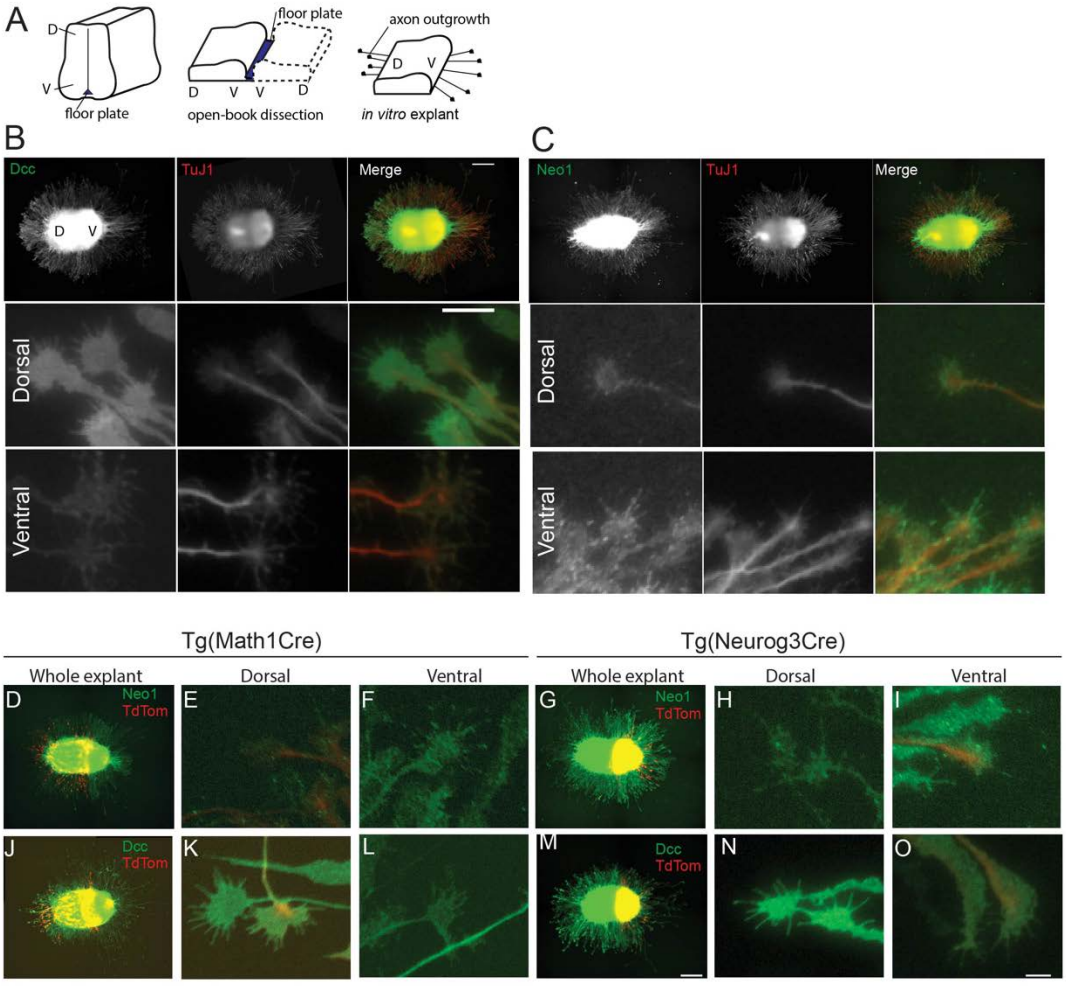
A
D
V
floor plate
floor plate
D V V D
open-book dissection
axon outgrowth
D V
in vitro explant
B
Dcc
TuJ1
Merge
D V
Dorsal
Ventral
C
Neo1
TuJ1
Merge
Dorsal
Ventral
Tg(Math1Cre)
Tg(Neurog3Cre)
Whole explant
Dorsal
Ventral
Whole explant
Dorsal
Ventral
D
Neo1
TdTom
E
F
G
Neo1
TdTom
H
I
J
Dcc
TdTom
K
L
M
Dcc
TdTom
N
O

In vitro Netrin receptor dynamics are similar in both dorsal and ventral populations

Because Dcc and Neo1 are differentially expressed in the various commissural neuron populations, we were curious whether ligand-mediated regulation of these receptors explain the differential effects in dorsal and ventral neuron populations from *Dcc*$^{-/-}$ embryos. Reduced Netrin-1 levels (e.g. in *Netrin-1*$^{gt/gt}$ embryos) correlate with an increase in the protein levels of both Dcc and Neo1 *in vivo* (Bin et al., 2015). When Dcc receptors bind Netrin-1, they are proteolytically down-regulated (Kim et al., 2005). Increased Dcc receptor expression in *Netrin-1* hypomorphs likely reflects a lack of proteolytic down-regulation of Dcc receptors. It remains unknown whether Netrin-1 similarly induces down-regulation of Neo1. Using 2D cultures of spinal cord explants, we examined the effect of recombinant Netrin-1 on Dcc and Neo1 protein expression in growth cones. We confirmed that addition of Netrin-1 causes a dose-dependent downregulation of Dcc receptors in both populations (Fig 3.8A-G). Similarly, Neo1 expression is reduced in response to increasing concentrations of Netrin-1 in both populations (Fig 3.8H-N). We also considered the possibility that downregulation of Dcc and Neo1 occurs over a different dynamic range of Netrin-1 concentrations, which could explain the apparent differences in Netrin receptor dependence between the dorsal and ventral commissural neuron populations. However, we found that in both populations, Dcc and Neo1 are downregulated over a similar range of Netrin-1 concentrations (Fig 3.8O-P). In summary, the dynamics of Dcc and Neo1 Netrin-1 induced downregulation are

similar in both dorsal and ventral populations, and this alone cannot account for their apparent different Netrin-1 receptor dependency.

Figure 3.8 *In vitro* Netrin-1 sensitivities of both dorsal and ventral populations are similar

(A-F) E11.5 spinal cord explants were cultured for 16 hr with a range of differing Netrin-1 concentrations, then fixed and stained for Dcc (green) and TuJ1 (red). Panels show representative growth cones in the absence of Netrin-1 (A and B), 50 ng mL^{-1} (C and D) or 1000 ng mL^{-1} (E and F) Netrin-1. Growth cones from axons extending from the dorsal (A, C and E) or ventral (B, D and F) explants are shown. As the *in vitro* Netrin-1 concentration increased, the levels of Dcc receptor decreased. The scale bar in F represents 10 μm, and applies equally to all panels. **(G)** The Dcc immunofluorescence intensity per unit area was quantified. For each embryo, at least 15 randomly selected growth cones from axons extending from the dorsal (black bars) or ventral (white bars) edge were measured, and the mean was calculated. Plotted are the mean ± SEM of *n*=4 embryos. These values were normalized to the average intensity of dorsal-derived growth cones cultured in the absence of Netrin-1. **(H-M)** Similar to (A-F), with the exception that cultures were stained for Neo1 instead of Dcc. **(N)** Similar to (G), with the exception that Neo1 immunofluorescence intensity was quantified here instead of Dcc. These values were normalized to the average intensity of ventral-derived growth cones cultured in the absence of Netrin-1. **(O-P)** The mean intensity of Dcc (O) or Neo1 (P) in at least five $TdTomato^{+}$ growth cones from *Tg(Math1:Cre);Rosa26*$^{Ai14/+}$ (*n*=4, white circles) or *Tg(Neurog3:Cre);Rosa26*$^{Ai14/+}$ (*n*=3, black circles) were measured. Plotted are the mean ± SEM of each embryo. As *in vitro* Netrin-1 concentrations increased, the levels of Dcc and Neo1 levels within the growth cones of both Math1 and Neurog3 populations decreased. **(Q)** A Neo1 stain was done for both *Neo1*$^{+/+}$ (left) or *Neo1*$^{-/-}$ growth cones (right). The loss of signal in *Neo1*$^{-/-}$ growth cones demonstrated the specificity of the antibody used in these conditions.

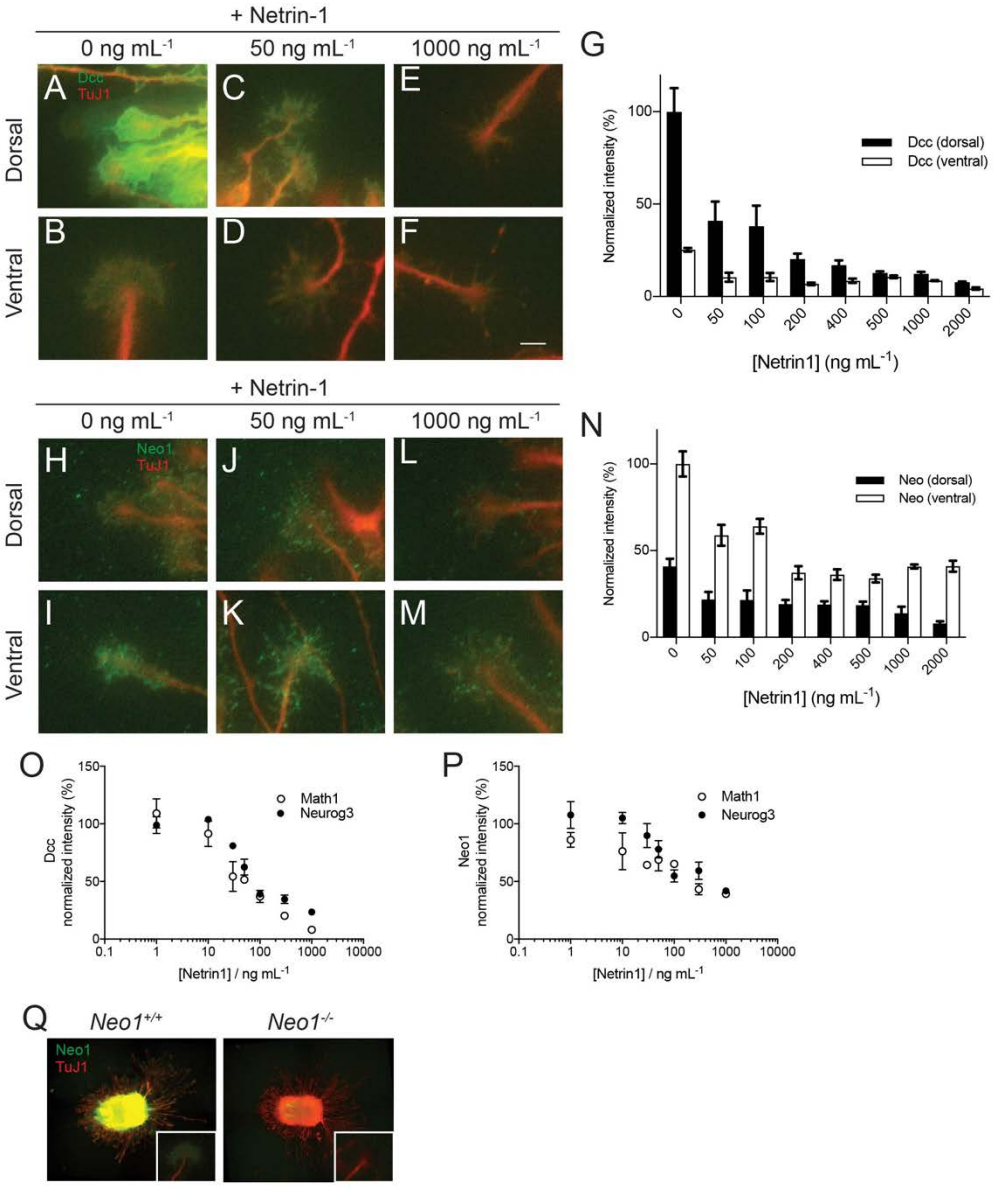
+ Netrin-1
0 ng mL-1
50 ng mL-1
1000 ng mL-1
Dorsal
Ventral
A
Dcc
TuJ1
B
C
D
E
F
G
Normalized intensity (%)
Dcc (dorsal)
Dcc (ventral)
[Netrin1] (ng mL-1)
+ Netrin-1
H
Neo1
TuJ1
I
J
K
L
M
N
Neo (dorsal)
Neo (ventral)
O
Dcc normalized intensity (%)
Math1
Neurog3
[Netrin1] / ng mL-1
P
Neo1 normalized intensity (%)
Q
Neo1+/+
Neo1-/-

Dcc and *Neo1* splice isoforms differ across both populations

Although Netrin-1 appears to bind to both Dcc and Neo1 with a similar affinity, the specific receptor isoform that Netrin-1 binds will determine the type of complex that is formed: a receptor-Netrin-1 continuous monomeric assembly or a 2:2 heterotetramer (Xu et al., 2014). To characterize which splice variants of Dcc and Neo1 are expressed by dorsal and ventral commissural neuron populations, we performed reverse transcription semi-quantitative PCR on purified dorsal and ventral commissural neuron populations (Fig 3.9).

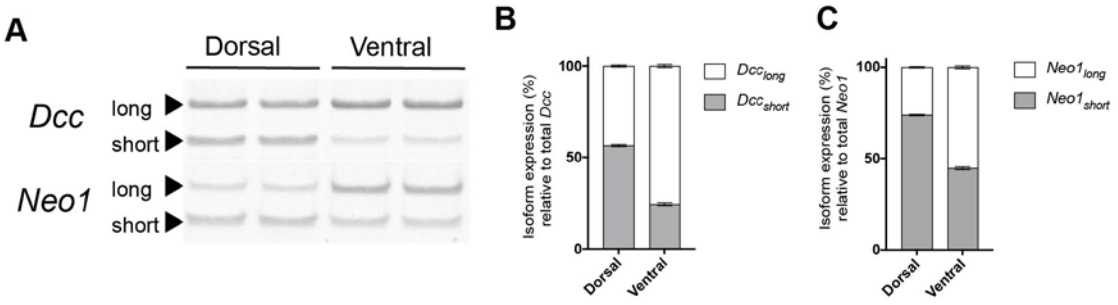

Figure 3.9 Differential expression of long and short isoforms of *Dcc* and *Neo1* in dorsal and ventral spinal cord

(A) Various *Dcc* and *Neo1* isoforms from dorsal or ventral spinal cord, separated on a PAGE gel after reverse-transcription semi quantitative PCR. Total RNA was extracted from microdissected dorsal and ventral spinal cords, reverse-transcribed and run with *Dcc* and *Neo1*-specific primers around the alternatively spliced loci. Two representative reactions from different embryos are shown here. **(B-C)** Band intensities from (A) were normalized to amplicon size and quantified for *Dcc* (B) and *Neo1* (C). Three embryos were used. Data are represented as the mean ± SEM.

Both the long and short isoform transcripts for Dcc and Neo1 were detected in dorsal and ventral spinal cord, but the relative proportion of each differed among the two populations (Fig 3.9A). Similar to what has been reported (Leggere et al., 2016), the Dcc_{short} transcript slightly predominated in dorsal commissural neuron populations, accounting for 56.5 ± 0.6 % of all *Dcc* transcripts. In contrast, Dcc_{long} transcripts accounted for the majority (75.7 ± 0.8 %) of all *Dcc* transcripts in the ventral spinal cord (Fig 3.9B). The relative amount of Dcc_{short} transcript differed significantly between dorsal and ventral populations (unpaired *t*-test, *n*=3, P<0.0001). For *Neogenin*, $Neo1_{short}$ transcripts accounted for the majority (73.8 ± 0.4 %) of *Neo1* transcripts in the dorsal spinal cord, while $Neo1_{long}$ transcripts slightly predominated and accounted for 55.5 ± 0.8 % of all *Neo1* transcripts in the ventral spinal cord (Fig 3.9C). The proportion of $Neo1_{short}$ differed significantly between dorsal and ventral populations (unpaired *t*-test, *n*=3, P<0.0001). To summarize, $Dcc/Neo1_{short}$ isoforms predominate in the dorsal spinal cord and $Dcc/Neo1_{long}$ isoforms predominate in the ventral spinal cord.

RGMb, a ligand of Neo1, is enriched in commissural neurons

To gain further insights into commissural axon guidance, we generated a novel *Robo3*$^{Cre/+}$ mouse line. Robo3 is exclusively expressed in commissural neurons in the developing spinal cord, thus this mouse can be crossed with Cre-dependent fluorescent reporter lines to selectively label and isolate commissural neurons. To obtain pure preparations of commissural neurons, spinal cords from E11.5 *Robo3*$^{Cre/+}$*;Rosa26*$^{Ai14/+}$ embryos were dissociated and then TdTomato^{+} neurons were sorted from TdTomato^{-} cells using fluorescence-activated cell sorting (FACS) (A detailed analysis of these candidates will be examined later in the next Chapter). RNA from both cell types was isolated and sequenced using RNA-Seq. The polyadenylated transcriptome of Robo3-expressing TdTomato^{+} neurons was compared against TdTomato^{-} cells. This unbiased next-generation sequencing approach yielded several candidates transcripts that were expressed at significantly higher levels in commissural neurons compared to other cell types. Repulsive guidance molecule b (*Rgmb*), was one of 8 candidates (see Chapter 4) that was found to be both enriched and highly expressed in commissural neurons (Fig 3.10A). RGMb was interesting to us because it belongs to the RGM family of proteins that are ligands for Neo1 (Bell et al., 2013). The commissural-specific expression pattern of *Rgmb* was confirmed by *in situ* hybridization (Fig 3.10B).

Figure 3.10 Identification and characterization of Rgmb expression in commissural neurons

(A) Expression plot of genes significantly enriched in Robo3-expressing neurons compared to other cells as determined by RNA-Seq. Spinal cords from E11.5 *Robo3*$^{Cre/+}$*;Rosa26*$^{Ai14/+}$ embryos (*n*=3) were dissected, dissociated and FACS sorted to separate TdTomato^{+} neurons from TdTomato^{-} cells. The transcriptome of these two cell types were then sequenced by RNA-Seq. Gene expression level in TdTomato^{+} neurons (measured in fragments per kb gene per million reads, or fpkm) of statistically significant genes was plotted against their fold enrichment relative to TdTomato^{-} cells. Any gene that was annotated in the Uniprot database to be transmembrane were color coded red. *Robo3* and *Rgmb* were the top transmembrane-encoding genes that were outliers. **(B)** Fluorescent *in situ* hybridization of *Rgmb* (green) of E11.5 *Robo3*$^{Cre/+}$*;Rosa26*$^{Ai14/+}$ spinal cord sections, co-stained with TdTomato (red) confirmed *Rgmb* expression in commissural neurons. The scale bar represents 100 μm. **(C)** Immunofluorescent stain of RGMb protein (green) and TuJ1 (red) on E11.5 wild-type sections revealed localization of protein in precrossing commissural axons (arrow). The scale bar is 20 μm, and applies to panel B as well. **(D)** Top, E11.5 wild-type spinal cord explants were cultured in 2D for 16 hr, then fixed and stained for RGMb (green) and TuJ1 (red). D, dorsal, V, ventral. Scale bar is 200 μm. Bottom, regions of interest showing growth cones from dorsal axons expressing higher levels of RGMb compared to ventral axons.

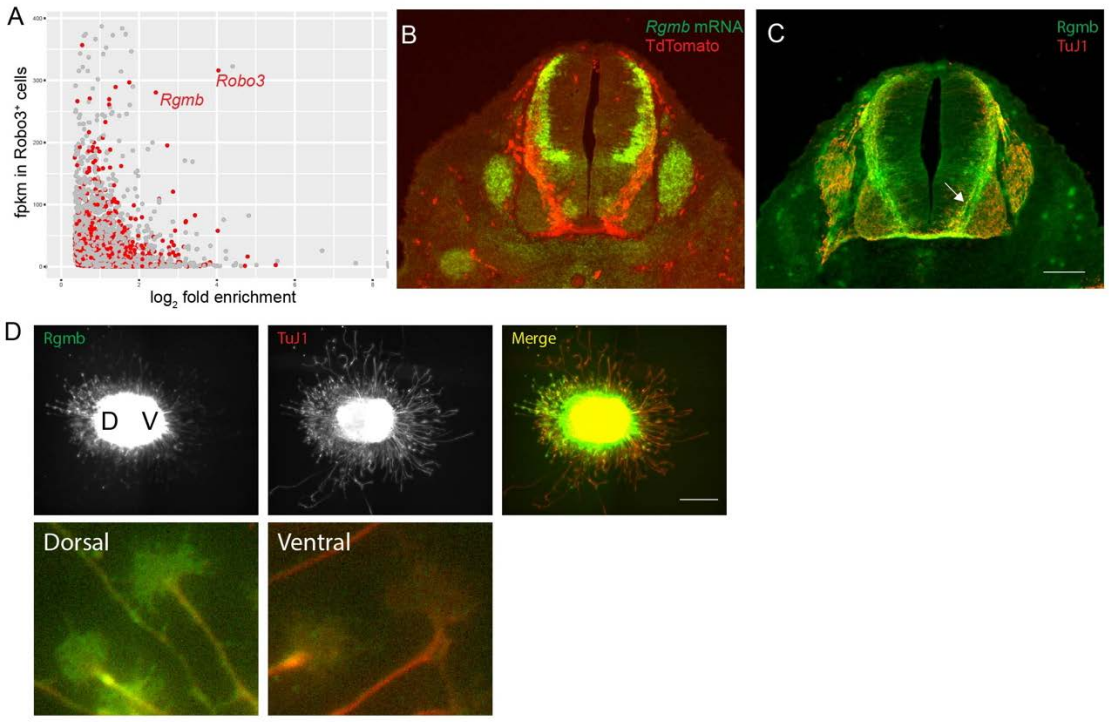
A
fpkm in Robo3+ cells
log2 fold enrichment
Robo3
Rgmb
B
Rgmb mRNA
TdTomato
C
Rgmb
TuJ1
D
Rgmb
TuJ1
Merge
D V
Dorsal
Ventral

RGMb is localized to precrossing and crossing axonal segments

To gain insight into RGMb function, we examined where RGMb protein was localized in commissural neurons. Using E11.5 frozen spinal cord sections, we detected RGMb protein prominently in precrossing axon commissures as they projected ventrally towards the midline. RGMb protein was also detected in the ventral commissure, but its levels decline post-crossing within the ventral funiculus (Fig 3.10C).

Given that Dcc and Neo1 are differentially expressed across commissural neuron populations, we examined whether RGMb expression might also vary between the various commissural neuron populations residing along the dorsoventral axis of the spinal cord. RGMb was expressed at higher levels in dorsal axons compared to ventral axons in E11.5 spinal explants cultured in 2D (Fig 3.10D), suggesting that RGMb may play an important role in the midline guidance of dorsal commissural neuron populations. A model that might account for the differential Netrin-1 receptor dependence of the dorsal and ventral population is summarized in Fig 3.11. In this model, RGMb and Netrin-1 compete for binding to Neo1. In the dorsal population, the low levels of Neo1, coupled with high expression of RGMb results in a non-functional Netrin-1 signaling pathway through Neo1, which could explain why the dorsal population is dependent on Dcc. In contrast, in the ventral population, the presence of high levels of Neo1 and low levels of RGMb results in a functional Netrin-1 signaling pathway through Neo1, so that Netrin-1 mediated attraction can be achieved in *Dcc*$^{-/-}$ embryos.

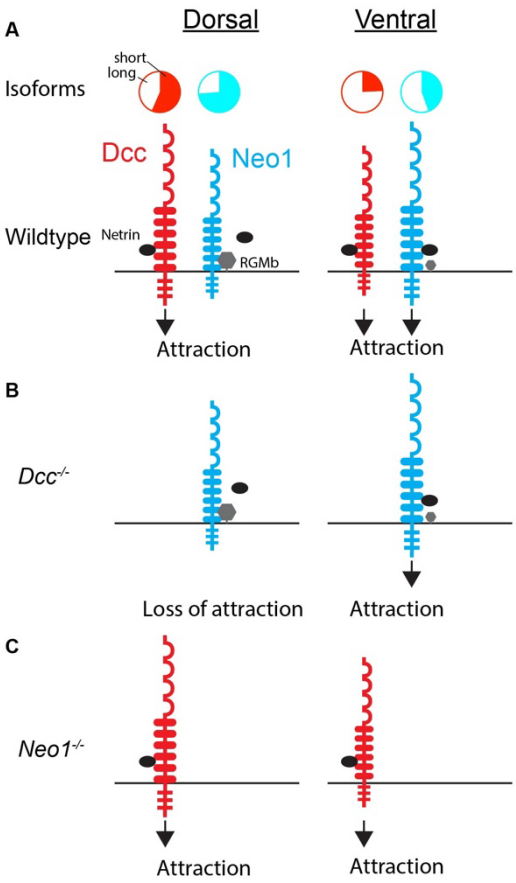

Figure 3.11 Model for Dcc and Neo1 population-specific functions in midline attraction

In this model, the size of the receptors (Dcc, red; Neo1, blue; RGMb, grey) are indicative of their enrichment relative to the other population. The abundance of long and short isoforms is also summarized in the pie charts (blank, long isoform; colored, short isoform). **(A)** In wild-type embryos, attraction is signaled through Dcc and Neo1, except in the dorsal population where RGMb, the ligand for Neo1, is enriched and could occlude Netrin-1 binding. It is also possible that the predominant $Neo1_{short}$ isoform is unable to signal attraction. **(B)** In the absence of Dcc, there is a loss of attraction in the dorsal population but not the ventral population. **(C)** In the absence of Neo1, Netrin signaling is unaffected.

Conclusions

Here, we have helped clarify the role of the Netrin receptors Dcc and Neo1 in commissural axon guidance with several important discoveries. First, we showed that Dcc and Neo1 are differentially expressed between the dorsal (dI1) and ventral (V0/V3) commissural neuron populations as are the splice isoforms for each receptor. As may be predicted from the receptor expression analysis, we found that *Dcc* is uniquely required for proper midline guidance of dorsal commissural neurons, but not the more ventral population. While *Dcc* can compensate for the loss of *Neo1* in both populations, and *Neo1* can compensate for the loss of *Dcc* in the ventral population, *Neo1* cannot compensate for the loss of *Dcc* in the dorsal population. Finally, we also identified a ligand of Neo1, RGMb. RGMb is a potentially novel mediator of axon guidance that is also differentially expressed between these two neuronal populations. A model describing the population-specific differences that might account for Netrin-1 mediated attraction is summarized in Fig 3.11. One or more of the differences reported here might account for the different Netrin-1 receptor dependency of the dorsal and ventral population.

Chapter 4. Revealing potentially new modulators of midline guidance factors using RNA-Seq of commissural neurons and floor plate

Rationale

While many of the major axon guidance programs involved in midline attraction of commissural axons have been well characterized, our understanding of the system remains fragmentary. Given that Robo3 is the most specific marker known presently, we generated a novel *Robo3*$^{Cre/+}$ reporter mouse line that allows us to flexibly label and/or manipulate commissural neurons for a variety of downstream analyses. Using this novel mouse line, we profiled the transcriptome of commissural neurons and unexpectedly identified RGMb, a ligand for the Netrin-1 receptor Neo1 in commissural neurons (Chapter 3). Here, I investigate whether newly identified commissural neuron-specific factors play a role in midline guidance. In addition to characterizing the transcriptome of commissural neurons, I also profiled the transcriptome of floor plate cells with the hope of uncovering additional floor plate-derived factors that influence midline guidance. The data from this unbiased approach should prove to be a valuable resource for unraveling the complex machinery that governs midline guidance.

Generation of a Robo3^{Cre} line to label commissural neurons and their axons

Existing commissural neuron markers only label either pre- (Tag1, Robo3) or post-crossing (L1CAM) segments of commissural neurons. The Robo3

knockout mice currently used by our lab expresses GFP from the Robo3 allele (Sabatier et al., 2004), but *in vivo,* GFP fluorescence can only be observed in highly fasciculated commissural axon bundles. Further underscoring the weakness of GFP expression in *Robo3*$^{GFP/+}$ mice, GFP fluorescence cannot be detected in individual axons *in vitro* when spinal cord explants are cultured from these mice (Sabatier et al., 2004). To overcome these limitations and create a mouse that is compatible with a broader set of downstream applications for commissural neuron analysis, we created a *Robo3*^{Cre} gene-targeted mouse line (Fig 4.1A-D). To test commissural neuron specificity, *Robo3*^{Cre} mice were crossed to a ß-actin promoter driven floxed-stop TdTomato reporter line (*Rosa26*$^{Ai14/Ai14}$). As expected, both pre- and post-crossing axon segments of commissural neurons were successfully and specifically labeled (Fig 4.1D).

Figure 4.1 Generation of a *Robo3*^{Cre} gene-targeted line

The targeting strategy is shown in **(A)**. The top line shows the wild-type *Robo3* locus, the second line shows the targeting vector. The translation initiation codon of *Robo3* exon 1 and subsequent 31 nucleotides was replaced by a targeting cassette containing Cre and a Neomycin resistance gene (*Neo*) flanked by a *Pgk1* promoter and a poly(A) tail, and by two FRT sites. The third line shows the correctly targeted locus. The fourth line shows the locus after mice were crossed to FlpE breeders to excise the Neomycin gene. **(B)** Southern blots of SspI (red, top) and BglI (green, bottom) genomic digests hybridized from *Robo3* heterozygotes and wild-type mice (before Flippase recombination) with the 5' and 3' probes shown in (A). **(C)** PCR genotyping using a common reverse primer and two wild-type- and mutant- specific forward primers (blue arrows, panel A) yielded PCR products of the expected sizes in heterozygotes (after Flippase recombination) and wild-type mice as shown here in an agarose gel. **(D)** Transverse E11.5 sections of embryos from a *Robo3*$^{Cre/+}$ *x Rosa26*$^{Ai14/Ai14}$ cross demonstrated that Cre recombination occurs in the anatomical locations of where commissural cell bodies are located. Pre- and post- crossing axons are also labeled.

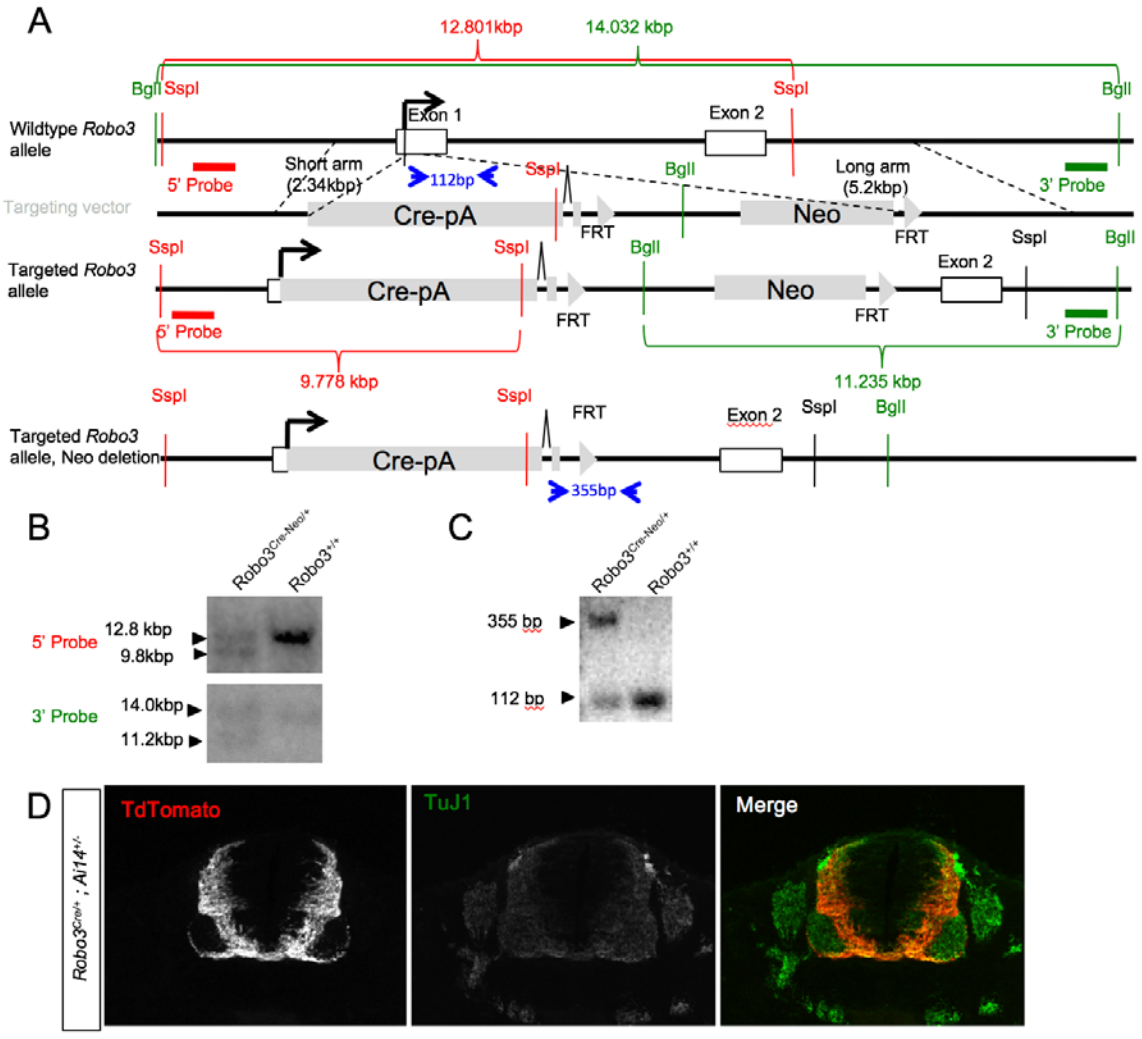
A
12.801kbp
14.032 kbp
BglI SspI
SspI
BglI
Wildtype Robo3 allele
Exon 1
Exon 2
5' Probe
Short arm (2.34kbp)
112bp
SspI
BglI
Long arm (5.2kbp)
3' Probe
Targeting vector
Cre-pA
FRT
Neo
FRT
SspI
BglI
Targeted Robo3 allele
SspI
SspI
BglI
Exon 2
Cre-pA
FRT
Neo
FRT
5' Probe
3' Probe
9.778 kbp
11.235 kbp
SspI
SspI
FRT
Exon 2
SspI
BglI
Targeted Robo3 allele, Neo deletion
Cre-pA
355bp
B
Robo3Cre-Neo/+
Robo3+/+
5' Probe
12.8 kbp
9.8kbp
3' Probe
14.0kbp
11.2kbp
C
Robo3Cre-Neo/+
Robo3+/+
355 bp
112 bp
D
Robo3Cre/+ ; Ai14+/-
TdTomato
TuJ1
Merge

Gene profiling of factors expressed in commissural neurons

Our initial plan for determining the translationally-active transcriptome of commissural neurons was to cross the *Robo3*$^{Cre/+}$ mouse line to a floxed-stop TRAP mouse line. Using this strategy, we found that the RNA yields from E11.5 embryos were too low for RNA-seq (data not shown). Therefore, we changed our strategy and crossed *Robo3*$^{Cre/+}$ to *Rosa26*$^{Ai14/Ai14}$ mice. This approach allowed us to utilize FACS to isolate commissural neurons based on their TdTomato signal. Briefly, we isolated *Robo3*$^{Cre/+}$*;Rosa26*$^{Ai14/+}$ E11.5 spinal cords, dissociated the cells and purified TdTomato-expressing commissural neurons by FACS sorting (Fig 4.2A). These neurons were then analyzed by RNA-Seq. The analysis yielded 3208 genes with significantly higher expression in commissural neurons relative to other cell types (Fig 4.2B). We then verified expression of these candidates using *in situ* hybridization on E11.5 spinal cord sections (Table 1), which narrowed the list to 8 candidates: *Sst, Rgmb, Dner, Thsd7a, Chl1, Kif26b, Lamp5* and *Mab21l2* (Fig 4.2C-J).

Figure 4.2 Expression of commissural neuron-specific transcripts

(A) Top, A representative FACS density plot showing how TdTomato$^+$ neurons were enriched from *Robo3$^{Cre/+}$;Rosa26$^{Ai14/+}$* E11.5 embryos (*n*=3 litters). The quadrilaterals were the gates used to segregate the TdTomato$^+$ and TdTomato$^-$ populations. Bottom, a representative histogram of cells from this run. A total of approximately 8% of cells sorted were TdTomato$^+$. **(B)** The gene expression level of RNA-Sequenced genes that were detected in TdTomato$^+$ neurons (measured in fragments per kb gene per million reads, or fpkm) were plotted against their enrichment compared to TdTomato$^-$ cells. Any gene that was annotated to be transmembrane in Uniprot were color coded red. Labeled genes were those whose expression was confirmed *in situ*. **(C-J)** Fluorescent *in situ* hybridization of *Robo3$^{Cre/+}$;Rosa26$^{Ai14/+}$* E11.5 embryos were stained for the gene of interest as labeled on the left (green) and TdTomato (red). Genes names that were color coded red were annotated as transmembrane in Uniprot. See Table 1 for the full name of each gene.

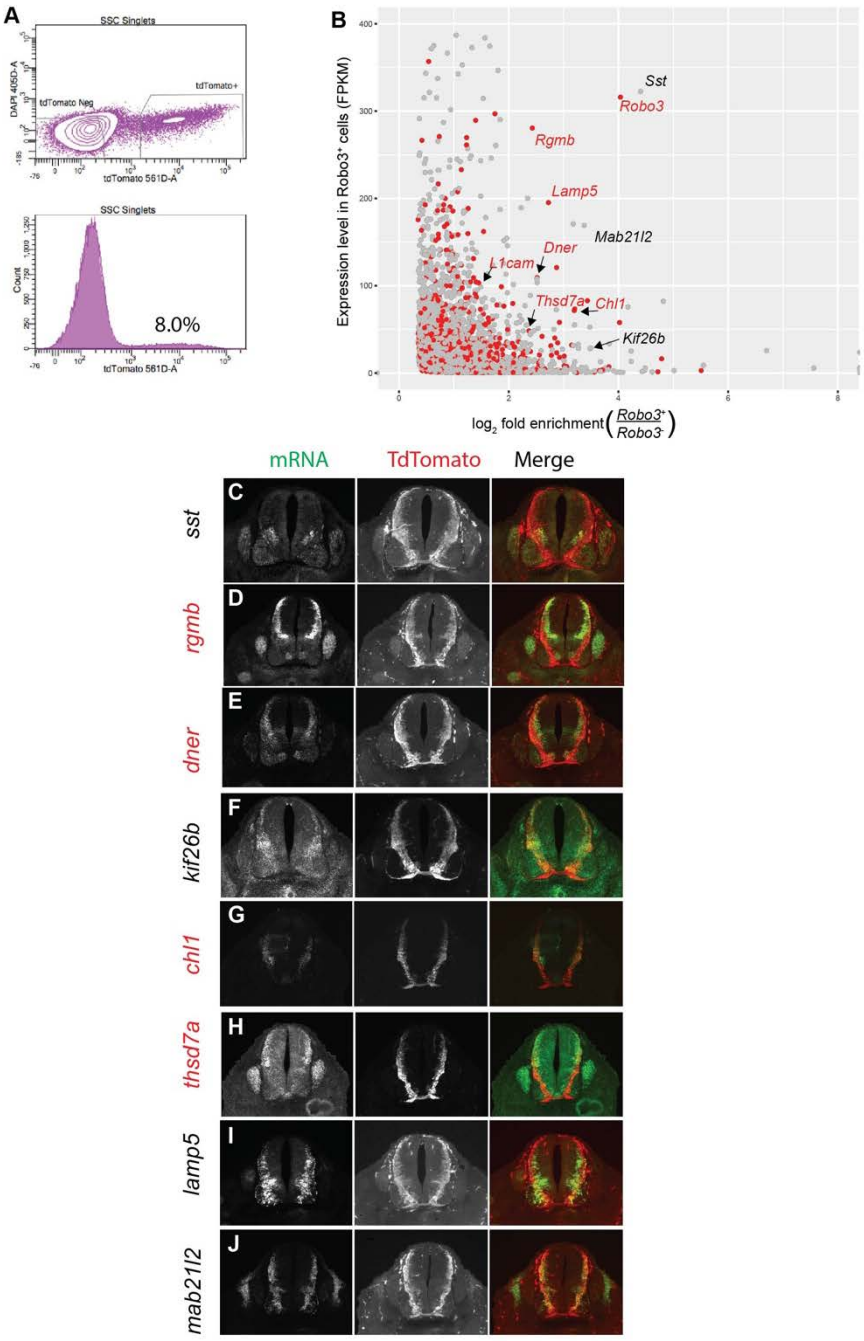
A
SSC Singlets
tdTomato Neg
tdTomato+
DAPI 405D-A
tdTomato 561D-A
SSC Singlets
Count
8.0%
tdTomato 561D-A
B
Expression level in Robo3+ cells (FPKM)
Sst
Robo3
Rgmb
Lamp5
Mab21l2
Dner
L1cam
Thsd7a
Chl1
Kif26b
log2 fold enrichment (Robo3+ / Robo3-)
mRNA
TdTomato
Merge
C
sst
D
rgmb
E
dner
F
kif26b
G
chl1
H
thsd7a
I
lamp5
J
mab21l2

Table 1 Candidate genes shortlisted from the RNA-Seq of commissural neurons and subsequent verification of gene expression by *in situ* hybridization

Subcellular location	Gene	Name	*In situ* Result
Transmembrane	*Sst*	*Somatostain*	Enriched*
	Dner	*Delta/Notch-Like EGF Repeat Containing*	Enriched
	Dlk1	*Protein delta homolog 1*	Not enriched
	Rtn1	*Reticulon 1*	Not enriched
	Lamp5	*Lysosomal-Associated Membrane Protein Family, Member 5*	Enriched
	Rgmb	*Repulsive guidance molecule family B*	Enriched
	Tmeff2	*Tomoregulin-2*	Not enriched
	Thsd7a	*Thrombospondin Type I, domain containing 7a*	Enriched
	Chl1	*Cell Adhesion Molecule L1-Like*	Enriched
Secreted	*Nxph4*	*Neurexophilin 4*	Not enriched
	Nms	*Neuromedin S*	Not enriched
Other	*Nrn*	*Neuritin 1*	Not enriched
	Crmp	*Collapsin response mediator protein 1*	Not enriched
	Mab21l2	*Mab-21-like 2*	Enriched
	Mtus2	*Microtubule Associated Tumor Suppressor Candidate 2*	Not enriched
	Cartpt	*Cocaine And Amphetamine Regulated Transcript*	Not enriched
	Skor2	*SKI family transcriptional corepressor 2*	Not enriched
	Kif26b	*Kinesin family member 26b*	Enriched

**Sst* was localized only very few commissural neurons in the middle of the dorsoventral axis.

The table lists all genes that were considered to be outliers in the plot, and whose expression was subsequently tested *in situ*. Their subcellular location was determined manually by their Uniprot annotation.

Functional knockdown screen for commissural-specific factors in axon guidance

To determine if validated commissural neuron specific candidates play a functional role in midline crossing, we examined the effects of knocking down each candidate by electroporating commercially available siRNAs into the dorsal spinal cord of E9.5 embryos (Chen et al., 2008). Following electroporation, embryos were incubated for 2 days *in vitro* using the whole-embryo culture (WEC) method (Fig 4.3A- H). As a proof-of-principle, knocking down Robo3 prevented axons from crossing to the contralateral side and increased the number of axons that invaded the ventral horn (Fig 4.3A and B). Knockdown of *Rgmb, Dner* or *Kif26b* moderately increased the number of aberrant axons invading the ventral horn (Fig 4.3C to E). However, no misprojections were observed following the knockdown of *Chl1, Lamp5* or *Mab21l2*. We were unable to knockdown *Thrombospondin 7a* (*Thsd7a)* because siRNAs against this target were not available in the siRNA library. The phenotypes observed in this screen suggest that *Rgmb, Dner* and *Kif26b* might play a role in midline axon guidance.

Figure 4.3 Characterization and genetic screening of commissural neuron-specific factors in axon guidance

(A-H) An *rfp* overexpression plasmid and a pool of 4 commercially available siRNAs against a single gene (shown in each panel) were co-electroporated into the dorsal spinal cord of E9.5 embryos. They were cultured for 2 days *in vitro* using the Whole Embryo Culture method (see Materials and Methods). The embryos were fixed, sectioned and stained for RFP (red). The autofluorescence of the tissue is shown in green for contrast. In (A), a control siRNA was used, and as expected, several axons successfully project cotralaterally (arrow). In (B), siRobo3 was used as a positive control. Consistent with an essential role of Robo3 in midline guidance, no axons were observed projecting contralaterally, and several axons invade the ventral horn (arrowhead). In (C) to (H), axons were able to project contralaterally. However, with knockdown of *Rgmb* (C), *Dner* (D) and *Kif26b* (E), several axons were observed invading the ventral horn. No obvious defects were observed with *Chl1* (F), *Lamp5* (G) and *Mab21l2* (H). **(I-J)** The ability of Dner ectodomain tagged with Alkaline phosphatase (AP) protein (DnerEc-AP, I) or Thsd7a ectodomain tagged with AP (Thsd7aEc-AP, J) protein to bind to spinal cord explants (spinal cord with floor plate, see Fig 1.3 for details) cultured in 2D were tested here. The presence of a purple precipitate denotes AP-protein binding. No binding was observed with DnerEc-AP. Binding to precrossing axons (red arrowhead, J') and post-crossing axons (red arrow, J'') were detected with Thsd7aEc-AP. **(K-N)** Genetic mutants of E11.5 *Dner* (L) and *Kif26b* (N) spinal cord sections were fixed and stained for Robo3 (green) and TuJ1 (red). Compared to their littermate controls (K and M), the morphology of commissural projections appeared similar.

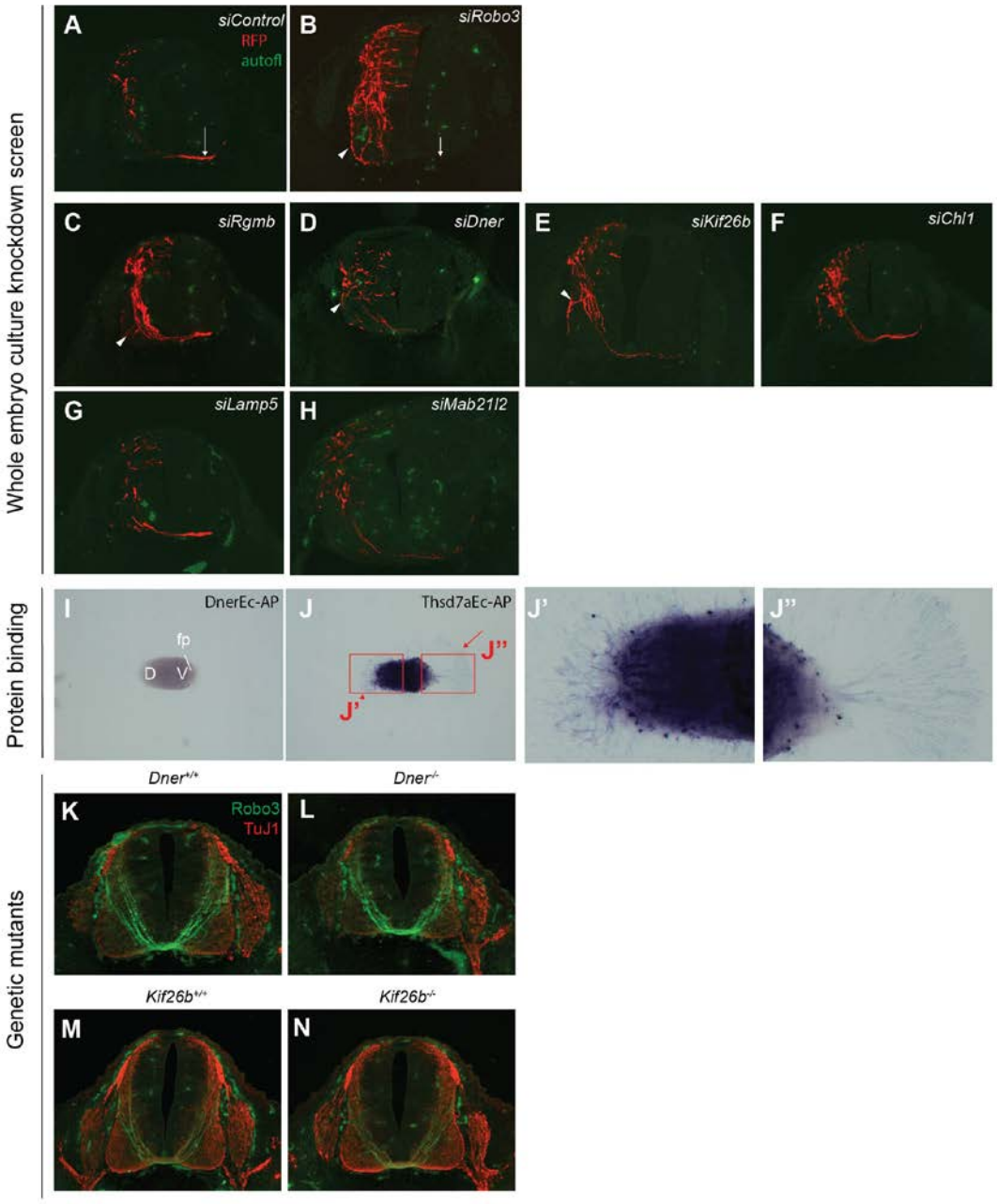
Whole embryo culture knockdown screen
A
siControl
RFP
autofl
B
siRobo3
C
siRgmb
D
siDner
E
siKif26b
F
siChl1
G
siLamp5
H
siMab21l2
Protein binding
I
DnerEc-AP
fp
D
V
J
Thsd7aEc-AP
J''
J'
J'
J''
Genetic mutants
Dner+/+
Dner-/-
K
Robo3
TuJ1
L
Kif26b+/+
Kif26b-/-
M
N

Shortlisting commissural-specific candidates for further characterization

Commissural neurons express several well-characterized transmembrane proteins such as Robos and Dcc that act as instructive guidance receptors (Yu and Bargmann, 2001; Bashaw and Klein, 2010). Of the candidates that resulted in modest guidance defects when knocked down, Rgmb and Dner (Fig 4.3C and D) are transmembrane. The other untested candidate Thsd7a contains thrombospondin domains (Wang et al., 2010) that are also present in the Unc-5 Netrin receptor family. Therefore, we wanted to determine if Rgmb, Dner and Thsd7a could bind with other proteins expressed by the developing spinal cord. Their binding properties could be indicative of a role as a guidance receptor. Rgmb was considered in the previous chapter and will not be discussed here.

Protein trafficking regulates guidance receptor levels on the extracellular surface of the growth cone, and therefore governs guidance decisions in the developing neuron (Winckler and Mellman, 2010). In the precrossing commissural axons of *Drosophila*, surface Robo receptor levels are kept low by the protein commissureless (comm), which acts to direct Robo to the endosomes instead of the plasma membrane, thereby preventing premature Slit repulsion (Keleman et al., 2002; Myat et al., 2002; Keleman et al., 2005). Similarly in the mouse, Robo1/2 levels are localized in post-crossing segments (Long et al., 2004), but the factor that regulates Robo trafficking is not known. Of the candidates that resulted in guidance defects when knocked down, Kinesin-like family protein 26b (Kif26b) is an attractive candidate for trafficking guidance receptors. It contains a kinesin motor domain (Uchiyama et al., 2010) that could

potentially regulate receptor trafficking. If true, it could serve a *Drosophila comm*-like trafficking function that has not yet been reported in the mouse. Therefore, we obtained *Kif26b* mutant embryos to determine if there are guidance phenotypes that could reveal a role for *Kif26b* in trafficking.

The Thsd7a ectodomain binds to axons *in vitro*

To visualize extracellular transmembrane protein interactions, cDNAs encoding for the ectodomains of each transmembrane protein were cloned in frame with alkaline phosphatase to produce alkaline phosphatase (AP) fusion proteins in HEK293 cells. Conditioned media of secreted DnerEc-AP or Thsd7aEc-AP fusion proteins were collected. Fusion proteins in conditioned media were then tested for their ability to bind to spinal cord explants that had been cultured *in vitro*. Briefly, DnerEc-AP or Thsd7aEc-AP conditioned media was added onto E11.5 spinal cord explants that were cultured in 2D for 16 hr *in vitro* (see Fig 1.3D). 2D cultures were washed several times before detection of AP enzymatic activity. No detectable binding on cultured explants was observed with Dner fusion protein (Fig 4.3I). However, Thsd7a specifically bound the axons of cultured explants (Fig 4.3J), making it a good midline guidance candidate.

Grossly normal axonal projections in *Dner* and *Kif26b* mutant spinal cords

We further tested potential roles for *Dner, Kif26b* and *Thsd7a* in midline guidance by analyzing the spinal cords of E11.5 homozygous mutant embryos for each candidate. Unfortunately, no *Thsd7a*$^{-/-}$ embryos were obtained from 3 independent crosses. Therefore, it seems likely that *Thsd7a*$^{-/-}$ embryos are not viable at this developmental stage, which precludes further analysis (data not

shown). Also, no guidance defects were observed in *Dner*$^{-/-}$ (Fig 4.3L) or *Kif26b*$^{-/-}$ (Fig 4.3N) E11.5 spinal cords: The number of Robo3^{+} axons invading the motor column and the ventral commissure size appeared comparable in both wild-types and mutants. Taken together, this suggests that these factors may not be involved in midline guidance.

Gene profiling factors expressed in the floor plate

To identify novel axon guidance factors that are expressed and enriched in the floor plate, we microdissected floor plate tissue from embryonic mice, performed RNA-Seq and compared the transcriptome of floor plate tissue to the transcriptome of dorsal spinal cord tissue (*n*=3 litters of 8 embryos each, Fig 4.4A). In this dataset, 5329 genes were found to be enriched in the floor plate (Fig 4.4B). These genes included well-documented floor plate-derived guidance cues such as *Netrin-1* (*Netrin-1*), *Slit1, Slit2* and *Shh*, thus validating this approach as a suitable method for uncovering additional guidance factors expressed by the floor plate.

Because floor plate-derived guidance factors must be presented to commissural axons in order to influence axon guidance, we reasoned that floor plate-derived guidance factors must either be secreted or expressed on the extracellular cell membrane (e.g. transmembrane or GPI-linked proteins). We used these parameters to restrict our search to candidates annotated as such in the Uniprot database. As a survey, we successfully confirmed the expression of

the top 23 genes through *in situ* hybridization (Fig 4.5A-W). A list of all the genes that were tested is summarized in Table 2.

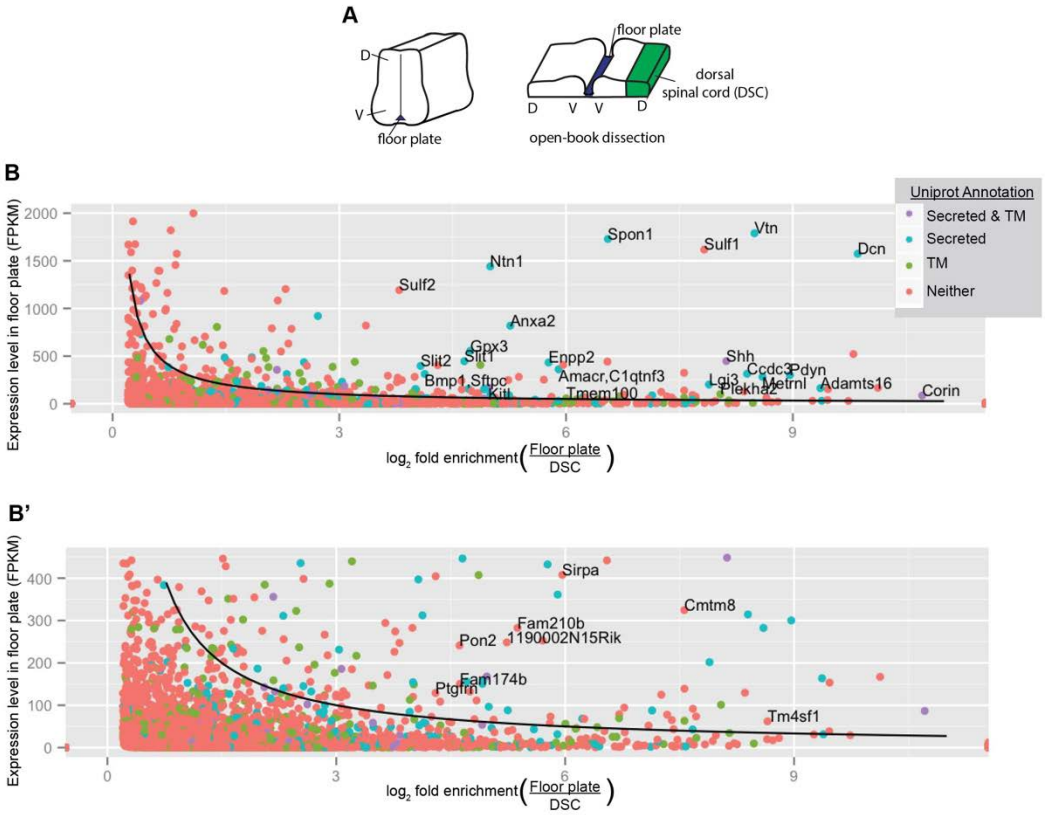

Figure 4.4 RNA-Seq identification of candidate genes enriched in floor plate cells

(A) Floor plate (blue) and dorsal spinal cord tissue (DSC, green) were isolated from three independent litters of 8 embryos for RNA-Seq. The DSC region was defined as the volume that excludes the ventral horn bulge. D, dorsal; V, ventral. **(B)** The gene expression level within the floor plate of all differentially expressed genes was plotted against their relative fold enrichment compared to DSC. For survey purposes, the black curve denotes the boundary that separates most of the top 23 'candidates' considered for further analysis from low expressers. Genes were color coded by their annotation of cell localization in the Uniprot database and summarized in the key (top right). TM, transmembrane. **(B')** shows the lower expressers of the plot in (B) (see range of vertical axis).

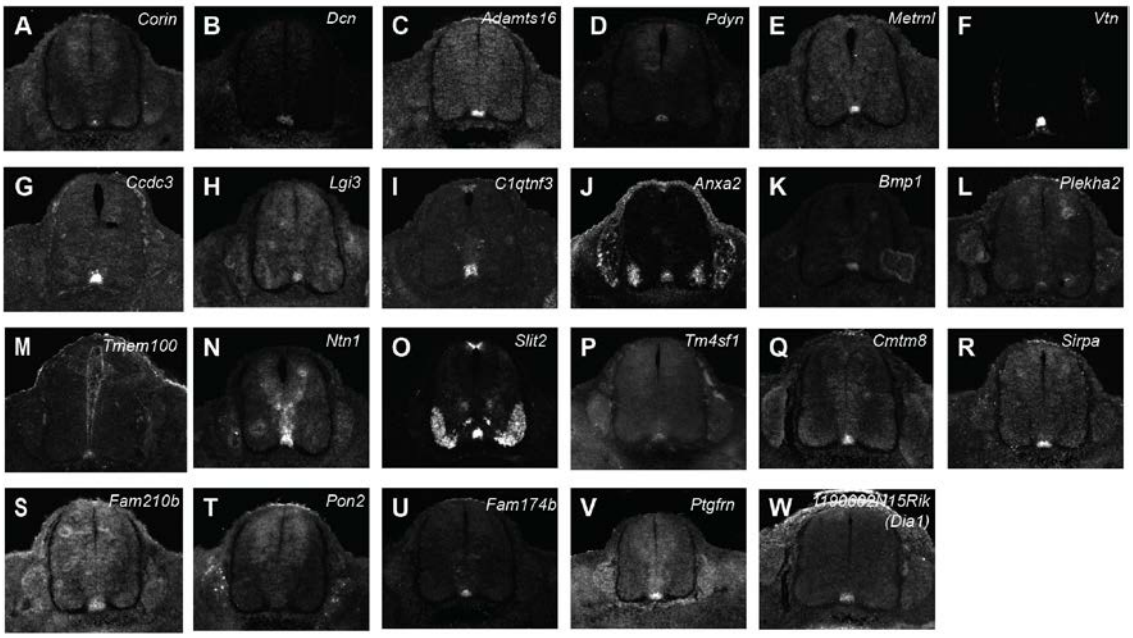

Figure 4.5 *In situ* validation of gene expression of floor plate candidates

(A-W) E11.5 fluorescent *in situ* hybridization of outliers identified through RNA-Seq of floor plate tissue. Note that in each instance, transcript was detected in the ventral midline floor plate tissue. Some genes were also detected in other regions. See Table 2 for the full name of each gene.

Table 2 Candidate genes shortlisted from the RNA-Seq of floor plate tissue and subsequent verification of gene expression by *in situ* hybridization

Subcellular location	Gene	Name
Secreted	*Dcn*	Decorin
	Adamts16	ADAM metallopeptidase with thrombospondin Type 1 Motif 16
	Pdyn	Prodynorphin
	Metrnl	Meteorin-like
	Vtn	Vitronectin
	Ccdc3	Favin
	Lgi3	LRR, glioma-inactivated 3
	C1qtnf3	C1q & TNF related protein 3
	Anxa2	Annexin-a2
	Netrin-1	Netrin1
	Bmp1	Bone morphogenetic protein 1
	Slit2	Slit2
	1190002N15Rik	Deleted in autism 1
Transmembrane	*Tm4sf1*	Tumor associated antigen L6
	Plekha2	Pleckstrin homology domain-containing family A member 2
	Cmtm8	Chemokine-like factor superfamily member 8
	Sirpa	Signal regulatory protein alpha
	Fam210b	Family with sequence similarity 210b
	Pon2	Arylesterase
	Fam174b	Family with Sequence Similarity 174, Member B
	Ptgfrn	Prostaglandin F2 receptor negative regulator
	Tmem100	Transmembrane100
Both	*Corin*	Atrial natriuretic peptide-converting enzyme

The table lists all genes whose expression was tested *in situ*. Gene expression was confirmed for all genes (see Fig 4.5). The subcellular location of each gene was manually verified using the Uniprot annotation of each gene.

Considerations for shortlisting floor plate-specific candidates for further characterization

In order to prioritize candidates that function as instructive guidance cues, we first focused on ones possessing evolutionarily conserved domains that are homologous to those present in already characterized guidance molecules. In this way, we narrowed down the list of 23 floor plate-enriched candidates by comparing their protein domains to known guidance molecules.

The first candidate that we focused on from our screen of floor plate-enriched transcripts was the Leucine Rich Glioma-Inactivated protein 3 (Lgi3) (Fig 4.5H). This secreted protein was of particular interest because it encodes a secreted protein containing leucine rich repeat (LRR) domains (Kegel et al., 2013) (Fig 4.6A), which are also present in the floor plate-derived classic Slit family of chemorepellent proteins (Brose et al., 1999). Both Slit-2 and Lgi3 can promote axon elongation in sensory neurons of the DRG as well (Wang et al., 1999; Park et al., 2010). The homology and outgrowth-promoting activity shared by both Slit2 and Lgi3 supports the idea that Lgi3 might have a guidance role in the developing spinal cord.

A second candidate that we focused on from our screen of floor plate-enriched transcripts was ADAM with thrombospondin motifs 16 (*Adamts16)* (Fig 4.5C). We focused on this candidate because Madd-4, a *C. elegans* ortholog to human Adamtsl-1, is expressed by midline cells and acts in guidance via the Unc-40/Dcc receptor (Seetharaman et al., 2011). We reasoned that Adamts16 could share an evolutionarily conserved guidance function as well. Furthermore,

as a metalloprotease, we considered that Adamts16 might process receptors on the surface membrane. Indeed, receptor processing plays a key role in modulating guidance signaling in neurons (Yu and Bargmann, 2001; Bashaw and Klein, 2010). Guidance receptors, such as Dcc, are known to undergo ectodomain shedding to regulate the level of full-length receptor, thereby inhibiting inappropriate Netrin-1 attraction (Galko and Tessier-Lavigne, 2000; Bai et al., 2011). In the fly, cleavage of the Dcc homolog Frazzled releases the transcriptionally-active intracellular domain of Fra/Dcc to regulate midline crossing (Yang et al., 2009; Neuhaus-Follini and Bashaw, 2015). Similarly, cleavage of Robo receptors by Kuzbanian (Kuz/Adam10) activates the receptor to signal midline repulsion (Coleman et al., 2010). Given the precedent that metalloproteases can regulate midline guidance across several species, we tested the hypothesis that floor plate-derived Adamts16 shares an evolutionarily conserved role with Madd-4 in regulating guidance through receptor processing on the surface of commissural axons.

Lgi3 as a candidate for mediating midline guidance

To determine if axons are responsive to Lgi3, we first produced Lgi3 protein. This was accomplished by cloning full-length Lgi3 and various fragments of Lgi3 into an alkaline phosphatase (AP) expression vector (Fig 4.6A). AP or Lgi3-AP conditioned media were applied to dorsal spinal cord (DSC) explants cultured in a 3D collagen matrix, and the effects of AP or Lgi3-AP on axonal outgrowth were measured. In explants cultured with AP, Netrin-1 application induced robust axonal outgrowth that peaked at a Netrin concentration of 400 ng

mL^{-1}. However, addition of Lgi3-AP reduced the Netrin concentration needed to produce maximal axonal outgrowth (200 ng mL^{-1}) (Fig 4.6B), indicating that Lgi3 modulates the Netrin1 sensitivity of axons.

Having shown that Lgi3 modulates the Netrin1 sensitivity of commissural axons, we tested whether Lgi3 achieves this modulatory effect by binding to either axons and/or floor plate tissue *in vitro*. Binding was detected on axons as well as floor plate tissue with full-length Lgi3-AP protein (Fig 4.6F). This result suggests that Lgi3 interacts with both axons and floor plate tissue, and this potential interaction could account for Lgi3's ability to modulate Netrin-1 sensitivity (Fig 4.6B).

Figure 4.6 *In vitro* and *in vivo* characterization of Lgi3 in midline guidance

(A) Schematic of the protein domains found in Lgi3, and various Lgi3 constructs tagged to alkaline phosphatase (AP) that were used in the study. **(B)** E11.5 spinal cord dorsal-only explants were cultured in 3D collagen gels and incubated in varying Netrin-1 concentrations for 24 hr, then fixed and stained for TuJ1. In the presence of AP as a control (red), peak outgrowth was achieved at 400 ng mL^{-1} Netrin-1. However, with Lgi3-AP, peak outgrowth occurred earlier at 100 ng mL^{-1} Netrin-1. **(C-H)** Various AP-tagged constructs were added to spinal cord explants cultured in 2D (with floor plate present). D, dorsal; fp, floor plate. The presence of purple precipitate indicates where AP activity was detected. Panels (D) and (E) are shown as controls: With DCCEc-AP (Ec, Ectodomain) (D), activity was detected in the floor plate where its ligand Netrin-1 is highly expressed; With AP-Netrin-1 (E), activity was detected in axons where its receptor Dcc and/or Neo1 is expressed. (F) Lgi3-AP binding was detected most strongly in the floor plate and less so in axons (F'). (G) LRR-AP binding was detected in distal axons. (H) EAR-AP binding was detected on dorsal axons (H') and floor plate. **(I)** Same as C, with the exception that instead of explants, the ability of Lgi3-AP to bind to COS cells singly overexpressing a guidance receptor was tested. No binding was observed with a negative control (EGFP) or any canonical guidance receptor (Dcc, Robo1/2/3). Lgi3 is a known ligand for Adam22 (Ozkaynak et al., 2010), and is shown here as a positive control. **(J)** Fluorescent *in situ* hybridization on E11.5 sections revealed that *Adam11* is detected within developing spinal interneurons and dorsal root ganglion neurons. **(K)** COS cell binding assay (similar to C-H) revealed that Lgi3-AP binding was detected on Adam11-expressing COS cells. **(L)** A frameshift mutation (red) was introduced to the coding sequence (CDS) of exon 1 of *Lgi3* by CRISPR/Cas9 gene editing in zygotes. PAM, protospacer adjacent motif; DSB, double stranded break. A mouse line with 1 basepair deletion was isolated and used in (M). **(M)** Spinal cord sections of control and $Lgi3^{-/-}$ from E11.5 embryos were stained for Robo3 (red) and L1 (green). No gross defects were detected: In mutants, the ventral commissure size appeared normal, and the $Robo3^{+}$ axon trajectories appeared comparable to wild-types.

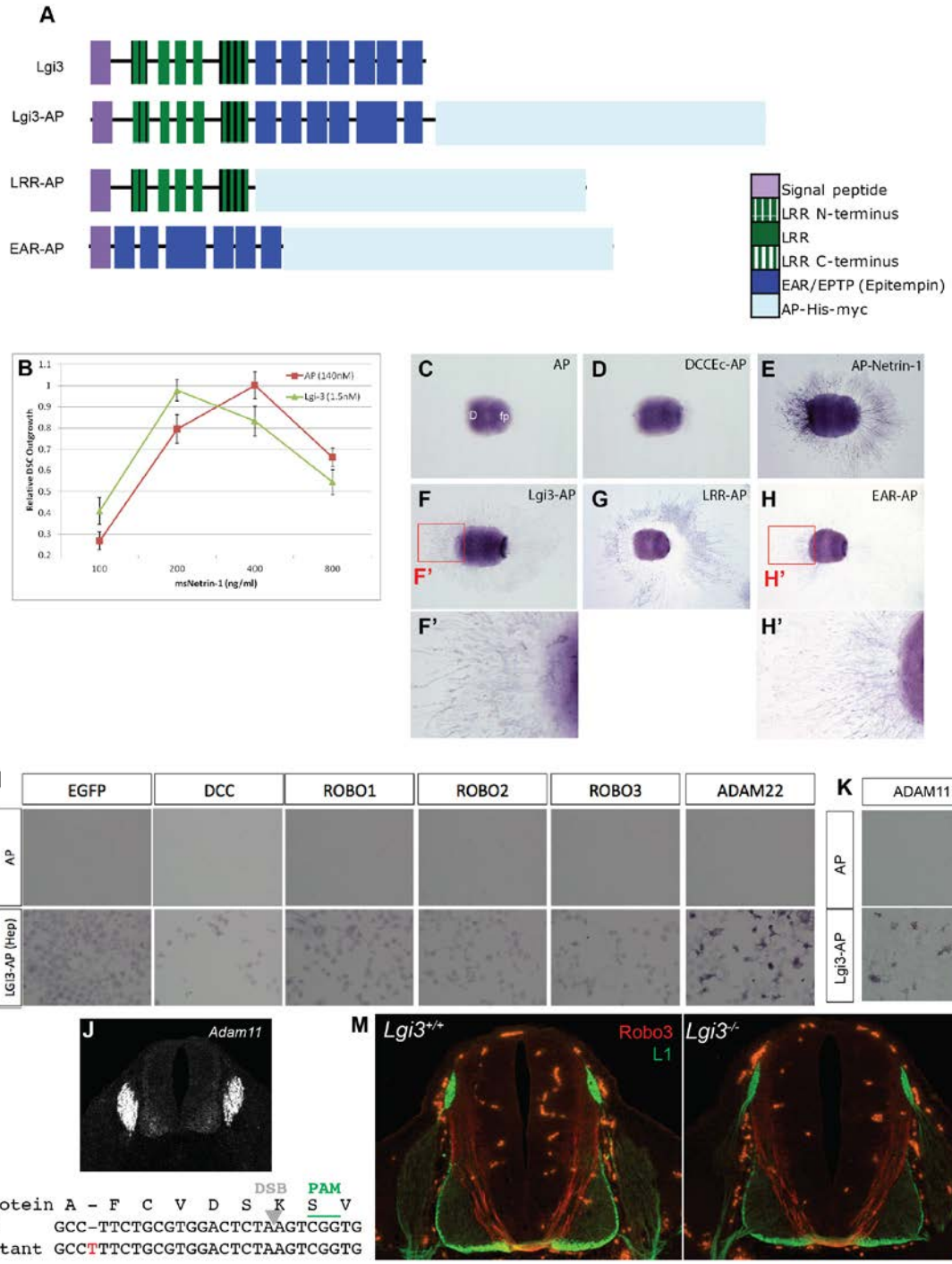
A
Lgi3
Lgi3-AP
LRR-AP
EAR-AP
Signal peptide
LRR N-terminus
LRR
LRR C-terminus
EAR/EPTP (Epitempin)
AP-His-myc
B
AP (140nM)
Lgi-3 (1.5nM)
Relative DSC Outgrowth
msNetrin-1 (ng/ml)
C
AP
D
DCCEc-AP
E
AP-Netrin-1
F
Lgi3-AP
G
LRR-AP
H
EAR-AP
F'
H'
I
EGFP
DCC
ROBO1
ROBO2
ROBO3
ADAM22
AP
LGi3-AP (Hep)
K
ADAM11
J
Adam11
L
DSB
PAM
Protein A - F C V D S K S V
WT GCC-TTCTGCGTGGACTCTAAGTCGGTG
Mutant GCCTTTCTGCGTGGACTCTAAGTCGGTG
M
Lgi3+/+
Robo3
L1
Lgi3-/-

Lgi3 comprises a series of N-terminal LRR domains, and a C-terminal Epilepsy Associated Repeat (EAR) domain with a predicted beta-propeller fold (Kegel et al., 2013) (Fig 4.6A). To delineate which domains account for the differential binding of Lgi3 to floor plate versus axons, we repeated the binding experiments using either the Lgi3 LRR-domain or Lgi3 EAR-domain tagged to AP (Fig 4.6G and H). Interestingly, we found that the LRR domain bound indiscriminately to all axons. In contrast, the Lgi3 EAR-domain bound specifically to precrossing axons as well as to floor plate cells (Fig 5H). This binding pattern raises the possibility that different domains within Lgi3 possess distinct functions that together modulate axonal sensitivity to Netrin1.

Given Lgi3's ability to bind to axons and modulate Netrin1 sensitivity, we postulated that Lgi3 may bind Dcc. However, we failed to detect Lgi3 binding to COS cells expressing Dcc (Fig 4.6D). The Robo receptors provide another potential receptor for Lgi3, as Robo3 is known to modulate Netrin-1 signaling and is highly expressed on precrossing commissural axons (Zelina et al., 2014). Further, Lgi3 bears homology to Slit proteins, the canonical ligands of the Robo receptors (Brose et al., 1999). However, we found that Lgi3 did not bind to COS cells expressing Robo1, 2 or 3 (Fig 4.6I).

Several ADAM (A disintegrin and metalloproteinase) proteins bind to Lgi3 (Kegel et al., 2013), so we next considered which ADAMs are expressed in commissural neurons. Of the ADAMs that were predicted to be expressed in commissural neurons based on the commissural neuron RNA-Seq transcriptome (Fig 4.2B and data not shown), we verified expression of only ADAM11 by *in situ*

hybridization (Fig 4.6J). Further, we confirmed that Lgi3 binds COS cells expressing ADAM11 (Fig 4.6K). This raises the possibility that Lgi3's ability to bind to axons (Fig 4.6F) could be mediated through axonal ADAM11, a molecule that is thought to mediate neuron-neuron and/or neuron-glial cell interactions during neurodevelopment (Rybnikova et al., 2002).

To determine if Lgi3 mediates midline guidance *in vivo*, we used CRISPR/Cas9 technology to generate a novel mouse mutant harboring a frameshift mutation within the coding sequence of exon 1 of the *Lgi3* locus (Fig 4.6L). Examination of E11.5 embryos revealed no gross defects in *Lgi3*$^{-/-}$ spinal cords: The number of Robo3^{+} axons invading the motor column and the ventral commissure size appeared comparable in both wild-types and *Lgi3*$^{-/-}$ (Fig 4.6M).

Taken together, the absence of a guidance phenotype does not support the hypothesis that Lgi3 is a mediator of axon guidance. However, the extensive protein interactions that have been characterized here suggest that Lgi3 may perform some other role in the developing spinal cord. It is also possible that subtle defects were missed, and a more extensive characterization *in vivo* will be required to definitely rule out a guidance role for Lgi3.

Adamts16 as a candidate for midline guidance

To determine whether Adamts16 plays a midline guidance role that is analogous to Madd-4, we attempted to express AP-tagged Adamts16 clones from both HEK293T cells and COS cells. However, we were unable to express recombinant protein, and this technical difficulty precluded our ability to study both the interactions between Adamts16 protein and commissural axons and

Adamts16's ability to cleave guidance receptors (data not shown). However, we successfully used CRISPR/Cas9 to generate a novel mouse mutant harboring a frameshift mutation within the coding sequence of exon 1 of the *Adamts16* locus (Fig 4.7A). Compared to wild-types, the ventral commissure size of *Adamts16*$^{-/-}$ at E12.5 was similar in size. No commissural axons were seen wandering in the motor column in both wild-types and mutants (Fig 4.7C). Since no obvious defects were observed in *Adamts16*$^{-/-}$ mice, the possible guidance role of floor plate-derived Adamts16 remains unknown. At this level of analysis, the possibility that subtle guidance defects were overlooked cannot be ruled out, and a more systematic study will be required to definitively rule out a guidance role for Adamts16.

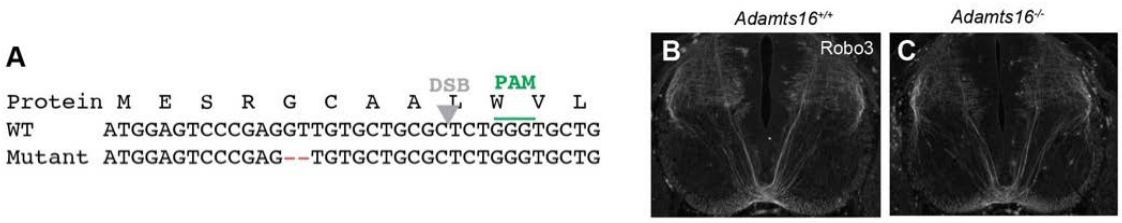

Figure 4.7 *In vivo* characterization of Adamts16 in midline guidance

(A) A frameshift mutation (red) was introduced to the coding sequence of exon 1 of *Adamts16* by CRISPR/Cas9 gene editing in zygotes. PAM, protospacer adjacent motif; DSB, double stranded break. A mouse line with a 2 basepair deletion was isolated and used in (C). **(B-C)** Spinal cord sections of control (B) and *Adamts16*$^{-/-}$ from E12.5 embryos were stained for Robo3. No gross defects were detected: The ventral commissure size appeared similar, and the trajectories of Robo3-axons were comparable between wild-types and mutants.

Eva1c as a candidate for midline guidance

While we were considering Adamts16's possible evolutionary relationship to Madd-4, it was reported that Madd-4-mediated chemoattraction to the midline is enhanced through the Unc-40/Dcc co-receptor, Eva-1 (Chan et al., 2014). Eva-1 can also bind to Slits and signal repulsion (Fujisawa et al., 2007). Immunohistochemical analysis of Eva1c, the mammalian Eva-1 homolog, revealed expression of Eva1c in axons across the mouse nervous system and, in particular, in neurons of the developing spinal cord (James et al., 2013). This supports the idea that Eva1c plays an evolutionarily conserved role in midline guidance.

To determine whether the *Eva1c* receptor may play an important role in axon guidance, we examined *Eva1c* using *in silico*, *in situ*, *in vitro* and *in vivo* analyses. We first turned to the two *in silico* transcriptomic datasets (commissural neuron and floor plate datasets, Fig 4.2 and 4.4) to determine where *Eva1c* is expressed. *Eva1c* transcripts were virtually undetected within commissural neurons (*Eva1c* FPKM=0.06). To our surprise, *Eva1c* expression was 208-fold enriched in floor plate tissue compared to the dorsal spinal cord (floor plate FPKM=23.0, dorsal spinal cord=0.110, false discovery rate-adjusted $P=1.05\times10^{-4}$). Despite its high enrichment, *Eva1c* was not part of the top 23 candidates considered earlier because of its low expression relative to the top expressers (Fig 4.8A). To verify this *in silico* result, we conducted an *in situ* hybridization of *Eva1c*. Significant expression was detected in the floor plate (Fig 4.8B). Taken together, these data suggest that neuronal expression of Eva1c is not conserved from *C. elegans* to mouse.

Figure 4.8 Characterization of Eva1c in midline guidance

(A) The gene expression level within the floor plate of all differentially expressed genes was plotted against their relative fold enrichment compared to DSC. For survey purposes, the black curve denotes the boundary that separates most of the top 23 'candidates' considered for further analysis from low expressers. Genes were color coded by their annotation of cell localization in the Uniprot database and summarized in the key (see Fig 4.4B). *Eva1c* was not in the list of top 23 genes, and was therefore not part of the initial *in situ* validation screen as shown in Fig 4.5. **(B)** Fluorescent *in situ* hybridization of *Eva1c* on E11.5 spinal cord sections confirmed gene expression within the floor plate. **(C-D)** Eva1c-AP was added to spinal cord explants cultured in 2D (with floor plate, fp). D, dorsal. The presence of purple precipitate indicates where AP activity was detected. Panel (C) shows no AP activity was detected with AP protein alone as a negative control, panel (D) shows AP activity detected across axons (D') and the explant with Lgi3-AP. **(E)** Slit1- and Slit2- AP were added to COS cells overexpressing EGFP (negative control), Eva1c, Robo1 and Robo2 (positive controls). Slit binding was not detected with Eva1c. **(F)** A mutant mouse line harboring a 19 basepair deletion (red) within the CDS of exon 1 of *Eva1c* was isolated after CRISPR/Cas9 gene editing in zygotes. **(G)** Spinal cord sections of control and *Lgi3*$^{-/-}$ from E12.5 embryos were stained for Robo3. No gross defects were detected: The ventral commissure size appeared similar, and the trajectories of Robo3-axons were comparable between wild-types and mutants.

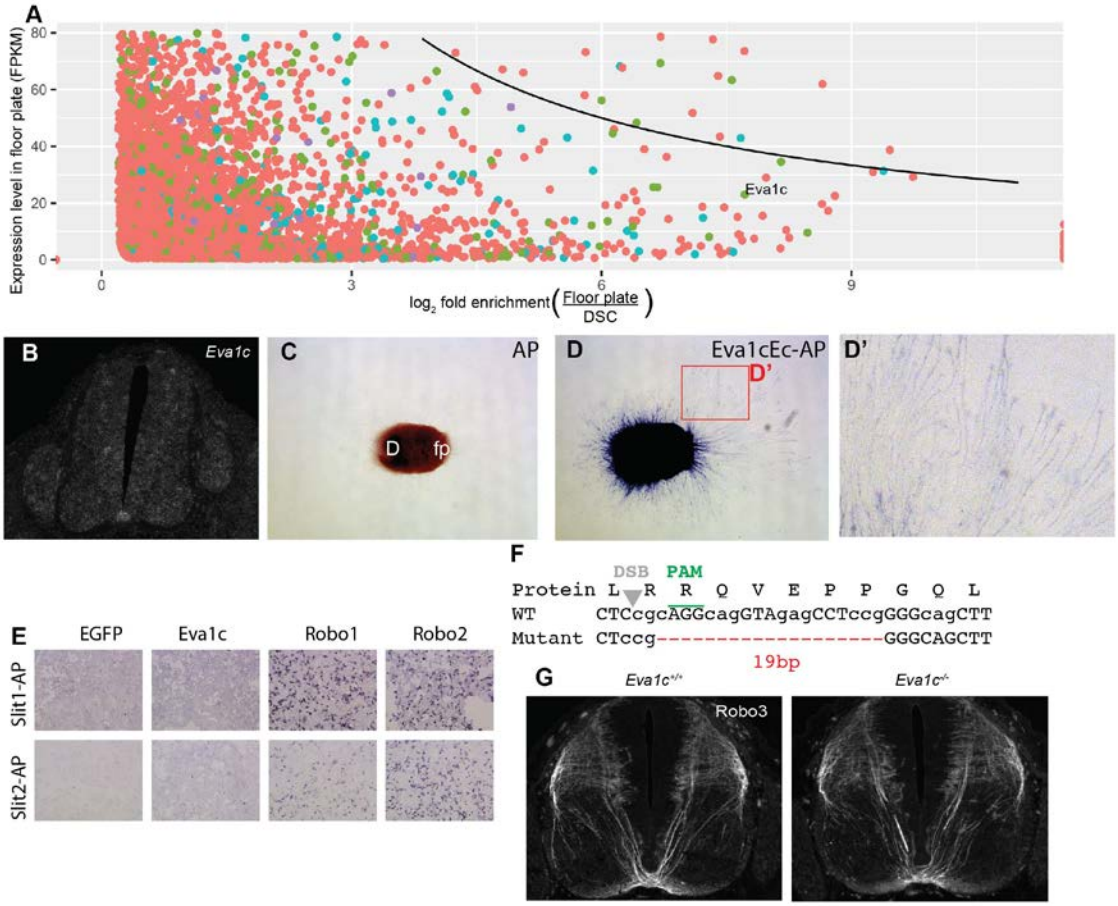
A
Expression level in floor plate (FPKM)
80
60
40
20
0
0
3
6
9
Eva1c
log2 fold enrichment (Floor plate / DSC)
B
Eva1c
C
AP
D
fp
D
Eva1cEc-AP
D'
D'
E
EGFP
Eva1c
Robo1
Robo2
Slit1-AP
Slit2-AP
F
DSB
PAM
Protein L R R Q V E P P G Q L
WT CTCcgcAGGcagGTAgagCCTccgGGGcagCTT
Mutant CTccg----------GGGCAGCTT
19bp
G
Eva1c+/+
Eva1c-/-
Robo3

To gain insight into which cells in spinal cord explants are influenced by Eva1c, we cloned and expressed the ectodomain of Eva1c protein fused to alkaline phosphatase (Eva1cEc-AP) in COS cells, and examined Eva1cEc-AP binding to spinal cord explants. Eva1cEc-AP binding was ubiquitous across cell bodies and axons (Fig 4.8C and D), indicating extensive Eva1c protein interactions.

Eva-1 is a Slit receptor in *C. elegans* (Fujisawa et al., 2007). To determine whether this function is conserved in mammals, COS cells expressing full-length Eva1c were generated and binding of Slit1-AP and Slit 2-AP fusion proteins was examined. We failed to detect binding of Slits to Eva1c (Fig 4.8E), suggesting that mammalian Eva1c has lost its ability to bind to Slits. Instead it must interact with other substrate(s) that is/are present on mouse axons *in vitro*.

Using CRISPR/Cas9, we generated a novel *Eva1c* mouse mutant harboring a frameshift mutation within the coding sequence of exon 1 in order to examine an *in vivo* role for *Eva1c* in axon guidance (Fig 4.8F). The size of the ventral commissure and the number of commissural axons misprojecting into the motor column were comparable between wild-type and *Eva1c*$^{-/-}$ embryos (Fig 4.8G). Therefore, no gross defects were observed in *Eva1c*$^{-/-}$ E12.5 embryos. Taken together, the data presented here suggests that Eva1c does not play a major neuronal role in midline guidance and is divergent from C. elegans *Eva-1*. It could require further phenotypic analysis in older mouse embryos when more axons have crossed the midline to definitely rule out any post-crossing guidance defects mutants might possess.

Conclusions

We have characterized the transcriptome of spinal commissural neurons and the floor plate in the developing mouse spinal cord. The high throughput RNA-Seq dataset allowed us to explore the possible roles of several relatively uncharacterized genes in the context of midline guidance. In commissural neurons, we identified *Dner, Rgmb, Thsd7a* and *Kif26b* as interesting candidates, and showed that Thsd7a protein binds to axons. In the floor plate, we identified *Lgi3, Adamts16* and *Eva1c* as interesting candidates, and showed that Lgi3 and Eva1c proteins binds to both axons and floor plate. However, we were unable to find obvious midline guidance phenotypes when these genes were mutated in either newly generated or existing mouse models. More fine-scaled analyses of phenotypes have to be done before we can conclusively rule out a role of these genes in midline guidance (see Discussion). The transcriptomes characterized in this Chapter have proven a useful starting point to test either new or evolutionarily-related hypotheses in midline guidance of the developing mouse spinal cord.

Chapter 5. Discussion

Floor plate-derived Netrin-1 is essential for midline guidance

Recently, two groups asserted that floor plate-derived Netrin-1 is dispensable for midline guidance (Dominici et al., 2017; Varadarajan et al., 2017). If that is indeed true, then the number of commissural axons reaching the midline, as well as the trajectory of commissural axons, should be similar in controls and floor plate-specific *Netrin-1* deletion mutants. However, significantly fewer axons reach the midline in floor plate-specific *Netrin-1* deletion mutants (Fig 2.2B). Furthermore, commissural axons in these mutants inappropriately invade the motor column and ventral funiculus, and display an aberrant "U-shaped" trajectory (Fig 2.3B and G). These data directly contradict the assertion that floor plate-derived Netrin-1 is expendable. The lack of quantification and the severe phenotype in ventricular zone-derived *Netrin-1* mutants in the recent studies by Dominici et al., 2017 and Varadarajan et al., 2017 likely led them to overlook the less severe, but still clear and statistically significant, 30.8% reduction in ventral commissure size that we observed. Indeed, as mentioned, the defects we observed can be seen in the images by these authors, who missed the phenotypes.

Evaluating the reduction in ventral commissure size as a measure for axon guidance defects

The reduction of the ventral commissure size is an established measure that reflects the loss of Netrin-1 attraction for commissural formation, and has been shown in *Netrin-1, Dcc* and *Neo1* mutants. Consistent with Netrin-1, Dcc

and Neo1 mediating midline attraction, commissural axons are observed wandering before reaching the midline (Serafini et al., 1996 and Xu et al., 2014). Similarly, we show here that the reduced ventral commissure in floor plate-specific *Netrin-1* mutants is associated with misprojections around the motor column. To more directly prove that the ventral commissure size is an accurate predictor of the number of axons at the midline, it will be important for future studies to enumerate the number of axons within the ventral commissure using electron microscopy. Future studies should also consider additional axon guidance-independent roles of Netrin-1, and in particular, whether Netrin-1 controls defasciculation of the ventral commissure. This can be addressed by comparing the axon density of the ventral commissure of control and floor-plate specific *Netrin-1* mutants under the electron microscope. It has also been proposed that Netrin-1 acts as an anti-apoptotic factor by binding to Dcc and Unc5 homologs that act as “dependence receptors” (Mehlen et al., 1998; Llambi et al., 2001; Mehlen and Guenebeaud, 2010), as is the case in the developing olfactory epithelium (Kam et al., 2016), and the decrease in ventral commissure size could be due to fewer surviving commissural neurons. However, this possibility has been ruled out in the developing spinal cord by analyzing the number of apoptotic cells in *Netrin-1*$^{-/-}$ mutants (Bin et al., 2015). Netrin-1 might also be required for the proper cell fate specification and early patterning of the spinal cord, although this has also been ruled out by analyzing progenitor and postmitotic markers in *Netrin-1*$^{-/-}$ mutants (Bin et al., 2015).

Netrin-1 maintains the integrity of the CNS

Netrin inhibits premature dorsal root ganglion (DRG) axons from entering the CNS (Watanabe et al., 2006; Masuda et al., 2008), and also prevents commissural axons from exiting into the periphery (Laumonnerie et al., 2014). Aberrant projections in the CNS of *Netrin-1*$^{-/-}$ (Fig 2.4 and Bin et al., 2015), *Netrin-1*$^{gt/gt}$ *Shh*^{Cre}*;Netrin-1*$^{fl/fl}$ (Fig 2.4) and possibly ventricular zone-specific *Netrin-1* deletion mutants originate from the DRG. Thus, Netrin-1 does not function to prevent commissural axons from growing around the ventricular zone as proposed by Varadarajan et al.,2017, but rather maintains the integrity of the CNS.

Relative tissue-specific contributions to the Netrin-1 gradient

Taken together with the evidence recently presented by two other groups that ventricular zone-derived Netrin-1 is required for midline guidance (Dominici et al., 2017; Varadarajan et al., 2017), we continue to favor a model in which floor plate-derived and ventricular zone-derived Netrin-1 collaborate to establish a proper Netrin-1 gradient. Inspired by the use of tissue-specific conditional *Netrin-1* deletion mutants, we are motivated to address questions that have been raised previously (Kennedy et al., 2006): What is the quantitative contribution of the floor plate and ventricular zone to the Netrin-1 gradient? How much does Netrin-1 diffusion versus local production contribute to the gradient? A head-to-head comparison of these two sources of Netrin-1 could be carried out using ventricular zone-specific *Netrin-1* mutants and floor plate-specific *Netrin-1* mutants. Understanding the phenotypes of these two mutants both quantitatively

and qualitatively will help clarify the common, and the specialized, roles of Netrin produced by the floor plate and ventricular zone in mediating midline attraction.

Floor plate-derived Netrin-1 has long-range effects in the developing spinal cord

The chemotropic axon-orienting activity of a floor plate-derived diffusible cue (later found to be Netrin) is ~150-250 μm (Placzek et al., 1990). In chick, the floor plate is the sole source of Netrin-1 in the spinal cord and the Netrin-1 gradient is distributed across 250 μm (Kennedy et al., 2006). Visualizing the gradient of floor plate-derived Netrin-1 in the mouse is confounded by ventricular zone production of Netrin-1. However, loss of floor plate Netrin-1 causes disorganization of commissural axons around the motor column at a considerable distance (but within 250 μm) in *Shh^{Cre};Netrin-1$^{fl/fl}$* embryos. This argues that floor plate Netrin-1 functions to orient commissural axons at a distance even before axons reach the ventral commissure, and that ventricular zone Netrin-1 is not sufficient to properly guide axons. Netrin-1 therefore exerts long-range effects at-a-distance.

The “canonical model” that the papers challenge is that floor plate-derived Netrin-1 attracts axons from the most distant reaches of the dorsal spinal cord (see Fig. 4Q in Varadarajan et al., 2017). However, the canonical model never proposed that Netrin-1 functions over this distance. Instead, previous work demonstrated that the range for long-range attraction of Netrin-1 is only ~150-250 μm (Placzek et al., 1990). The canonical model predicts that “at least one role for the chemoattractant [now identified to be Netrin-1] may be to direct axons

that have to grow to the ventral midline through the cellular environment of the motor column" (Colamarino and Tessier-Lavigne, 1995). Consistent with this model, we find that the loss of floor plate-derived Netrin-1 causes commissural axons to project through the motor column instead of avoiding it, and the subsequent loss of separation of precrossing axons from postcrossing axons in the ventral funiculus (Fig 2.3). The misprojections in the motor column have been previously reported in *Netrin-1*$^{gt/gt}$ mutants as well (Xu et al., 2014) and further verified in this study (Fig 3.3I-J). The original model indeed has correctly predicted Netrin's crucial guidance role around the motor column and not the ventricular zone.

In contrasting the proposed "growth substrate model" (Dominici et al., 2017 and Varadarajan et al, 2017) with the "canonical model", the long-range action of Netrin-1 has been mistakenly pitted against its short-range action. Both Dominici et al., 2017 and Varadarajan et al., 2017 appropriately cite developmental systems in support of the short-range action of Netrins (Timofeev et al., 2012; Akin and Zipursky, 2016). However, these studies were performed on a different cell type that might have different adaptations to Netrin signaling when compared to the developing mouse spinal cord, where we show long-range effects of floor plate Netrin-1. It is also worth noting that long- and short-range modes of Netrin action are not mutually exclusive. Co-existence of short- and long-range Netrin actions has been shown in *C. elegans* (Wadsworth et al., 1996; Adler et al., 2006) and *Drosophila* (Brankatschk and Dickson, 2006). We show here that floor plate-derived Netrin exerts long-range attractive effects on

commissural axons even before they reach the midline. Taken together with the data that ventricular zone Netrin exerts short-range attractive effects (Dominici et al., 2017; Varadarajan et al., 2017), Netrin-1 has both short- and long-range effects in the developing spinal cord.

Netrin-1 has haptotactic modes of action and travels from its site of production

The “canonical model” of Netrin-1 acting “simply as a soluble cue” (Dominici et al., 2017) that Dominici et al., 2017 and Varadarajan et al., 2017 question, has never been the proposed mode of Netrin action. As originally proposed upon their discovery, Netrins are diffusible. However, because of their avid binding to the cell surface and extracellular matrix, Netrin can become partially immobilized and function haptotatically (Kennedy et al., 1994; 2006). Indeed, in the case of the optic nerve head, it has been proposed that the extent of Netrin’s action depend on the balance of Netrin production versus binding sites that capture Netrin and prevent it from spreading (Deiner et al., 1997). Netrin-1’s diffusibility and subsequent enrichment in membranes *in vivo* is confirmed by (1) the ability of floor plate-derived Netrin-1 to contribute to Netrin-1 immunoreactivity in the ventral pial surface (Fig. 2.5C-D) and (2) the presence of Netrin-1 immunoreactivity in the ventral commissure despite the lack of Netrin-1 expression in the floor plate of *Shh^{Cre};Netrin-1$^{fl/fl}$* mutants (Fig 2.5A-B and see Fig 1M by Varadarajan et al., 2017). These data contradict the assertion by Dominici et al., 2017 and Varadarajan et al., 2017 that Netrin-1 is confined to its source of production. Consistent with the biochemical characteristics of Netrins (Kennedy

et al., 1994), Netrin-1 can be simultaneously soluble, diffusible and haptotactically exert long-range guidance functions.

The canonical model of Netrin-1 in midline guidance revisited

Given that the majority of Netrin-1 is enriched at particular regions of the spinal cord, we favor a model whereby Netrin-1 functions haptotactically by first diffusing to predefined regions in the spinal cord where it is immobilized. Given the solubility of Netrin-1 and its ability to exert long-range effects, Netrin-1 may still function in solution, so we find that it premature for Dominici et al., 2017 and Varadarajan et al., 2017 to rule out a major role for Netrin-1 in mediating midline guidance chemotactically.

In contradiction to the assertion that Netrin has only local, short-range, haptotactic guidance effects in the spinal cord, we show that floor plate-derived Netrin-1 can diffuse from its local source to exert long-range effects on commissural axons. Our findings are consistent with the “canonical model” (Colamarino and Tessier-Lavigne, 1995) which has successfully predicted that Netrin-1 functions at a distance to guide commissural axons around the motor column. The work here represents the first step in determining to what extent Netrin-1 acts at-a-distance or locally from the floor plate and other sites of expression in mammals, as Netrins do in invertebrates.

Dcc and Neo1 mediate Netrin-dependent midline attraction

Despite recognition that Netrin-1 is a key guidance cue required for the wiring of vital brain circuitry, how different levels and combinations of Netrin receptors influence Netrin-1 signaling and, ultimately, neuronal responses remain

incompletely understood. It is well known that Dcc is a receptor that mediates Netrin-1 chemoattraction in commissural axons (Keino-Masu et al., 1996; Fazeli et al., 1997). We have also shown that Neo1 receptors also play a role in Netrin-mediated midline guidance (Xu et al., 2014), but we were unable to ascertain at that time whether or not additional Netrin-1 receptors exist because the *Netrin-1* and *Neo1* alleles available at that time were hypomorphs. Using null alleles, we show for the first time that the severity of *Dcc*$^{-/-}$*;Neo1*$^{-/-}$ mutants phenocopies that of *Netrin-1*$^{-/-}$ mutants, demonstrating that in this system, Dcc and Neo1 mediate a majority, if not all, of Netrin-1 attraction.

Population-specific mechanisms for midline attraction

Here, we show that axons of two discrete populations of commissural neurons are guided to the midline by Netrin-1 mediated attraction. However, they utilize distinct combinations of Netrin-1 receptors to achieve this shared outcome. Our *in vivo* and *in vitro* data show that Dcc and Neo1 are differentially expressed by commissural neurons in the developing spinal cord. Whereas the dorsal population expresses higher levels of Dcc, the ventral population expresses Neo1 to a greater extent than neurons located more dorsally. Both Dcc and Neo function in midline attraction, which helps explain why single receptor mutants have guidance defects that are less severe than those observed in mice lacking the guidance cue that activates these receptors, Netrin-1.

Dcc is not required for midline attraction for the ventral population, but this is only true at a later stage (E12.5 but not E11.5). The developmental delay observed in the ventral population could reflect a role of Dcc in regulating the rate

of axon extension, which is the case with thalamocortical axons *en route* to the ventral telencephalon (Castillo-Paterna et al., 2015). If this is true, it would suggest that despite having the shared property of having Netrin-1 as a ligand, Dcc and Neo1 diverge in their ability to regulate the rate of axon extension of spinal commissural axons. This would be consistent with the observation that at E11.5, the guidance of ventral axons is affected in *Dcc*$^{-/-}$ but not *Neo1*$^{-/-}$ mutants. Alternatively, the delay could also reflect the additional time that is required to restore total Netrin-1 receptor levels in *Dcc*$^{-/-}$ mutants, possibly through a compensatory increase in Neo1 expression. Future studies will have to confirm if this increase in Neo1 expression within the ventral population occurs at a mRNA transcript level and/or a protein level.

Molecular correlates of differential Netrin-1 sensitivity: Receptor isoforms and modulators of Neo1 signaling

The dorsal and ventral populations have unique Netrin-1 receptor expression profiles. This may provide the molecular basis for the differential Netrin sensitivity of these two populations, as well as contrasting effects in *Netrin-1*$^{gt/gt}$ animals. The affinity of Netrin-1 for Dcc and Neo1 is similar (Xu et al., 2014). Therefore, the greater Netrin-1 sensitivity of the dorsal population may reflect a different receptor architecture upon Netrin-1 binding. The energetics of the receptor-Netrin-1 continuous monomeric assembly or the 2:2 heterotetramer is determined by which isoform(s) of Dcc is expressed (Xu et al., 2014). We find that the *Dcc/Neo1*$_{short}$ predominates in the dorsal population, whereas the Dcc/*Neo1*$_{long}$ isoform is dominant in the ventral population. It has been reported

that the *Dcc*$_{long}$ splice variant is crucial for proper guidance, at least in the dorsal population (Leggere et al., 2016). However, several questions remain unanswered: How does the balance of splice variants affect Netrin-1 receptor assembly at the growth cone? How do these complexes differ in their ability to transduce Netrin-1 attraction?

Another possible molecular correlate of Netrin-1 sensitivity is RGMb, which is expressed at higher levels in the dorsal population. Neo1's unique ability to flexibly signal attraction with Netrins (Wilson and Key, 2006; Xu et al., 2014) and repulsion with the RGM family members (Rajagopalan et al., 2004) sets it apart from Dcc. RGMs interact with a loop in FNIII 5 and the FNIII 6 domain of Neo1, thereby forming a 2:2 heterotetramer (Bell et al., 2013). Neo1 shares 50% amino acid homology with the more well studied Dcc receptor (Vielmetter et al., 1994). However, the specificity of RGM binding for Neo1 (Rajagopalan et al., 2004; Zhang et al., 2005) can be explained by lack of conservation of the interacting FNIII 5 domain loop in Dcc (Bell et al., 2013).

It is unclear if, and how, Netrin-1 and RGMb compete with each other for binding to Neo1. Both ligands are present in the developing spinal cord and the FNIII 5 domain of Neo1 is involved in binding to both Netrin and RGMs. This competitive binding forms the basis of our model of differential Netrin-1 receptor dependence in distinct neuronal populations (Fig 3.11). Consistent with our model, Netrin suppresses RGMa-mediated growth cone collapse in dorsal root ganglion axons (Conrad et al., 2007).

Given that RGMb expression is greater in dorsal commissural axons and Neo1 is greater in ventral axons, RGMb is likely to signal in *trans*, i.e. RGMb expressed on dorsal axons present themselves to its receptor, Neo1 that is expressed at higher levels on the ventral axons. How this non-cell autonomous interaction between RGMb and Neo1 modulates Netrin-1 chemoattraction within the ventral population should become clearer by analyzing *Rgmb* mouse mutants. Despite several attempts, we were unable to gain access to this published mouse line.

RNA-Seq transcriptomes provide a useful starting tool for identifying and verifying candidate guidance factors

The transcriptome of both commissural neurons and floor plate provides unprecedented detail into possible midline guidance factors. For example, the list allowed us to identify RGMb as a potential modulator of Neo1 signaling. Coupled with AP protein binding assays and CRISPR/Cas9 technology, the transcriptome offers an invaluable starting point to test the properties and *in vivo* guidance roles of potential guidance factors.

The transcriptome analysis was informative because it allowed us to compare the expression of guidance factors that are already described in other animal models and determine if their functions are evolutionarily conserved. For example, based on the axonal localization of Eva1c protein in mice, Eva1c was thought to function as a Slit-receptor for commissural axons (James et al., 2013), a role that has remained evolutionarily conserved from *C. elegans* (Fujisawa et al., 2007; Chan et al., 2014). However, floor plate-specific *Eva1c* expression and

lack of a detectable midline crossing phenotype in *Eva1c*$^{-/-}$ mutants argues against this model. Eva1c binds to neurons (Fig 4.7D) and Eva1c protein is detected mostly on axons in mice (James et al., 2013), raising the interesting possibility that transmembrane floor plate-derived Eva1c is cleaved, secreted and presented as a guidance cue to commissural axons rather than acting as a cell-autonomous signal-transducing receptor in axons. However, the precise role *Eva1c* plays in mice remains to be defined.

Several candidate mutants characterized in this study, including *Dner, Kif26b, Lgi3, Adamts16* and *Eva1c*, did not demonstrate a gross guidance phenotype. Proteins such as Lgi3 and Eva1c bind to axons *in vitro*, so we find it unlikely that these cues do not at the very least modulate axon guidance. It will be important to ascertain that these knockouts generated by CRISPR/Cas9 are true loss-of-function mutants by ruling out the possibility that there are unintended exon skipping events that result in mRNA that encode for fully or partially functional proteins (Kapahnke et al., 2016; Lalonde et al., 2017). It is also possible that subtle defects were missed in this analysis, and before completely ruling out a role for these genes in midline guidance, it will be important to conduct fine-scale analyses of guidance phenotypes. For example, a DiI lipophilic tracer can be used to trace individually misguided axons that could potentially reveal stalled growth cones within the floor plate (Gore et al., 2008) or post-crossing misprojections (Zou et al., 2000). Even if these fine-scaled analyses do not yield guidance phenotypes, this may not be surprising, as the floor plate has a number of other developmental functions, in addition to guiding

commissural neurons. The floor plate establishes several dorsoventral gradients that specify various neuronal and glial identities (Placzek and Briscoe, 2005). It is also important for repelling motor axons away from the midline (Bai et al., 2011).

Concluding remarks

We have consolidated evidence to support and reaffirm the canonical model of Netrin in midline guidance. We also discovered how distinct commissural axon populations utilize two receptors, Dcc and Neo1, in different ways to reach the midline, which potentially could explain the disparity in phenotypic severity between genetic deletion of the guidance cue Netrin and single cognate receptors. Potential modulators of Netrin signaling were also identified in the transcriptomic analysis, along with a full repertoire of potential guidance candidates for further analysis. At a more general level, future studies that follow the line of inquiry this thesis has taken will continue to help us appreciate how a single chemotactic cue, Netrin-1, is used by distinct neuronal populations that express unique sets of receptors, receptor isoforms and modulators to achieve identical guidance outcomes (i.e. accurate midline guidance) during neural circuit formation.

Chapter 6. Materials and Methods

Mice

Animals were bred and used according to IACUC protocols at The Rockefeller University. The use of various mutant mouse lines used in this study have been described previously: *Netrin-1*$^{flox/flox}$ (Brunet et al., 2014), *Netrin-1*$^{gt/+}$ hypomorph (Serafini et al., 1996), *Dcc*$^{+/-}$ (Fazeli et al., 1997), *Dner*$^{+/-}$ (EM:08394) (Skarnes et al., 2011), *Kif26b*$^{+/-}$ (JAX 022085) (Skarnes et al., 2011), *Shh*^{Cre} (JAX 005622) (Harfe et al., 2004), *Neo1*$^{+/-}$ (Kam et al., 2016), *Neo1*$^{gt/+}$ (Bae et al., 2009), *Thsd7a*$^{+/-}$ (KOMP, JAX 027218), transgenic Math1:Cre (JAX 011104) (Matei et al., 2005), transgenic Neurogenin3:Cre (JAX 006333) (Schonhoff et al., 2004), transgenic Neurogenin1:mCherry (a kind gift from Dr. Jane Johnson), Dbx1$^{Cre/+}$ (Bielle et al., 2005), transgenic Sim1-Cre (a kind gift from Dr. Hongkui Zeng from The Allen Brain Institute), and the tdTomato Cre-expression reporter *Rosa26*$^{Ai14/Ai14}$ (JAX 007908) (Madisen et al., 2010).

To generate a colony harboring a Netrin-1 null-allele (*Netrin-1*$^{+/-}$), *Netrin-1*$^{flox/flox}$ mice were crossed with a EIIA-Cre mice that expresses Cre in the germline (Lakso et al., 1996).

Genotyping of embryos (with the exception of the *Netrin-1*^{gt} allele) were done using genomic DNA extracted from tail tissues according to the manufacturer's instructions (Sigma, Extract-N-Amp), and the PCR primers used for each mouse line have been previously described according to published protocols. For genotyping of the *Netrin-1*^{gt} allele in the transgenic Math1 and

Neurog3 colonies, fresh tail and hindlimb tissue was incubated for 1 hr with shaking in 1 mL of X-gal reaction solution (1 mg mL^{-1} X-gal previously dissolved in dimethyl formamide, 2.12 mg mL^{-1} potassium ferrocyanide, 1.64 mg mL^{-1} potassium ferricyanide, 2 mM $MgCl_2$, 0.01% deoxycholate, 0.02% NP-40, 100 mM sodium phosphate, pH 7.3). The intensity of dark blue precipitate was used to estimate the number of *LacZ gene-trap* alleles that are present. For genotyping of the *Netrin-1^{gt}* allele in other non-Cre colonies, the DNA was extracted from the tail and hindlimb tissue according to the manufacturer's instructions (Qiagen, DNEasy blood and tissue kit). These genomic extractions were used as template for a copy number variation qPCR analysis using TaqMan *LacZ* (Mr00529369_cn) as a target probe and *Tfrc* as a reference probe according to the manufacturer's instructions (Applied Biosystems).

Robo3^{Cre} mutant mice were generating using the strategy as detailed in Fig 4.1A by standard recombineering techniques. ES cell clones were generated by using standard techniques at the Gene Targeting facility at the Rockefeller University. ES cell clones were screened by Southern blotting with ^{32}P DNA probes generated by Prime-It II random primer labeling kit (Agilent). Correctly targeted ES cells clones were injected into B6 blastocysts at the Transgenic Services Laboratory at The Rockefeller University. The frt-flanked neomycin cassette was removed by crossing germline-transmitted *Robo3$^{Cre\text{-}Neo/+}$* mice with a FLP deletor strain (JAX 009086) (Farley et al., 2000). For genotyping of *Robo3^{Cre}*, the allele was detected by PCR (primer sequences: wild-type ctgcgctacctgcttaaaacacta, mutant atcataatcagccataccaca, common reverse

primer ctgccagcgaggagttgaag) from genomic DNA, with the wild-type and mutant amplicon size is 112 base pairs and 335 base pairs. The *Robo3*$^{Cre/+}$ colony was maintained on a C57BL/6 background.

Mutant E11.5 embryos were harvested from pregnant heterozygote dams crossed to heterozygote males, with E0.5 used as the day of the vaginal plug.

Histology and immunohistochemistry

Mouse embryos were harvested, fixed in PBS/4% PFA overnight at 4°C, briefly washed in PBS, and cryopreserved in PBS/10% sucrose for at least overnight at 4°C. Embryos were embedded in gelatin-sucrose, and 20 μm sections were cut on a cryostat. Sections were then permeabilized in PBS/0.1% Triton-X, and blocked with 3% donkey serum in PBS/0.1% Triton-X for at least 1 hour at room temperature. The following primary antibodies were used: polyclonal goat anti-human Robo3 (1:500, R&D), monoclonal mouse neuron-specific class III β-tubulin (TuJ1, 1:2000, Covance), monoclonal rat anti-L1 (1:1000, Millipore), monoclonal rat anti-neurofilament M (NF, 1:1000, DSHB 2H3) (Dodd et al., 1988), polyclonal goat anti-TAG-1 (1:500, R&D), polyclonal rabbit anti-Netrin-1 (Abcam, ab126729), (Bin et al., 2015), polyclonal rabbit anti-Hb9 antibody (1:10,000) (Thaler et al., 1999), polyclonal goat anti-mouse DCC (1:500, R&D), polyclonal goat-anti human Neo1 pre-adsorbed to E13.5 *Neo1*$^{-/-}$ embryos (1:500, R&D), polyclonal rabbit anti-RFP (1:1000, Rockland Immunochemicals), polyclonal sheep anti-RGMb (1:500, R&D). For Netrin-1 immunostaining, antigen retrieval was done prior to blocking by boiling in citrate buffer (pH 6.0) briefly in the microwave (adapted from Bin et al., 2015). Alexa 488, 568 or 647 secondary

antibodies (1:500-1:1000, Invitrogen) were used. Hoechst staining was done at 1:10 000. Sections were mounted in Fluoromount G (Electron Microscopy Sciences) and then examined with a fluorescent microscope (Eclipse 90i, Nikon) coupled to a Nikon QiMc camera.

Image processing and quantification

Quantification of Robo3-stained ventral commissural bundle size normalized to spinal cord length (defined as the distance between the roof plate and the base of the ventral commissure) were measured using ImageJ (Schneider et al., 2012) on at least 5 evenly spaced brachial spinal cord sections. *Netrin-1* control ratios were further normalized to 100%. One-way ANOVA analysis followed by Bonferroni post-test was performed to compare the mean normalized ratios across genotypes.

Quantification of Robo3^{+} aberrant axons in the motor column was done in ImageJ on at least 7 evenly spaced brachial spinal cord sections. For each section, the motor column area was traced manually using only Hb9 images, and the mean intensity of Robo3-staining was then measured in the motor column. The average background staining was then determined using the mean intensity of Robo3 in the ventricular zone (where no Robo3 expression is expected) of 1 section from each embryo of both genotypes, and this same value was equally subtracted from all datapoints. The average Robo3+ axon staining intensity was normalized to the mean from *Netrin-1* controls, which was defined as 100%. An unpaired t-test was performed to compare the mean Robo3+ staining intensity.

Quantification of the bilateral length of precrossing and crossing axons in the ventral commissure and ventral funiculus was done in ImageJ on at least 7 evenly spaced brachial spinal cord sections. An unpaired t-test was performed to compare the mean normalized length across both genotypes.

2D explant cultures

E11.5 CD1 mouse (Charles River) spinal cords were dissected in the open-book configuration as previously described (Keino-Masu et al., 1996) in ice-cold L-15 media (Gibco 11415) supplemented with 5% heat-inactivated horse serum (Gibco 26050). Explants were then cut and trimmed into ~200 μm segments longitudinally. These explants were then plated onto glass slides that were coated with 20 $\mu g\ mL^{-1}$ poly D-Lysine (Sigma, P6407) followed by 3 $\mu g\ mL^{-1}$ of recombinant human N-Cadherin (R&D Systems, 1388-NC), and cultured in growth media (0.5% methyl cellulose (Sigma M0512), 0.8% glucose, B-27 (Gibco), penicillin/streptomycin/glutamine (Gibco) in Neurobasal (Gibco)) in a 5% CO_2 humidified 37°C incubator for 16 hours. For receptor dynamics experiments in response to Netrin-1, recombinant mouse Netrin-1 (R&D 1109-N1-025) was added at the indicated concentrations to the culture media.

For immunohistochemical analysis of these 2D explant cultures, the same method was used as reported above with treatment of histological sections, with these exceptions: 0.2% Tween20 was used as detergent instead of Triton-X. An additional 1 hour 0.3M glycine in PBS/0.2% Tween-20 block at room temperature prior to the blocking step in donkey serum. The blocking step with donkey serum was also increased to 4 hours. Images were acquired using an inverted

fluorescent microscope (Eclipse Ti, Nikon) coupled to a Neo sCMOS camera (Andor Technology), and multiple images of whole explants were stitched with the software supplied by the manufacturer (NIS-Elements AR, Nikon).

3D explant cultures

Explants were dissected in the same manner as in 2D explant cultures. Explants were then cultured according to the standard procedure as described elsewhere (Xu et al., 2014).

RNA extraction for RT-PCR

The dorsal and ventral halves were dissected in ice-cold L-15 media (Gibco), and the tissues were protected in RNAlater stabilization solution (Qiagen) at 4°C until ready for RNA extraction. Total RNAs were extracted using the RNeasy Mini Kit (Qiagen) with a genomic DNA digest step. Total RNA was measured using a Nanodrop (ThermoScientific). The same amount of RNA from each sample was reverse transcribed with SuperScipt IV VILO (Invitrogen). All PCRs were performed using a StepOnePlus Real-Time PCR system (Applied Biosystems). 2 To verify equal loading, we measured the relative expression of the housekeeping gene by using a *gapdh* TaqMan probe (Applied Biosystems Mm99999915_g1), and found that all samples had the same C_T value (data not shown).

The relative isoforms of Dcc and Neo1 were generated using PowerUp Sybr Green (Applied Biosystems) to generate 2 isoforms of a gene in a single reaction well. The forward and reverse primers used for each gene were from (Leggere et al., 2016), except for *Dcc* forward: gagttctcattatgtaatctccttaaaagc. A

complete run with 40 cycles was first done to determine an appropriate cycle that ended within log amplification phase. A separate and final run using this cycle number was then done, and the PCR products from this reaction were then separated using PAGE (BioRad). Each sample was run in triplicate. Band densitometries were measured using ImageStudio Lite (LI-COR Biosciences), and subsequently normalized to their respective amplicon sizes.

Tissue dissociation and FACS sorting of *Robo3$^{Cre/+}$;Rosa26$^{Ai14/+}$* cells

Robo3$^{Cre/+}$;Rosa26$^{Ai14/+}$ E11.5 spinal cords from the same litter were dissected in the open-book configuration in ice-cold L-15 (Gibco), and cut into 4 smaller sections longitudinally. The tissue was pooled, then digested with half a vial of papain (Worthington, PAP2) with 1mM $CaCl_2$, DNAase (Worthington, D2) dissolved in 5 mL of HBSS-supplemented solution (HBSS (Gibco 14710), 0.3% glucose, 10mM HEPES) at 37°C for 7 minutes, with gentle mixing. The supernatant was replaced by a 5mL of 2.5mg mL^{-1} trypsin inhibitor (Sigma T6522) and 0.1% BSA in HBSS-supplemented solution (Sigma T6522). The suspension was triturated and filtered through a 70 μm nylon cell filter (Falcon). The cell suspension was resuspended to 10^6 cells mL^{-1} in 0.1% BSA in HBSS-supplemented solution (Sigma T6522) with DAPI added as a marker of cell death.

Cells were FACS sorted using a BD FACSAria Cell Sorter system at the The Rockefeller University Flow Cytometry Center. Sorting was gated according to TdTomato expression, and live cells were collected into vials containing lysis

buffer from the RNeasy kit (Qiagen). RNA extraction was immediately done using the RNeasy kit according to manufacturer's instructions (Qiagen).

RNA extraction of floor plate and dorsal spinal cord for RNA-Seq

Spinal cords from 3 C57BL/6 (JAX) E11.5 litters were dissected in the open-book configuration in ice-cold L-15 (Gibco), and floor plate tissue was separated from dorsal spinal cord. The tissues were protected in RNAlater stabilization solution (Qiagen) until ready for RNA extraction. Total RNAs were extracted using RNeasy Mini Kit (Qiagen) with a genomic DNA digest.

RNA library preparation

All RNA samples were verified on a Bioanalyzer Picochip, and had RNA integrity number of > 8.5 (Agilent). 100 ng total RNA of each sample was used as input material for cDNA library preparation using TruSeq RNA Sample Prep Kit v2 (Illumina). Libraries were prepared simultaneously to minimize batch variation. Libraries were multiplexed and sequenced on HiSeq 2500 (Illumina) at the Genomics Resource Center at The Rockefeller University to generate 30×10^6 of single-end 100 base pair reads per library.

RNA-Seq alignment and analysis

RNA-Seq reads were aligned to the GRCm38 (mm10) Reference genome. Read alignment, transcriptome alignment and differential analysis were done using the Tuxedo protocol as published (Trapnell et al., 2012). The RNA-Seq expression-enrichment plots were explored and graphed in R (R Core Team, 2017).

In situ hybridization

The generation of *Slit2* (Brose et al., 1999) and *Netrin-1* (Serafini et al., 1996) probes have been previously described. To generate the other probes used in this study, we obtained cDNA library clones of target genes (Dharmacon). Then, we used gene-specific primer sequences (Table 3) with T7 and T3 promoters incorporated into the 5' ends of the forward and reverse primer respectively, so that upon amplification, the PCR product is flanked by T7 and T3 promoters. Digoxigenin-11-D-UTP (DIG)-labeled probes were then generated by *in vitro* transcription with DIG RNA labeling mix (Roche).

The *in situ* hybridization of *Netrin-1* and detection with colorimetric alkaline-phosphatase activity was done according to standard procedures as described previously (Marillat et al., 2002).

Fluorescence *in situ* hybridization was done on embryos lightly fixed for 30 minutes in 4%PFA/1X PBS at room temperature, and samples cryoprotected with 10% sucrose/1X PBS overnight at 4°C. They were embedded in gelatin-sucrose, frozen and 14 μm sections were made. Glass slides containing these sections were post-fixed for 10 minutes, rinsed three times in PBS, then acetylated for 8 minutes. The slides were washed for 30 minutes in PBS/0.5% Triton-X, followed by 3 rinses in PBS. Sections were pre-hybridized for 2 hours at room temperature in hybridization solution (50% formamide, 5X SSC, 5X Denhardt's solution, 0.5mg mL^{-1} salmon testes DNA, 0.24 mg mL^{-1} baker's yeast tRNA), then with a coverslip with DIG-labeled riboprobe in hybridization solution overnight at 72°C in a humidified chamber. The next day, sections were dipped into a 5X SSC

solution at 72°C, then 0.2X SSC at 72°C for 90 minutes. The slides were cooled to room temperature and blocked with TNB solution (0.5% TSA blocking reagent (PerkinElmer), 100mM Tris HCl pH7.6, 0.15M NaCl). Sections were incubated for 1 hour with 1:500 anti-DIG HRP antibody (Roche) in TNB. Slides were washed five times with TNT buffer (0.1% Tween 20, 100mM Tris HCl pH7.6, 0.15M NaCl). DIG signal on sections were amplified using the TSA Cy3 system for 10 minutes exactly according to manufacturer's instructions (PerkinElmer). The reaction was quenched using 1% NaN_3 in TNT buffer for 10 minutes, then washed five times for 5 minutes in TNT buffer. For further TdTomato staining, sections were first blocked in 3% donkey serum in PBS/0.1% Triton-X, and the subsequent steps as according to the standard procedure (See section on Histology and Immunohistochemistry).

Table 3 Primers used to generate *in situ* probes

Gene	Forward primer	Reverse primer
Sst	ggagacgctaccgaagccgtcgctgctgc	cataatctcaccataattttattttgtat
Dner	tgactcccattgcctacgaggattacagt	cctcgacctgctaacgtttattcaatatt
Dlk1	tggctttcttcccgctggacgcccgtgc	cccgatgtcggtgcagacgccatcgttct
Rtn1	aatcccgcccagagccatcgtctggagat	tagcaacacgaaatcaaaaaccacatcta
Lamp5	cgcctacacactcagaatgctctttgtaa	caagacatgccttccatccctgggtttaa
Rgmb	tgaggtccttccgatccacgcacgtcga	ggtgcctatgtagcgggcatgcatctcta
Tmeff2	gagaacaccacataccttgcccagaacat	tgcattttattttgagccacaaaacactt
Thsd7a	agaattttgttggattgtcccaggaaaag	gcaaggattttagttttagtcttcctttg
Chl1	cctttgccccagtgatccagctttaggag	actggatatgtggagttggtaggccctcc
Nxph4	gtgagcacccctactttggataacgcccc	ggatttcgctttattttgttccctccccg
Nms	ctctggaccctcgggaaatgctcatcacc	gttcgattgttccatgcccaaatcagtaa
Nrn	gccttcccagtgcataaagtctctgtcgc	caggatttcccacaatcccatatgagtgt
Crmp	cctcagatgagccagatatgcaagagtgaa	cacaagctttgaattcagaaataagagcc
Mab21l2	gcaaacctcagagtgcgctgcggcctga	gatcttgcgcgcagaaaggtagccagacg
Mtus2	gagcgaaagagcccttgcgaaagaaaagg	gtggacaccagactctgctgcttacacct
Cartpt	cagaaccatggagagctcccgcctgcggc	gatgtcaaatcttttattttgaagcaaca
Skor2	gtgcctggcgcagatctccaacactcttc	ccttgacggaactgagtgggtgacaggcc
Kif26b	ttggggaaccattcgaaattaaagtctatg	gacagttaacatttattcagctgcaatacc
Dcn	ttgggcaaaatgacttctgccgagctgga	tagagttcggcggcatttgactttatgtc
Adamts16	taactctgatgtgcatggtggaatcgctg	agaaatgctgcttttgtgaggggccaaga
Pdyn	ggcttttgcgcaaataccccaagaggag	gtttctctggattctgggatgggcaggga
Metrnl	ccgccgccaccgctgctgttgctgctactac	aaggggtcagagcagcatgtaccttcccag
Vtn	atggcacccctgaggccctttttcatactag	ctacttctcagaggtcgggcagcccagcca
Ccdc3	acggtggtccaggactactcttatttcttc	ttggaaacatgagtgatgaaatatggtatg
Lgi3	ttctgctacatgcctgctggagatgcccag	ttggctgatttttttttatatatccagtca
Anxa2	atgtctactgtccacgaaatcctgtgcaagc	tcagtcatccccaccacacaggtacagcag
Bmp1	taaagctgactttcgtggagatggatattg	ctttctgtttattggctggggtgccctggt
1190002N15Rik	cattccgtgctatgcggtacatacttaaa	gatgttctgatatctagcaactgagtaaa
Tm4sf1	tcattgtggcatcactgggtttggcagaa	tggtccttcttggtcttaaaaaggaaatcg
Plekha2	ggtgatgtgaacagagcccaggaatgcct	accagacactcgtgagtcttgagaacatc
Cmtm8	ggacacttgcggacctgaccctggagatc	tttctttcttttaataacagtgggattcg
Sirpa	aaatgacatcaacgacatcacatacgcag	attttctaacaccttagctttaagactgc
Fam210b	ttcccgagtgggcacactggagctgcgc	caccagatgtttgatgataaaagtaaaac
Pon2	agaagaagttaaactggtggcagaaggat	atgctaaaagcgcatcagaattgcaaggc
Fam174b	aacttcgctggcttgtcagcgtcctgtgg	gttggcaaacatacacatatatagaggca
Ptgfrn	tggaattcttgctgcaagtgcatggctct	cactcgattgttacatatcagaaagtgcc
Tmem100	ggacacttgcggacctgaccctggagatc	tttctttcttttaataacagtgggattcg
Corin	ggctgtcctcagaagctggtgactgctaa	agtcatggtccccatcgcacacccactca
Adam11	agagtccagagggctctgaggtcaca	tgcttattccacatcatgcccaagtt
Eva1c	ttcccaagaacatactcacggcagtggatc	tacagataggattgcaagaca

All sequences are listed from 5’ to 3’.

siRNA knockdown using whole embryo culture

Whole embryo culture was done as described elsewhere (Chen et al., 2008), except that an *rfp* overexpression plasmid was used instead of *gfp*. siRNAs were obtained from the siGENOME mouse library (Dharmacon). The siRNA sequence that was used to knock down *Robo3* has been described elsewhere (Chen et al., 2008).

AP-protein binding assay

Overexpression constructs for *Dner, Rgmb, Lgi3*, *Adam22* and *Adam11, Eva1c* were cloned from Mammalian Gene Collection (MGC) cDNAs obtained from Dharmacon. Full length *Thsd7a* and *Adamts16* cDNA clones were unavailable, and therefore were generated from SMARTer RACE (Clontech) of spinal cord-extracted RNA.

AP-tagged protein binding experiments were done on either Lipofectamine 2000 (Invitrogen) transiently-transfected COS7 cells cultured on glass slides coated with 100 μg mL^{-1} poly-D-lysine, or on E11.5 spinal cord explants as described in 2D explant cultures.

AP-fusion constructs were cloned in-frame into the pAPtag plasmid (GenHunter). To collect AP-fusion protein, the plasmid was transiently transfected using Lipofectamine 2000 (Invitrogen) into HEK293T cells. The cells were cultured in Optimem for 2 days on 10 cm dishes, and the supernatant was filter-sterlized using a 0.2 μm filter. AP enzymatic activity was assayed using para-nitrophenyl phosphate as a substrate, and the amount of reaction product generated was measured 12 minutes later using a Nanodrop at 405nm. Lgi3-AP

and EAR-AP protein expression was found to be low, and these proteins were concentrated using a 100 kD Centricon filter (Millipore).

AP-binding experiments were done as described elsewhere (Xu et al., 2015). Binding of AP control ligands was done at 500 nM, and all other -AP tagged protein ligands was done at 100 nM in the presence of 10 ng mL^{-1} heparin.

CRISPR/Cas9 knockout mice generation

At least 2 single guide RNAs (sgRNAs) to exon 1 of the gene of interest were designed, and the sgRNA that gave the highest efficacy in ES cells was picked. Standard procedures were applied and described as previously (Yang et al., 2014). These procedures were done at the Gene Targeting Facility at The Rockefeller University. Germline transmission of mutant alleles was tested by PCR around the gene-edited locus followed by Sanger sequencing. Sanger sequencing tracers with overlapping spectral peaks near the double-stranded break were considered to be gene-edited. To determine the exact sequence of these edits, PCR products were TOPO cloned into vectors and transformed into bacteria according to manufacturer's instructions (Invitrogen), and at least 6 single colonies were sequenced. Mice with mutations that gave rise to a frameshift mutation were used.

Statistics

Unless stated otherwise, all statistics and graphs were prepared using GraphPad Prism v7.0c for Mac OS X (GraphPad Software). All bar graphs were plotted as the mean ± SEM.

References

Adler CE, Fetter RD, Bargmann CI (2006) UNC-6/Netrin induces neuronal asymmetry and defines the site of axon formation. Nat Neurosci 9:511–518.

Akin O, Zipursky SL (2016) Frazzled promotes growth cone attachment at the source of a Netrin gradient in the Drosophila visual system. Elife 5.

Alaynick WA, Jessell TM, Pfaff SL (2011) SnapShot: spinal cord development. Cell 146:178–178.e1.

Altman J, Bayer SA (1984) The development of the rat spinal cord. Adv Anat Embryol Cell Biol 85:1–164.

Bae G-U, Yang Y-J, Jiang G, Hong M, Lee H-J, Tessier-Lavigne M, Kang J-S, Krauss RS (2009) Neogenin regulates skeletal myofiber size and focal adhesion kinase and extracellular signal-regulated kinase activities in vivo and in vitro. Mol Biol Cell 20:4920–4931.

Bai G, Chivatakarn O, Bonanomi D, Lettieri K, Franco L, Xia C, Stein E, Ma L, Lewcock JW, Pfaff SL (2011) Presenilin-dependent receptor processing is required for axon guidance. Cell 144:106–118.

Bashaw GJ, Klein R (2010) Signaling from axon guidance receptors. Cold Spring Harb Perspect Biol 2:a001941.

Bell CH, Healey E, van Erp S, Bishop B, Tang C, Gilbert RJC, Aricescu AR, Pasterkamp RJ, Siebold C (2013) Structure of the repulsive guidance molecule (RGM)-neogenin signaling hub. Science 341:77–80.

Bermingham NA, Hassan BA, Wang VY, Fernandez M, Banfi S, Bellen HJ, Fritzsch B, Zoghbi HY (2001) Proprioceptor pathway development is dependent on Math1. Neuron 30:411–422.

Bielle F, Griveau A, Narboux-Nême N, Vigneau S, Sigrist M, Arber S, Wassef M, Pierani A (2005) Multiple origins of Cajal-Retzius cells at the borders of the developing pallium. Nat Neurosci 8:1002–1012.

Bin JM, Han D, Lai Wing Sun K, Croteau L-P, Dumontier E, Cloutier J-F, Kania A, Kennedy TE (2015) Complete Loss of Netrin-1 Results in Embryonic Lethality and Severe Axon Guidance Defects without Increased Neural Cell Death. Cell Rep 12:1099–1106.

Blasiak A, Lee GU, Kilinc D (2015) Neuron Subpopulations with Different Elongation Rates and DCC Dynamics Exhibit Distinct Responses to Isolated Netrin-1 Treatment. ACS Chem Neurosci 6:1578–1590.

Bouvier J, Thoby-Brisson M, Renier N, Dubreuil V, Ericson J, Champagnat J, Pierani A, Chédotal A, Fortin G (2010) Hindbrain interneurons and axon guidance signaling critical for breathing. Nat Neurosci 13:1066–1074.

Bovolenta P, Dodd J (1991) Perturbation of neuronal differentiation and axon guidance in the spinal cord of mouse embryos lacking a floor plate: analysis of Danforth's short-tail mutation. Development 113:625–639.

Brankatschk M, Dickson BJ (2006) Netrins guide Drosophila commissural axons at short range. Nat Neurosci 9:188–194.

Brose K, Bland KS, Wang KH, Arnott D, Henzel W, Goodman CS, Tessier-Lavigne M, Kidd T (1999) Slit proteins bind Robo receptors and have an evolutionarily conserved role in repulsive axon guidance. Cell 96:795–806.

Brunet I et al. (2014) Netrin-1 controls sympathetic arterial innervation. J Clin Invest 124:3230–3240.

Cajal RY (1899) Le Retine des vertebres. La Cellule 9:119–2560.

Castillo-Paterna M, Moreno-Juan V, Filipchuk A, Rodríguez-Malmierca L, Susín R, López-Bendito G (2015) DCC functions as an accelerator of thalamocortical axonal growth downstream of spontaneous thalamic activity. EMBO Rep 16:851–862.

Chan KKM, Seetharaman A, Bagg R, Selman G, Zhang Y, Kim J, Roy PJ (2014) EVA-1 functions as an UNC-40 Co-receptor to enhance attraction to the MADD-4 guidance cue in Caenorhabditis elegans. PLoS Genet 10:e1004521.

Chan SS, Zheng H, Su MW, Wilk R, Killeen MT, Hedgecock EM, Culotti JG (1996) UNC-40, a C. elegans homolog of DCC (Deleted in Colorectal Cancer), is required in motile cells responding to UNC-6 netrin cues. Cell 87:187–195.

Chao DL, Ma L, Shen K (2009) Transient cell-cell interactions in neural circuit formation. Nat Rev Neurosci 10:262–271.

Charron F, Stein E, Jeong J, McMahon AP, Tessier-Lavigne M (2003) The morphogen sonic hedgehog is an axonal chemoattractant that collaborates with netrin-1 in midline axon guidance. Cell 113:11–23.

Chen Z, Gore BB, Long H, Ma L, Tessier-Lavigne M (2008) Alternative splicing of the Robo3 axon guidance receptor governs the midline switch from attraction to repulsion. Neuron 58:325–332.

Chédotal A, Richards LJ (2010) Wiring the brain: the biology of neuronal guidance. Cold Spring Harb Perspect Biol 2:a001917.

Chilton JK, Guthrie S (2016) Axons get ahead: Insights into axon guidance and congenital cranial dysinnervation disorders. Dev Neurobiol.

Cho KR, Oliner JD, Simons JW, Hedrick L, Fearon ER, Preisinger AC, Hedge P, Silverman GA, Vogelstein B (1994) The DCC gene: structural analysis and mutations in colorectal carcinomas. Genomics 19:525–531.

Colamarino SA, Tessier-Lavigne M (1995) The role of the floor plate in axon guidance. Annu Rev Neurosci 18:497–529.

Coleman HA, Labrador JP, Chance RK, Bashaw GJ (2010) The Adam family metalloprotease Kuzbanian regulates the cleavage of the roundabout receptor to control axon repulsion at the midline. Development 137:2417–2426.

Conrad S, Genth H, Hofmann F, Just I, Skutella T (2007) Neogenin-RGMa signaling at the growth cone is bone morphogenetic protein-independent and involves RhoA, ROCK, and PKC. J Biol Chem 282:16423–16433.

Deiner MS, Kennedy TE, Fazeli A, Serafini T, Tessier-Lavigne M, Sretavan DW (1997) Netrin-1 and DCC mediate axon guidance locally at the optic disc: loss of function leads to optic nerve hypoplasia. Neuron 19:575–589.

Dickson BJ (2002) Molecular mechanisms of axon guidance. Science 298:1959–1964.

Dickson BJ, Gilestro GF (2006) Regulation of commissural axon pathfinding by slit and its Robo receptors. Annu Rev Cell Dev Biol 22:651–675.

Dickson BJ, Zou Y (2010) Navigating intermediate targets: the nervous system midline. Cold Spring Harb Perspect Biol 2:a002055.

Dodd J, Morton SB, Karagogeos D, Yamamoto M, Jessell TM (1988) Spatial regulation of axonal glycoprotein expression on subsets of embryonic spinal neurons. Neuron 1:105–116.

Dominici C, Moreno-Bravo JA, Puiggros SR, Rappeneau Q, Rama N, Vieugue P, Bernet A, Mehlen P, Chédotal A (2017) Floor-plate-derived netrin-1 is dispensable for commissural axon guidance. Nature 545:350–354.

Engle EC (2010) Human genetic disorders of axon guidance. Cold Spring Harb Perspect Biol 2:a001784.

Farley FW, Soriano P, Steffen LS, Dymecki SM (2000) Widespread recombinase expression using FLPeR (flipper) mice. Genesis 28:106–110.

Fazeli A, Dickinson SL, Hermiston ML, Tighe RV, Steen RG, Small CG, Stoeckli ET, Keino-Masu K, Masu M, Rayburn H, Simons J, Bronson RT, Gordon JI,

Tessier-Lavigne M, Weinberg RA (1997) Phenotype of mice lacking functional Deleted in colorectal cancer (Dcc) gene. Nature 386:796–804.

Fujisawa K, Wrana JL, Culotti JG (2007) The slit receptor EVA-1 coactivates a SAX-3/Robo mediated guidance signal in C. elegans. Science 317:1934–1938.

Gad JM, Keeling SL, Wilks AF, Tan SS, Cooper HM (1997) The expression patterns of guidance receptors, DCC and Neogenin, are spatially and temporally distinct throughout mouse embryogenesis. Dev Biol 192:258–273.

Galko MJ, Tessier-Lavigne M (2000) Function of an axonal chemoattractant modulated by metalloprotease activity. Science 289:1365–1367.

Geisbrecht BV, Dowd KA, Barfield RW, Longo PA, Leahy DJ (2003) Netrin binds discrete subdomains of DCC and UNC5 and mediates interactions between DCC and heparin. J Biol Chem 278:32561–32568.

Gore BB, Wong KG, Tessier-Lavigne M (2008) Stem cell factor functions as an outgrowth-promoting factor to enable axon exit from the midline intermediate target. Neuron 57:501–510.

Harfe BD, Scherz PJ, Nissim S, Tian H, McMahon AP, Tabin CJ (2004) Evidence for an expansion-based temporal Shh gradient in specifying vertebrate digit identities. Cell 118:517–528.

Hedgecock EM, Culotti JG, Hall DH (1990) The unc-5, unc-6, and unc-40 genes guide circumferential migrations of pioneer axons and mesodermal cells on the epidermis in C. elegans. Neuron 4:61–85.

His W (1888) Zur Geschichte des Gehirns, sowie der centralen und peripherischen Nervenbahnen beim menschlichen Embryo. Abh. K. Sachs. Ges. Wiss. Math.-Phys. Kl.

Ishii N, Wadsworth WG, Stern BD, Culotti JG, Hedgecock EM (1992) UNC-6, a laminin-related protein, guides cell and pioneer axon migrations in C. elegans. Neuron 9:873–881.

James G, Foster SR, Key B, Beverdam A (2013) The Expression Pattern of EVA1C, a Novel Slit Receptor, Is Consistent with an Axon Guidance Role in the Mouse Nervous System. PLoS ONE 8:e74115.

Jamuar SS et al. (2017) Biallelic mutations in human DCC cause developmental split-brain syndrome. Nature Genetics 49:606–612.

Jaworski A, Tom I, Tong RK, Gildea HK, Koch AW, Gonzalez LC, Tessier-Lavigne M (2015) Operational redundancy in axon guidance through the multifunctional receptor Robo3 and its ligand NELL2. Science 350:961–965.

Jen JC et al. (2004) Mutations in a human ROBO gene disrupt hindbrain axon pathway crossing and morphogenesis. Science 304:1509–1513.

Kadison SR, Kaprielian Z (2004) Diversity of contralateral commissural projections in the embryonic rodent spinal cord. J Comp Neurol 472:411–422.

Kam JWK, Dumontier E, Baim C, Brignall AC, Mendes da Silva D, Cowan M, Kennedy TE, Cloutier J-F (2016) RGMB and neogenin control cell differentiation in the developing olfactory epithelium. Development 143:1534–1546.

Kapahnke M, Banning A, Tikkanen R (2016) Random Splicing of Several Exons Caused by a Single Base Change in the Target Exon of CRISPR/Cas9 Mediated Gene Knockout. Cells 5.

Kappler J, Franken S, Junghans U, Hoffmann R, Linke T, Müller HW, Koch KW (2000) Glycosaminoglycan-binding properties and secondary structure of the C-terminus of netrin-1. Biochem Biophys Res Commun 271:287–291.

Kaprielian Z, Imondi R, Runko E (2000) Axon guidance at the midline of the developing CNS. Anat Rec 261:176–197.

Kegel L, Aunin E, Meijer D, Bermingham JR (2013) LGI proteins in the nervous system. ASN Neuro 5:167–181.

Keino-Masu K, Masu M, Hinck L, Leonardo ED, Chan SS, Culotti JG, Tessier-Lavigne M (1996) Deleted in Colorectal Cancer (DCC) encodes a netrin receptor. Cell 87:175–185.

Keleman K, Rajagopalan S, Cleppien D, Teis D, Paiha K, Huber LA, Technau GM, Dickson BJ (2002) Comm sorts robo to control axon guidance at the Drosophila midline. Cell 110:415–427.

Keleman K, Ribeiro C, Dickson BJ (2005) Comm function in commissural axon guidance: cell-autonomous sorting of Robo in vivo. Nat Neurosci 8:156–163.

Kennedy TE, Serafini T, la Torre de JR, Tessier-Lavigne M (1994) Netrins are diffusible chemotropic factors for commissural axons in the embryonic spinal cord. Cell 78:425–435.

Kennedy TE, Wang H, Marshall W, Tessier-Lavigne M (2006) Axon guidance by diffusible chemoattractants: a gradient of netrin protein in the developing spinal cord. Journal of Neuroscience 26:8866–8874.

Kiehn O (2006) Locomotor circuits in the mammalian spinal cord. Annu Rev Neurosci 29:279–306.

Kiehn O, Kullander K (2004) Central pattern generators deciphered by molecular

genetics. Neuron 41:317–321.

Kim T-H, Lee HK, Seo IA, Bae HR, Suh DJ, Wu J, Rao Y, Hwang K-G, Park HT (2005) Netrin induces down-regulation of its receptor, Deleted in Colorectal Cancer, through the ubiquitin-proteasome pathway in the embryonic cortical neuron. J Neurochem 95:1–8.

Klämbt C, Jacobs JR, Goodman CS (1991) The midline of the Drosophila central nervous system: a model for the genetic analysis of cell fate, cell migration, and growth cone guidance. Cell 64:801–815.

Kolodziej PA, Timpe LC, Mitchell KJ, Fried SR, Goodman CS, Jan LY, Jan YN (1996) frazzled encodes a Drosophila member of the DCC immunoglobulin subfamily and is required for CNS and motor axon guidance. Cell 87:197–204.

Kruger RP, Lee J, Li W, Guan K-L (2004) Mapping netrin receptor binding reveals domains of Unc5 regulating its tyrosine phosphorylation. Journal of Neuroscience 24:10826–10834.

Labrador JP, O'keefe D, Yoshikawa S, McKinnon RD, Thomas JB, Bashaw GJ (2005) The homeobox transcription factor even-skipped regulates netrin-receptor expression to control dorsal motor-axon projections in Drosophila. Current Biology 15:1413–1419.

Lai Wing Sun K, Correia JP, Kennedy TE (2011) Netrins: versatile extracellular cues with diverse functions. Development 138:2153–2169.

Lakso M, Pichel JG, Gorman JR, Sauer B, Okamoto Y, Lee E, Alt FW, Westphal H (1996) Efficient in vivo manipulation of mouse genomic sequences at the zygote stage. Proc Natl Acad Sci USA 93:5860–5865.

Lalonde S, Stone OA, Lessard S, Lavertu A, Desjardins J, Beaudoin M, Rivas M, Stainier DYR, Lettre G (2017) Frameshift indels introduced by genome editing can lead to in-frame exon skipping. PLoS ONE 12:e0178700.

Laumonnerie C, Da Silva RV, Kania A, Wilson SI (2014) Netrin 1 and Dcc signalling are required for confinement of central axons within the central nervous system. Development 141:594–603.

Leggere JC, Saito Y, Darnell RB, Tessier-Lavigne M, Junge HJ, Chen Z (2016) NOVA regulates Dcc alternative splicing during neuronal migration and axon guidance in the spinal cord. Elife 5.

Llambi F, Causeret F, Bloch-Gallego E, Mehlen P (2001) Netrin-1 acts as a survival factor via its receptors UNC5H and DCC. EMBO J 20:2715–2722.

Long H, Sabatier C, Ma L, Plump A, Yuan W, Ornitz DM, Tamada A, Murakami

F, Goodman CS, Tessier-Lavigne M (2004) Conserved roles for Slit and Robo proteins in midline commissural axon guidance. Neuron 42:213–223.

Lyuksyutova AI, Lu C-C, Milanesio N, King LA, Guo N, Wang Y, Nathans J, Tessier-Lavigne M, Zou Y (2003) Anterior-posterior guidance of commissural axons by Wnt-frizzled signaling. Science 302:1984–1988.

Madisen L, Zwingman TA, Sunkin SM, Oh SW, Zariwala HA, Gu H, Ng LL, Palmiter RD, Hawrylycz MJ, Jones AR, Lein ES, Zeng H (2010) A robust and high-throughput Cre reporting and characterization system for the whole mouse brain. Nat Neurosci 13:133–140.

Marillat V, Cases O, Nguyen-Ba-Charvet KT, Tessier-Lavigne M, Sotelo C, Chédotal A (2002) Spatiotemporal expression patterns of slit and robo genes in the rat brain. J Comp Neurol 442:130–155.

Marsh APL et al. (2017) Mutations in DCC cause isolated agenesis of the corpus callosum with incomplete penetrance. Nature Genetics 49:511–514.

Masuda T, Watanabe K, Sakuma C, Ikenaka K, Ono K, Yaginuma H (2008) Netrin-1 acts as a repulsive guidance cue for sensory axonal projections toward the spinal cord. Journal of Neuroscience 28:10380–10385.

Matei V, Pauley S, Kaing S, Rowitch D, Beisel KW, Morris K, Feng F, Jones K, Lee J, Fritzsch B (2005) Smaller inner ear sensory epithelia in Neurog 1 null mice are related to earlier hair cell cycle exit. Dev Dyn 234:633–650.

Matise MP, Lustig M, Sakurai T, Grumet M, Joyner AL (1999) Ventral midline cells are required for the local control of commissural axon guidance in the mouse spinal cord. Development 126:3649–3659.

Mehlen P, Guenebeaud C (2010) Netrin-1 and its dependence receptors as original targets for cancer therapy. Curr Opin Oncol 22:46–54.

Mehlen P, Rabizadeh S, Snipas SJ, Assa-Munt N, Salvesen GS, Bredesen DE (1998) The DCC gene product induces apoptosis by a mechanism requiring receptor proteolysis. Nature 395:801–804.

Michalski N, Babai N, Renier N, Perkel DJ, Chédotal A, Schneggenburger R (2013) Robo3-driven axon midline crossing conditions functional maturation of a large commissural synapse. Neuron 78:855–868.

Moore SW, Tessier-Lavigne M, Kennedy TE (2007) Netrins and their receptors. Adv Exp Med Biol 621:17–31.

Myat A, Henry P, McCabe V, Flintoft L, Rotin D, Tear G (2002) Drosophila Nedd4, a ubiquitin ligase, is recruited by Commissureless to control cell surface levels of the roundabout receptor. Neuron 35:447–459.

Neuhaus-Follini A, Bashaw GJ (2015) The Intracellular Domain of the Frazzled/DCC Receptor Is a Transcription Factor Required for Commissural Axon Guidance. Neuron 87:751–763.

Nugent AA, Kolpak AL, Engle EC (2012) Human disorders of axon guidance. Current Opinion in Neurobiology 22:837–843.

Okada A, Charron F, Morin S, Shin DS, Wong K, Fabre PJ, Tessier-Lavigne M, McConnell SK (2006) Boc is a receptor for sonic hedgehog in the guidance of commissural axons. Nature 444:369–373.

Ozkaynak E, Abello G, Jaegle M, van Berge L, Hamer D, Kegel L, Driegen S, Sagane K, Bermingham JR, Meijer D (2010) Adam22 is a major neuronal receptor for Lgi4-mediated Schwann cell signaling. Journal of Neuroscience 30:3857–3864.

Park W-J, Lim YY, Kwon NS, Baek KJ, Kim D-S, Yun H-Y (2010) Leucine-rich glioma inactivated 3 induces neurite outgrowth through Akt and focal adhesion kinase. Neurochem Res 35:789–796.

Placzek M, Briscoe J (2005) The floor plate: multiple cells, multiple signals. Nat Rev Neurosci 6:230–240.

Placzek M, Tessier-Lavigne M, Jessell T, Dodd J (1990) Orientation of commissural axons in vitro in response to a floor plate-derived chemoattractant. Development 110:19–30.

R Core Team (2017) R: A language and environment for statistical computing. R Foundation for Statistical Computing, Vienna, Austria Available at: http://www.R-project.org/.

Rabe N, Gezelius H, Vallstedt A, Memic F, Kullander K (2009) Netrin-1-dependent spinal interneuron subtypes are required for the formation of left-right alternating locomotor circuitry. Journal of Neuroscience 29:15642–15649.

Rajagopalan S, Deitinghoff L, Davis D, Conrad S, Skutella T, Chédotal A, Mueller BK, Strittmatter SM (2004) Neogenin mediates the action of repulsive guidance molecule. Nat Cell Biol 6:756–762.

Renier N, Schonewille M, Giraudet F, Badura A, Tessier-Lavigne M, Avan P, De Zeeuw CI, Chédotal A (2010) Genetic dissection of the function of hindbrain axonal commissures. PLoS Biol 8:e1000325.

Rybnikova E, Kärkkäinen I, Pelto-Huikko M, Huovila A-PJ (2002) Developmental regulation and neuronal expression of the cellular disintegrin ADAM11 gene in mouse nervous system. Neuroscience 112:921–934.

Sabatier C, Plump AS, Le Ma, Brose K, Tamada A, Murakami F, Lee EYHP, Tessier-Lavigne M (2004) The Divergent Robo Family Protein Rig-1/Robo3 Is a Negative Regulator of Slit Responsiveness Required for Midline Crossing by Commissural Axons. Cell 117:157–169.

Schneider CA, Rasband WS, Eliceiri KW (2012) NIH Image to ImageJ: 25 years of image analysis. Nat Methods 9:671–675.

Schonhoff SE, Giel-Moloney M, Leiter AB (2004) Neurogenin 3-expressing progenitor cells in the gastrointestinal tract differentiate into both endocrine and non-endocrine cell types. Dev Biol 270:443–454.

Seetharaman A, Selman G, Puckrin R, Barbier L, Wong E, D'Souza SA, Roy PJ (2011) MADD-4 is a secreted cue required for midline-oriented guidance in Caenorhabditis elegans. Dev Cell 21:669–680.

Serafini T, Colamarino SA, Leonardo ED, Wang H, Beddington R, Skarnes WC, Tessier-Lavigne M (1996) Netrin-1 is required for commissural axon guidance in the developing vertebrate nervous system. Cell 87:1001–1014.

Serafini T, Kennedy TE, Galko MJ, Mirzayan C, Jessell TM, Tessier-Lavigne M (1994) The netrins define a family of axon outgrowth-promoting proteins homologous to C. elegans UNC-6. Cell 78:409–424.

Shen H, Illges H, Reuter A, Stuermer CAO (2002) Cloning, expression, and alternative splicing of neogenin1 in zebrafish. Mech Dev 118:219–223.

Skarnes WC, Rosen B, West AP, Koutsourakis M, Bushell W, Iyer V, Mujica AO, Thomas M, Harrow J, Cox T, Jackson D, Severin J, Biggs P, Fu J, Nefedov M, de Jong PJ, Stewart AF, Bradley A (2011) A conditional knockout resource for the genome-wide study of mouse gene function. Nature 474:337–342.

Sommer L, Ma Q, Anderson DJ (1996) neurogenins, a novel family of atonal-related bHLH transcription factors, are putative mammalian neuronal determination genes that reveal progenitor cell heterogeneity in the developing CNS and PNS. Mol Cell Neurosci 8:221–241.

Srour M, Rivière J-B, Pham JMT, Dubé M-P, Girard S, Morin S, Dion PA, Asselin G, Rochefort D, Hince P, Diab S, Sharafaddinzadeh N, Chouinard S, Théoret H, Charron F, Rouleau GA (2010) Mutations in DCC cause congenital mirror movements. Science 328:592.

Tanabe Y, Jessell TM (1996) Diversity and pattern in the developing spinal cord. Science 274:1115–1123.

Tessier-Lavigne M, Goodman CS (1996) The molecular biology of axon guidance. Science 274:1123–1133.

Tessier-Lavigne M, Placzek M, Lumsden AG, Dodd J, Jessell TM (1988) Chemotropic guidance of developing axons in the mammalian central nervous system. Nature 336:775–778.

Thaler J, Harrison K, Sharma K, Lettieri K, Kehrl J, Pfaff SL (1999) Active suppression of interneuron programs within developing motor neurons revealed by analysis of homeodomain factor HB9. Neuron 23:675–687.

Timofeev K, Joly W, Hadjieconomou D, Salecker I (2012) Localized netrins act as positional cues to control layer-specific targeting of photoreceptor axons in Drosophila. Neuron 75:80–93.

Tran TS, Carlin E, Lin R, Martinez E, Johnson JE, Kaprielian Z (2013) Neuropilin2 regulates the guidance of post-crossing spinal commissural axons in a subtype-specific manner. Neural Development 8:15.

Trapnell C, Roberts A, Goff L, Pertea G, Kim D, Kelley DR, Pimentel H, Salzberg SL, Rinn JL, Pachter L (2012) Differential gene and transcript expression analysis of RNA-seq experiments with TopHat and Cufflinks. Nat Protoc 7:562–578.

Uchiyama Y, Sakaguchi M, Terabayashi T, Inenaga T, Inoue S, Kobayashi C, Oshima N, Kiyonari H, Nakagata N, Sato Y, Sekiguchi K, Miki H, Araki E, Fujimura S, Tanaka SS, Nishinakamura R (2010) Kif26b, a kinesin family gene, regulates adhesion of the embryonic kidney mesenchyme. Proceedings of the National Academy of Sciences 107:9240–9245.

Varadarajan SG, Kong JH, Phan KD, Kao TJ, Panaitof C, Cardin J, Eltzschig H, Kania A, Novitch BG, Butler SJ (2017) Netrin1 Produced by Neural Progenitors, Not Floor Plate Cells, Is Required for Axon Guidance in the Spinal Cord. Neuron.

Vielmetter J, Kayyem JF, Roman JM, Dreyer WJ (1994) Neogenin, an avian cell surface protein expressed during terminal neuronal differentiation, is closely related to the human tumor suppressor molecule deleted in colorectal cancer. J Cell Biol 127:2009–2020.

Wadsworth WG, Bhatt H, Hedgecock EM (1996) Neuroglia and pioneer neurons express UNC-6 to provide global and local netrin cues for guiding migrations in C. elegans. Neuron 16:35–46.

Wang C-H, Su P-T, Du X-Y, Kuo M-W, Lin C-Y, Yang C-C, Chan H-S, Chang S-J, Kuo C, Seo K, Leung LL, Chuang Y-J (2010) Thrombospondin type I domain containing 7A (THSD7A) mediates endothelial cell migration and tube formation. J Cell Physiol 222:685–694.

Wang KH, Brose K, Arnott D, Kidd T, Goodman CS, Henzel W, Tessier-Lavigne M (1999) Biochemical purification of a mammalian slit protein as a positive

regulator of sensory axon elongation and branching. Cell 96:771–784.

Watanabe K, Tamamaki N, Furuta T, Ackerman SL, Ikenaka K, Ono K (2006) Dorsally derived netrin 1 provides an inhibitory cue and elaborates the “waiting period” for primary sensory axons in the developing spinal cord. Development 133:1379–1387.

Whitman MC, Engle EC (2017) Ocular Congenital Cranial Dysinnervation Disorders (CCDDs): Insights into Axon Growth and Guidance. Hum Mol Genet.

Wilson NH, Key B (2006) Neogenin interacts with RGMa and netrin-1 to guide axons within the embryonic vertebrate forebrain. Dev Biol 296:485–498.

Winckler B, Mellman I (2010) Trafficking guidance receptors. Cold Spring Harb Perspect Biol 2:a001826.

Xu K, Olsen O, Tzvetkova-Robev D, Tessier-Lavigne M, Nikolov DB (2015) The crystal structure of DR6 in complex with the amyloid precursor protein provides insight into death receptor activation. Genes & Development 29:785–790.

Xu K, Wu Z, Renier N, Antipenko A, Tzvetkova-Robev D, Xu Y, Minchenko M, Nardi-Dei V, Rajashankar KR, Himanen J, Tessier-Lavigne M, Nikolov DB (2014) Structures of netrin-1 bound to two receptors provide insight into its axon guidance mechanism. Science 344:1275–1279.

Yam PT, Kent CB, Morin S, Farmer WT, Alchini R, Lepelletier L, Colman DR, Tessier-Lavigne M, Fournier AE, Charron F (2012) 14-3-3 proteins regulate a cell-intrinsic switch from sonic hedgehog-mediated commissural axon attraction to repulsion after midline crossing. Neuron 76:735–749.

Yang H, Wang H, Jaenisch R (2014) Generating genetically modified mice using CRISPR/Cas-mediated genome engineering. Nat Protoc 9:1956–1968.

Yang L, Garbe DS, Bashaw GJ (2009) A frazzled/DCC-dependent transcriptional switch regulates midline axon guidance. Science 324:944–947.

Yu TW, Bargmann CI (2001) Dynamic regulation of axon guidance. Nat Neurosci 4 Suppl:1169–1176.

Yung AR, Nishitani AM, Goodrich LV (2015) Phenotypic analysis of mice completely lacking netrin 1. Development 142:3686–3691.

Yurchenco PD, Wadsworth WG (2004) Assembly and tissue functions of early embryonic laminins and netrins. Curr Opin Cell Biol 16:572–579.

Zelina P, Blockus H, Zagar Y, Péres A, Friocourt F, Wu Z, Rama N, Fouquet C,

Hohenester E, Tessier-Lavigne M, Schweitzer J, Roest Crollius H, Chédotal A (2014) Signaling switch of the axon guidance receptor Robo3 during vertebrate evolution. Neuron 84:1258–1272.

Zhang A-S, West AP, Wyman AE, Bjorkman PJ, Enns CA (2005) Interaction of hemojuvelin with neogenin results in iron accumulation in human embryonic kidney 293 cells. J Biol Chem 280:33885–33894.

Zou Y, Stoeckli E, Chen H, Tessier-Lavigne M (2000) Squeezing axons out of the gray matter: a role for slit and semaphorin proteins from midline and ventral spinal cord. Cell 102:363–375.